Online Assessment of Distributed Generation Connection for Smart Grid

by

Ayman Bahgat Abdelazim Ibrahim Eltantawy

A thesis
presented to the University of Waterloo
in fulfillment of the
thesis requirement for the degree of
Doctor of Philosophy
in
Electrical and Computer Engineering

Waterloo, Ontario, Canada, 2014

I hereby declare that I am the sole author of this thesis. This is a true copy of the thesis, including any required final revisions, as accepted by my examiners.

I understand that my thesis may be made electronically available to the public.

Abstract

Increasing renewable energy generation is among the most important objectives of smart grid, especially due to the increased environmental concerns, energy demand, and depletion of fossil energy resources. Introducing incentive feed-in tariff (FIT) programs to promote renewable distributed generation (DG) in distribution systems is an essential step towards smart grid implementation. However, current regulations of FIT programs for small-scale DG sources strictly limit the aggregated installed DG capacity to a small fraction of the system peak load. Limiting the DG capacity avoids the need for detailed connection impact assessment studies for the DG connection. Conducting detailed CIA studies for each small-scale DG project application is impractical due to the large number of applications, which can lead to delaying the DG connection process. However, avoiding assessment studies and imposing such strict limits result in rejecting numerous applications for renewable DG projects, and therefore losing a significant amount of renewable DG capacity.

Such situations underscore the need for research that suggests new directions for increasing small-scale renewable DG projects under FIT programs. In order to accomplish this target, this thesis presents a planning model and a management scheme for DG connection online assessment in smart grids. The planning model achieves two objectives: insuring an adequate profit for DG owners and maximizing the number of installed DG sources in the systems. The management scheme controls the curtailment of the connected DG units to satisfy the system operational constrains. Implementing the proposed work evades the need for detailed connection impact assessment studies prior to installing small-scale DG units since the assessment is performed on an online basis. This feature can therefore reduce the number of rejected applications for renewable DG projects under FIT programs while accelerating the DG connection process.

The proposed planning model and management scheme for DG connection online assessment are based on dividing the output power of each DG unit into two components: unconditional and conditional. The unconditional DG component refers to the portion of DG output power that is not subject to curtailment for all online conditions of the system; this component guarantees an adequate profit for the DG investors. The conditional DG component denotes the portion of the DG output power that is subject to curtailment. The curtailment of the conditional DG component is controlled using the proposed management scheme for DG connection online assessment.

The first phase of this work introduces an economic model for calculating the unconditional DG component. This model ensures that the unconditional DG component, which is not susceptible to curtailment, yields adequate profit for DG investors. The first part

also presents a techno-economic planning model that maximizes the number of DG units installed based on the technical and economic constraints.

The second phase of this work presents a novel algorithm for DLF analysis that can interact with the continual changes of load and network topology in smart grids. This algorithm can solve the DLF problem in a specific area of interest in a distribution system without necessitating the inclusion of all of the system buses. This "zooming" feature leads to a significant reduction in the required DLF solution time, especially for large distribution systems. This DLF algorithm is utilized in obtaining load flow results in the proposed management scheme for DG connection online assessment, presented in the third phase of this work.

The third phase of this work introduces a management scheme for DG connection online assessment in smart grids. The assessment is performed using a novel scalable optimization model that utilizes the "zooming" feature of the proposed DLF algorithm, presented in the second phase of this work. The scalable optimization model can therefore minimize the curtailment of the conditional DG components in a specific area of interest in the system without including all the system buses in the optimization problem. This feature ensures fast calculation of the minimum DG power to be curtailed based on the online condition of the system.

The simulation results include a comparison between two maximum renewable DG capacities - that which can be installed according to the current FIT rules in Ontario and that which can be installed by implementing the proposed planning model with the management scheme for DG connection online assessment. The comparison indicates that implementing the proposed work would significantly increase the number of small-scale renewable DG projects that can be installed.

Acknowledgements

All praise is due to Allah for granting me the strength and knowledge to achieve this work.

I would like to thank my supervisor Professor Magdy Salama for his continuous encouragement, helpful discussion, and insightful guidance throughout my PhD.

I would like to thank the members of my doctoral committee: Professor Sheshakamal Jayaram, Dr. Tarek El-Fouly, Professor Amir Khajepour, and Professor Elham Makram for investing time in reading and providing many valuable comments on my thesis.

I would like to thank my wife for her continuous understanding, unlimited encouragement, and unending love during the years of my Ph.D. studies.

I would like to express my deepest gratitude and respect to my parents, Dr. Bahgat Eltantawy and Dr. Hala Nagati, for their continuous encouragement, support, patience, and prayers. I also would like to thank my grandparents, my brothers, and my sister for their unlimited support and encouragement.

Last but not least, I wish to thank Eng. Aly El-Kholy, my dearest friend and brother, whose valuable suggestions and discussions were always helpful and inspiring.

Dedication

To my parents,
my grandparents,
my wife,
and my son Yassine ...

Table of Contents

List of Tables **xi**

List of Figures **xiii**

Nomenclature **xvi**

1 Introduction **1**

1.1 General 1

1.2 Motivation 2

1.3 Research Objectives 4

1.4 Thesis Outline 5

2 Background and Literature Survey **6**

2.1 Introduction 6

2.2 Technical Interconnection Requirements (TIR) for microFIT DG Projects . 6

2.3 Potential Solutions for Increasing the Interconnection of Renewable Energy DG in Distribution Systems 8

2.3.1 Reduction of Distribution Transformer Secondary Voltage 8

2.3.2 Application of Voltage Regulating Devices 8

2.3.3 Network Upgrading 8

2.3.4 Application of Energy Storage Devices 9

2.3.5 Reactive Power Compensation 9
2.3.6 DG Active Power Curtailment 9
2.4 Distribution Load Flow (DLF) Analysis 11
2.4.1 Newton Raphson (NR) Method 12
2.4.2 Forward/Backward (F/B) Method 13
2.5 Distribution System Modeling for DLF Analysis 16
2.5.1 Line Modeling 17
2.5.2 Load Modeling 18
2.5.3 DG Modeling 18
2.6 Summary 19

3 A Techno-Economic Planning Model for Increasing the Connectivity of Small-Scale Renewable DG in Distribution Systems 20

3.1 Introduction 20
3.2 Economic Assessment of Renewable DG Investments for Calculating the Unconditional and Conditional Components 21
3.2.1 Classification of Investment Alternatives 22
3.2.2 Selecting the Best Project among Mutually Exclusive Investment Alternatives 23
3.2.3 After-Tax Cash Flow for Renewable DG Projects 23
3.2.4 Calculation of Unconditional and Conditional DG Components . . . 27
3.3 Techno-Economic Planning Model for Increasing the Connectivity of Renewable Energy Sources in Distribution Systems 28
3.4 Simulation Results 32
3.4.1 Calculation of the Unconditional and Conditional DG Components 35
3.4.2 Calculation of the Maximum DG Capacity to be Installed in the System 38
3.5 Summary 42

4 A "Zooming" Algorithm for Distribution Load Flow Analysis in Smart Grids 43

4.1 Introduction . . . 43
4.2 Proposed System Lumping Technique . . . 44
4.3 System Configuration Modeling . . . 46
4.3.1 *PC* Matrix Characteristics . . . 46
4.3.2 *PC* Matrix Building Algorithm . . . 47
4.4 Proposed DLF Zooming Algorithm . . . 51
4.5 Simulation Results . . . 54
4.5.1 Accuracy Validation . . . 55
4.5.2 DLF Solution Speed Evaluation . . . 59
4.5.3 Network Topology Changes . . . 60
4.6 Summary . . . 61

5 A Management Scheme for Online Assessment of DG Connection in Smart Grids 62

5.1 Introduction . . . 62
5.2 Proposed Management Scheme . . . 63
5.2.1 Determination of the Zone of Interest . . . 63
5.2.2 Formulation of the Scalable Optimization Model Problem . . . 67
5.3 Simulation Results . . . 71
5.3.1 System Description . . . 71
5.3.2 Case #1: Simulation Results for a Winter Day . . . 74
5.3.3 Case #2: Simulation Results for a Summer Day . . . 79
5.4 Summary . . . 83

6 Conclusions 84

6.1 Summary and Conclusions . . . 84
6.2 Contributions . . . 85
6.3 Directions for Future Work . . . 86

A Cash Flows of the Candidate DG Capacities Studied in Chapter 3 **88**

B Distribution Load Flow Results for the Forward/Backward Method and the Proposed Zooming Algorithm Presented in Chapter 4 **95**

References **98**

List of Tables

3.1 Economic parameters of a renewable energy DG project 24

3.2 After-tax cash flow for the DG project example given in Table 3.1 25

3.3 Calculated IRR values for the DG project example given in Table 3.1 . . . 27

3.4 Economic model parameters 36

3.5 Capital cost and IRR for the candidate DG capacities 37

3.6 Unconditional and conditional DG components for the output power of the candidate DG capacities 37

3.7 Number of installed DG units in Scenario #2 (7 kW capacity) per distribution transformer in the modified IEEE 123-bus system 39

3.8 Number of installed DG units in Scenario #3 (10 kW capacity) per distribution transformer in the modified IEEE 123-bus system 41

4.1 Recursive process output for the IEEE 13-bus system 53

4.2 Input and output of the proposed DLF zooming algorithm 54

4.3 Effect of increasing the system size on the results produced by the F/B method presented in [49] and the proposed zooming algorithm 59

4.4 IEEE 123-bus system switches for the system reconfiguration 61

A.1 After-tax cash flow for a 2 kW rooftop PV DG unit using the analysis described in Section 3.2.3 89

A.2 After-tax cash flow for a 3 kW rooftop PV DG unit using the analysis described in Section 3.2.3 90

A.3 After-tax cash flow for a 4 kW rooftop PV DG unit using the analysis described in Section 3.2.3 91

A.4 After-tax cash flow for a 5 kW rooftop PV DG unit using the analysis described in Section 3.2.3 92

A.5 After-tax cash flow for a 7 kW rooftop PV DG unit using the analysis described in Section 3.2.3 93

A.6 After-tax cash flow for a 10 kW rooftop PV DG unit using the analysis described in Section 3.2.3 94

B.1 DLF results of the IEEE 37-bus system for the zone of interest using the F/B method for the entire system and the proposed zooming method . . . 96

B.2 DLF results of the IEEE 123-bus system for the zone of interest using the F/B method for the entire system and the proposed zooming method . . . 97

List of Figures

2.1 Flow chart of the forward/backward DLF method 14

2.2 Line section in a ladder network 15

2.3 Three-phase line model 17

3.1 Single-line diagram of the modified IEEE 123-bus system, indicating the locations and phases of the 77 secondary-distribution residential networks . 33

3.2 Configuration of a 240-120 V secondary-distribution residential network . . 34

3.3 Four-season daily residential load profiles given in [77] for a house in Canada 34

3.4 Maximum PV DG capacity for the three scenarios examined for the distribution system under study 40

4.1 The IEEE 13-bus system 47

4.2 PC_{13} matrix of the IEEE 13-bus system 48

4.3 Flowchart of the PC matrix building algorithm 49

4.4 Ordered BI matrix of the IEEE 13-bus system 50

4.5 Flowchart of the proposed DLF zooming algorithm 52

4.6 Configuration of the (a) IEEE 37-bus system and (b) the zone of interest of the IEEE 37-bus system, showing the zooming-in on bus 741. The greyed parts of the system represent the lumped laterals 55

4.7 Configuration of the (a) IEEE 123-bus system and (b) the zone of interest of the IEEE 123-bus system, showing the zooming-in on bus 114. The greyed parts of the system represent the lumped laterals 56

4.8 DLF results of phase 'a' using the method presented in [49] for all the system buses and using the proposed DLF zooming algorithm (zooming on the farthest bus). (a) The IEEE 37-bus system. (b) The IEEE 123-bus system 58

5.1 Flowchart of the proposed management scheme 64

5.2 Simple radial distribution system, the shaded portions denote the zone of interest 66

5.3 Single-line diagram of the modified IEEE 123-bus system, indicating the locations and phases of the 77 secondary-distribution residential networks. The zone of interest for Case #1 is indicated. 70

5.4 Configuration of a 240-120 V secondary-distribution residential network . . 71

5.5 Hourly variations in (a) the temperature, (b) solar irradiance, and (c) PV DG output power for a Summer day; and (d) the temperature, (e) solar irradiance, and (f) PV DG output power for a Winter day. The unconditional power in (c) and (f) equals 85 % of the total output PV DG power. 73

5.6 Summer and Winter daily residential load profiles given in [77] for a house in Canada 74

5.7 Hourly variations in (a) the maximum voltage unbalance with and without the proposed management scheme and (b) the total curtailed PV DG power in the system using the proposed management scheme during a Winter day 75

5.8 Hourly variations in the maximum V_{max} and the minimum V_{min} of the system using the proposed management scheme during a Winter day 76

5.9 Hourly variations in the maximum percentage reverse power in the system using the proposed management scheme during a Winter day 77

5.10 Times required for the execution of the management scheme, which runs every 15 min, during a Winter day 77

5.11 Total generated power from the 286 PV DG units during a Winter day . . 78

5.12 Hourly variations in (a) the maximum reverse power flow with and without the proposed management scheme, (b) the total curtailed PV DG power in the system using the proposed management scheme, and (c) times required for the execution of the management scheme, which runs every 15 min, during a Summer day 80

5.13 Hourly variations in (a) the maximum V_{max} and the minimum V_{min} and (b) the maximum voltage unbalance of the system using the proposed management scheme during a Summer day 81

5.14 Total generated power from the 286 PV DG units during a Summer day . . 82

Nomenclature

α	Load model parameter (0 for constant power, 1 for constant current, and 2 for constant impedance)
β	Unconditional DG component, %
$\Delta\theta$	Change in voltage angle, p.u.
ΔP	Active power mismatch, p.u.
ΔQ	Reactive power mismatch, p.u.
ΔV	Bus voltage drop vector, p.u.
Δv	Change in voltage magnitude, p.u.
δ	Voltage phase angle, degree
ϵ	Tolerance value for load flow solution, p.u.
η	Overall efficiency of the DG PV inverter, %
a_{ij}	Bus incidence matrix element of row i and column j
B	Set of buses
B_r	Set of buses in the zone of interest
B_{3ph}	Set of 3-phase buses
$B_{r_{3ph}}$	Set of 3-phase buses in the zone of interest
$BCBV$	Branch-current to bus-voltage matrix

BI	Bus incidence matrix
$BIBC$	Bus-injection to branch-current matrix
C_t	Project net cash flow of the period t, \$
DG	Set of DG units
dg	DG unit index
DG_r	Set of DG units with conditional components in the interest-zone
DT	Set of distribution transformers
dt	Distribution transformer index
f	Index of lateral feeders
G	Solar irradiance, W/m^2
I	Line current, p.u.
i	Bus index
I_{br}	Branch current vector, p.u.
I_{bus}	Bus-injection current vector, p.u.
I_{mp}	PV panel current at maximum power, p.u.
I^0_{mp}	Value of I_{mp} at standard test conditions ($G = 1000$ W/m^2 and $T = 25$°C), p.u.
IRR	Internal rate of return, %
J	Jacobian matrix
k	Iteration index
L	Set of lines
l	Line index
L_r	Set of lines in the zone of interest

$LIC_{I_{mp}}$	Light intensity coefficient of I_{mp}
$LIC_{V_{mp}}$	Light intensity coefficient of V_{mp}
$MARR$	Minimum attractive rate of return, %
N	Project lifetime, years
N_p	Number of parallel PV modules
N_s	Number of series PV modules
n_x	Number of buses of the lateral feeder f including its sublaterals
$N_{DG_{dt_{min}}}$	Minimum number of DG units per distribution transformer dt
$N_{DG_{dt}}$	Number of DG units to be connected to distribution transformer dt
$P_{cur_{dg}}$	Curtailed active power of DG unit dg, p.u.
$P_{DG_{cap}}$	DG capacity, p.u.
P_{dg}	Output active power of DG unit dg, p.u.
$P_{load_{f_x}}$	Total active power load connected to phase x of the lateral feeder f, p.u.
$P_{load_{s_x}}$	Active power load connected to phase x of the feeder section s, p.u.
$P_{loss_{f_x}}$	Reactive power loss of phase x of the lateral feeder f, p.u.
$P_{loss_{s_x}}$	Active power loss of phase x of the feeder section s, p.u.
$P_{permitted_{dg}}$	Permitted output power for DG unit dg, p.u.
P_{rev-l_x}	Active reverse power flow of phase x of line l, p.u.
$P_{rev-l_{x_{max}}}$	Maximum allowable active reverse power flow of phase x of line l, p.u.
PC	Physical connection matrix
PW	Present worth value, $
$Q_{load_{f_x}}$	Total Reactive power load connected to phase x of the lateral feeder f, p.u.

$Q_{load_{s_x}}$	Reactive power load connected to phase x of the feeder section s, p.u.
$Q_{loss_{f_x}}$	Reactive power loss of phase x of the lateral feeder f, p.u.
$Q_{loss_{s_x}}$	Reactive power loss of phase x of the feeder section s, p.u.
$R_{base_{f_x}}$	Equivalent base resistance for phase x of the lateral feeder f, p.u.
R_{s_x}	Resistance of phase x of the feeder section s, p.u.
s	Index of feeder sections fed by the lateral feeder f
S_0	Load apparent power consumed at rated voltage, p.u.
$S_{cap_{dt}}$	Capacity of distribution transformer dt, p.u.
S_{f_x}	Equivalent load of the lateral feeder f including its sublaterals, p.u.
$S_{min_{dt}}$	Minimum load of distribution transformer dt, p.u.
T	PV cell temperature, °C
$TC_{I_{mp}}$	Temperature coefficient of I_{mp}
$TC_{V_{mp}}$	Temperature coefficient of V_{mp}
UB_i	Voltage unbalance index of bus i
UB_{max}	Maximum allowable voltage unbalance index
V	Bus voltage, p.u.
V_0	Load rated voltage, p.u.
V_{f_x}	Voltage of phase x of the connection bus of the lateral feeder f, p.u.
V_{i_x}	Voltage of phase x at bus i, p.u.
$V_{i_{avg}}$	Average voltage at bus i, p.u.
V_{max}	Maximum allowable system voltage, p.u.
V_{min}	Minimum allowable system voltage, p.u.
V_{mp}	PV panel voltage at maximum power, p.u.

V_{mp}^{0}	Value of V_{mp} at standard test conditions ($G = 1000\ \mathrm{W/m^2}$ and $T = 25°\mathrm{C}$), p.u.
V_{s_x}	Voltage of phase x of the connection bus of the feeder section s, p.u.
x	Phase index, $x \in \{a, b, c\}$
$X_{base_{f_x}}$	Equivalent base reactance for phase x of the lateral feeder f, p.u.
X_{s_x}	Reactance of phase x of the feeder section s, p.u.
Z_{line}	Line impedance, p.u.

Chapter 1

Introduction

1.1 General

In recent years, there has been a growing interest in increasing renewable energy distributed generation (DG) sources due to the increased environmental concerns, energy demand, and depletion of fossil energy resources. This interest is reflected in the growing trend toward introducing incentive feed-in tariff (FIT) programs to promote the installation of renewable DG sources in distribution systems. Promoting and facilitating renewable generation through FIT programs is a key step towards smart grids.

A FIT is a policy mechanism for accelerating renewable energy investments [1]. FIT programs provide long-term purchase agreements (10-25 years) for renewable energy producers. A FIT purchase agreement offers a per-kWh price for the produced renewable energy. This price is determined by the project size and the cost of generation of each technology [2–5]. A FIT policy has three main components [1]: a guaranteed DG connection to the grid, a fixed long-term purchase agreement, and a per-kWh price based on the cost of generation.

Implementing FIT programs faces many challenges. Typically, current distribution networks are not designed to accommodate high penetration levels of renewable DG sources. The adverse effects of installing renewable DG sources on distribution systems include overvoltage, reverse power flow, and system unbalance problems [6–8]. Therefore, the connection of DG sources under FIT programs must comply with a set of technical interconnection requirements (TIR). The TIR include constraints on the impact of connecting a DG source on the system operation such as operating voltage range, system protection

scheme, system unbalance, and equipment overloading. The TIR are set to ensure safe penetration of the DG source while maintaining efficient and reliable system operation. A connection impact assessment (CIA) study for DG connection is required prior to connecting a DG source under FIT rules to ensure the DG source satisfy all the TIR constraints. The IEEE Std 1547 series provides standards for interconnecting DG sources with electric power systems. The main guidelines for conducting impact studies for DG interconnection are given in the IEEE Std 1547.7-2003 [9].

1.2 Motivation

The Ontario Power Authority (OPA) has developed a FIT program for the province of Ontario [10]. This program supports a variety of renewable energy technologies including wind, photovoltaic (PV), waterpower, biomass, biogas, and landfill gas. The DG capacity in this program should be greater than 10 kW for single-phase DG or greater than 30 kW for three-phase DG. The OPA has also developed a micro feed-in tariff program (microFIT) that enables the installation of small-scale renewable energy DG sources [11]. The microFIT program enables homeowners and other eligible participants to install a small or "micro" renewable energy generation project (single-phase DG less than 10 kW or three-phase DG less than 30 kW) on their property. The connection of DG sources under the FIT and microFIT programs must comply the TIR given in [12] and [13], respectively. The TIR have been developed in accordance with Ontario and Canadian regulations and international standards.

The FIT and the microFIT programs are different in terms of their TIR. A CIA is required for connecting a DG project under the FIT program. On the other hand, no CIA is required for DG projects under the microFIT program. Conducting CIA studies for each microFIT application is infeasible due to the large number of applications, which can result in delaying the connection process. Alternatively, one of the microFIT TIR constraints explicitly restrict the aggregated interconnected generation to a small fraction (7 %) of the annual system peak load.

Imposing strict limits on the total interconnected microFIT generation ensures insignificant effect of the DG connection on the system operation, hence avoiding any possible violations to the system operational constraints. These limits therefore alleviates the need for detailed CIA studies of the impact of DG connections. However, such strict limits also result in the rejection of significant renewable DG capacity available for installation in distribution systems. The latest 2013 microFIT biweekly report shows that the unsuccessful microFIT applications represent 42.6 % of the total DG capacity submitted for version

3.0 of the microFIT program [14]. This deficiency contributed to the failure to achieve the 30 MW procurement target of version 3.0 of the microFIT program in 2013. Only 14.65 MW were considered applicable to the 30 MW procurement target by the end of 2013 [15].

The high rejection rates of the microFIT program have highlighted the need for developing a new approach for small-scale renewable DG planning and operation. This can be achieved by the application of DG power curtailment in the microFIT program. DG power curtailment is very appropriate to the situation that, when installing a DG project, only several days have violation issues to the TIR constraints during one year time long. The application of DG power curtailment can therefore allow small-scale renewable generation to access capacity not currently available under the microFIT regulations. DG power curtailment is also advantageous in the case of inverter-based generating technology, which is currently used with all renewable energy technologies. This is because implementing power curtailment requires minor modifications in the inverter controller [16].

There is a strong trend toward using power curtailment as a means to increase renewable energy penetration in distribution systems [17]. However, implementing power curtailment as an alternative to conducting detailed CIA studies prior to the small-scale DG installation still faces several challenges:

1. Typically, applying a DG power curtailment technique results in revenue loss for DG owners. The power curtailment techniques presented in the literature provide effective solutions for limiting the overvoltage problems caused by renewable DG integration [16, 18–23]. However, these techniques are unsuitable for implementation under FIT programs. These curtailment techniques cannot guarantee an adequate rate of return on investment for DG owners. To address this deficiency, a full examination of the power curtailment technique must include consideration of economic as well as technical factors.

2. There is a lack of a planning model for increasing DG capacity while a curtailment method is in place. The current DG planning practice under FIT programs is based on a worst-case scenario, such as considering minimum loading with maximum DG output. This approach, however, falls short in manifesting the effect of implementing power curtailment on the DG capacity assessment.

3. DG power curtailment is implemented to preserve the system within its operating constrains. Achieving this objective depends on the availability of up-to-date DLF results that reflect the actual load flow conditions of the systems. Providing fast

and accurate DLF results is necessary to identify any violations in the system operating constraints, such as overvoltage and reverse power flow. However, current DLF techniques are unsuitable for online interaction with continual changes in loads, renewable DG sources, and network topology. Addressing this problem is of a particular importance especially in the context of smart grid.

4. The majority of power curtailment methods presented in the literature focus only on one aspect: the overvoltage problem [16, 18–21]. However, this approach overlooks the need for considering other problems that can also be solved by curtailment, such as voltage unbalance and reverse power flow. DG sources connected under microFIT programs are single phase. Increasing the installed DG capacity in microFIT programs can therefore significantly increase reverse power and voltage unbalance. Solving these problems in addition to the overvoltage problem using power curtailment can allow for installing higher DG capacity in distribution systems.

1.3 Research Objectives

The primary goal of the research presented in this thesis is to enable accommodating high penetration of renewable energy generation in distribution systems. In order to accomplish this goal, this thesis suggests new directions for increasing small-scale renewable DG projects under FIT programs. Accordingly, the objectives of the research presented in this thesis are outlined as follows:

1. The development of an economic model for calculating the component of the DG output power that is not susceptible to curtailment for small-scale renewable DG sources.

2. The development of a techno-economic planning model for increasing DG capacity in distribution systems.

3. The development of a fast and accurate DLF algorithm for large distribution systems with continual changes of loads and network topology.

4. The development of a management scheme to control DG power curtailment based on an online assessment of DG connection.

1.4 Thesis Outline

The remainder of this thesis is organized as follows:

Chapter 2 presents the necessary background and a literature survey pertaining to the technical assessment of small-scale DG projects, potential solutions for increasing renewable DG penetration, and DLF analysis.

Chapter 3 introduces a techno-economic planning model for increasing the capacity of small-scale renewable DG sources that can be installed in distribution systems. This planning model is called techno-economic since it is based on both an economic and technical assessment of the DG projects. The "unconditional" DG component, which is not susceptible to curtailment, is first calculated based on an economic evaluation model. Then, the number of DG units to be installed in the system is maximized considering technical and economic constraints. This techno-economic planning model represents the main framework on which the proposed online assessment management scheme, presented in Chapter 5, is based.

Chapter 4 presents a novel "zooming" algorithm for DLF analysis for systems with flexible network topologies. The proposed DLF algorithm is utilized in the management scheme for DG connection online assessment, presented in Chapter 5, since it offers two exceptional features. First, the proposed DLF algorithm enables solving distribution systems with continual changes in network topology. Second, the algorithm can significantly reduce the DLF solution time by solving the DLF problem in a specific area of interest in the distribution system without necessitating the inclusion of all of the system buses.

Chapter 5 presents a management scheme for the online assessment of DG connection. The management scheme is based the output of the techno-economic planning model, presented in Chapter 3. This scheme utilizes the smart grid communication and metering infrastructure to manage the curtailment of the "conditional" DG components, that are subject to curtailment. The management scheme is implemented based on a novel scalable optimization model to minimizes the DG curtailment based on the system online conditions. The scalable optimization model utilizes the DLF proposed in Chapter 4.

Chapter 6 presents the thesis conclusions, contributions, and directions for future work.

Chapter 2

Background and Literature Survey

2.1 Introduction

In Chapter 1, the research motivations and objectives have been discussed. This chapter presents the necessary background and a literature survey pertaining to increasing the penetration level of small-scale DG sources in distribution systems. This chapter includes two main parts. In the first part, Section 2.2 presents an overview of the technical interconnection requirements (TIR) of the microFIT program, and Section 2.3 introduces a review of the potential solutions introduced in the literature for increasing renewable DG interconnection in distribution systems. In the second part, Section 2.4 and Section 2.5 include a review on DLF techniques and distribution systems modeling for DLF analysis, respectively.

2.2 Technical Interconnection Requirements (TIR) for microFIT DG Projects

As discussed earlier in Chapter 1, DG sources under the microFIT program must comply with a set of technical interconnection requirements (TIR). The TIR include constraints on the impact of connecting a DG source on the system operation. The TIR are set to avoid the adverse effects of installing renewable DG sources on distribution systems. In the case of small-scale renewable DG sources, these adverse effects typically include overvoltage, reverse power flow, and system unbalance problems [6–8]. The following is a summary of the microFIT TIR constraints that affect the amount of DG installed capacity [13]:

1. The DG capacity must be less than the capacity of the existing electrical service.
2. The DG must have an operating voltage range compatible with the standard voltage range.
3. The voltage rise caused by the total installed DG capacity must not exceed the operating voltage by more than 1 %. The CSA CAN3-C235 standard [24] provides the recommended service voltage variation limits for systems up to 50 kV.
4. For distribution transformers rated 50 kVA or higher, the total connected DG capacity must be limited to the distribution transformer rating.
5. For distribution transformers rated less than 50 kVA, the total connected DG capacity must be limited to 50 % of the distribution transformer rating.
6. The total connected DG capacity must not cause a protective device to exceed 100 % of its short circuit capacity.
7. Connecting a DG source must not cause the voltage unbalance to exceed 2 %.
8. The total connected DG capacity must not exceed 7 % of the total annual system load.

Aside from the last constraint, all the aforementioned constraints limit the DG capacity based on technical system parameters, such as overvoltage or equipment capacity limits. On the other hand, the DG capacity limit imposed by the last constraint is not based on a technical system parameter. As discussed earlier in Chapter 1, the goal of this constraint is to avoid conducting CIA studies for each microFIT DG application. This constraint represents a very conservative limit on renewable DG capacity. This conservative limit ensures the compliance of the DG project to all the other microFIT constraints.

As a result of this practice, 42.6 % of the microFIT applications were rejected in version 3.0 of the microFIT program in 2013 [15]. The rejected applications are equivalent to 10747.6 kW of renewable energy [15]. Several potential solutions are presented in the literature for increasing the interconnection of renewable energy DG in distribution systems. These solutions are discussed in the next section.

2.3 Potential Solutions for Increasing the Interconnection of Renewable Energy DG in Distribution Systems

Previous studies have reported a number of potential solutions for increasing the interconnection of renewable energy DG in distribution systems [16, 25, 26]. These solutions focus on solving the most two adverse impacts of installing DG sources in distributions systems: overvoltage and reverse power flow [27]. The potential solutions are listed in the following subsections:

2.3.1 Reduction of Distribution Transformer Secondary Voltage

In this method, distribution transformer secondary voltage is reduced by setting the transformer tap [25]. This method is impractical in case of high DG penetration. The tap setting has to be changed frequently due to the randomness of load and DG output [19, 21].

2.3.2 Application of Voltage Regulating Devices

Voltage regulating devices can mitigate overvoltage problems in systems with high DG penetration. In [28], a coordinated control strategy for on-load tap changers and storage devices is presented for reducing overvoltage in low-voltage networks with high PV penetration. The objective of the presented control strategy is to reduce the system losses and relieve the tap changer transformer operation stress. However, the authors in [18, 23] questioned the suitability of using voltage regulating devices in presence of high renewable DG penetration. The intermittency of the renewable DG output can cause frequent tap operations [23].

2.3.3 Network Upgrading

Increasing conductor size results in reducing the line impedance [25] hence reducing the voltage drop/rise. The effect of the line impedance on the overvoltage problem in systems with high DG penetration is discussed in [6]. Network upgrading is considered the most straightforward method for reducing the overvoltage caused by high connected DG capacity. However, this method is expensive especially in the case of underground lines [16].

2.3.4 Application of Energy Storage Devices

Energy storage devices provide a very effective way for accommodating the intermittency of renewable energy DG sources [29]. Storage systems can store the surplus DG generated power hence preventing reverse power flow and overvoltage. The stored power can be used to supply the loads at the system peak. The work in [27] presents the application of energy storage devices in low-voltage systems with high photovoltaic (PV) penetration. In [30], several local voltage control strategies are presented for improving the PV grid integration.

Given the technical advantages for using energy storage devices with renewable DG sources, a primary concern of energy storage devices is, however, their low cost benefit ratio [16, 23].

2.3.5 Reactive Power Compensation

Reactive power compensation is one of the approaches for overvoltage mitigation. Inverter-based DG sources can be controlled to absorb reactive power, hence reducing the overvoltage [25, 26]. Typically, the R/X ratio is high in distribution systems. Consequently, the effect of reactive power compensation is limited [22, 23, 26]. Therefore, the reactive power compensation method is always implemented along with active power curtailment in the literature [19, 20, 22, 23, 26].

The main advantage of this approach is that it utilizes the inverter capacity without adding extra investments [23]. However, this approach can lead to higher current flow, hence increasing power losses [27]. Also, this approach may require increasing the inverter capacity [16]. Another limitation of this approach is that, according to the IEEE Std 1547-2003 [31], DG sources cannot actively regulate the system voltage.

2.3.6 DG Active Power Curtailment

DG power curtailment is one of the most effective options for avoiding overvoltage caused by increasing DG capacity [16, 32]. This method is very appropriate for accommodating high DG penetration. Typically when installing a DG project, only several days have violation issues with system operational constraints during one year time long. The application of DG power curtailment can therefore allow DG sources to access capacity not currently available under the FIT regulations.

Recently, researchers have shown an increased interest in applying DG power curtailment in distribution systems. The developed methods for DG power curtailment fall in

two categories. In the first category, the curtailed power is determined using a droop-based scheme. In the second category, the curtailed power is determined based on an optimization model. The two categories are discussed in the following paragraphs.

In the first category, the curtailed DG power is determined using droop-control [16, 19, 21]. This method is first proposed in [16]. According to this method, DG power is curtailed linearly with the DG voltage rise. A droop coefficient is used for calculating the curtailed power. Using this method, however, results in unfair sharing of the curtailed power among DG sources. DG units closer to the distribution transformer will have less curtailed power than downstream DG sources. Accordingly, to address this deficiency, the work in [16] also presents a different method for calculating the curtailed power. This method, alternatively allows for equal curtailed power sharing. It employs a voltage sensitivity matrix to calculate the curtailed power. This method, however, requires full information for calculating the sensitivity matrix. In order to avoid this, the authors in [21] proposed a Thevenin equivalent-based control method. This method is implemented online to find dynamic Thevenin equivalent circuits at the DG connection points. This equivalent circuit is then used for calculating the curtailed power. Another development for the droop-based curtailment method is presented in [19] that considers reactive power compensation besides active power curtailment.

In the second category, the curtailed DG power is determined using an optimization model [22, 23]. The optimization model presented in [22] is based on an optimal power flow (OPF) formulation. The objective of this optimization model is to minimize the curtailed power. It also includes reactive power compensation; the reactive power is included in the objective function using a penalty factor. This method includes a constraint for sharing the curtailed power among DG units with the same percentage of their capacities. In [23], a multi-objective optimization model is presented. The objectives include minimizing network losses, voltage rise/drop, voltage unbalance, DG generation cost, and DG curtailment cost.

Despite this review shows a wide body of literature that has been carried out on developing DG power curtailment methods, the previous work falls short in two main issues:

1. The power curtailment techniques presented in the literature provided effective solutions for limiting the overvoltage problems caused by renewable DG integration. The main limitation of the implementation of these techniques under FIT programs, however, is that they overlook the importance of ensuring an adequate profit for DG investors. This point is of a particular importance in the case of implementing power curtailment under FIT programs. Many researchers have discussed the importance

of developing fair participation of the curtailed power. However, they provide no maximum limit for the curtailed power. This approach offers no guarantee for an adequate profit for DG investors.

2. All the methods presented in the literature focus on the operation and control of DG power curtailment. However, there is a lack of research on developing a planning model to calculate the DG capacity while a curtailment method is in place. This problem has been realized in [32]. The work presented in [32] proposed assigning a curtailment factor for each DG unit in the planning model. However, the calculation criteria of these curtailment factors is not discussed.

2.4 Distribution Load Flow (DLF) Analysis

Integrating renewable energy in distribution systems on a large scale depends on the availability of fast and accurate DLF solutions. The information provided by DLF analysis are utilized to assess the effect of renewable DG sources on the distribution system operation. The information provided by DLF analysis include the voltage magnitude and angle at each bus, the line flow in each line, the power loss in each line, the load active and reactive powers considering the load model, and the total system input active and reactive powers [33].

In a smart grid, the information provided by DLF analysis are employed by the control systems for monitoring and controlling the distribution system components. However, existing DLF analysis entails numerous challenges. First, system power flow conditions can change quickly because of the high penetration level of renewable distributed generation (DG) sources, such as wind and photovoltaic (PV). Second, the system topology also changes continually due to the self-healing capabilities and grid reconfiguration applications that are features of smart grids [34]. Third, a distribution system and its inherent imbalance significantly increase both the size of the DLF problem and the associated calculation burden [35]. Improper handling of these issues can increase the time required to produce the DLF solution and decrease the update rate of the DLF solution. If the update rate is slower than the system changes or the speed of the control systems, the control systems will be acting on outdated DLF results and will consequently be unable to function effectively.

The literature contains reports of numerous DLF techniques that have been developed as a means of addressing these challenges [36]. Recently developed DLF techniques fall into two categories. The first category is based on the implementation of the Newton-Raphson

(NR) method. The second category is based on the forward/backward (F/B) method. The details of each category are explained in the next two subsections.

2.4.1 Newton Raphson (NR) Method

The NR method is one of the most popular load flow methods. It is based on representing the load flow problem by a Taylor Series and ignoring the higher order terms [37]. The standard NR load flow method is given by

$$\begin{bmatrix}\Delta P\\ \Delta Q\end{bmatrix} = \begin{bmatrix}\frac{\partial P}{\partial \theta} & \frac{\partial P}{\partial v}\\ \frac{\partial Q}{\partial \theta} & \frac{\partial Q}{\partial v}\end{bmatrix} \begin{bmatrix}\Delta \theta\\ \Delta v\end{bmatrix} = [J] \begin{bmatrix}\Delta \theta\\ \Delta v\end{bmatrix} \tag{2.1}$$

where ΔP and ΔQ are the active and reactive power mismatches, respectively, and Δv and $\Delta \theta$ are the change in the voltage magnitude and angle, respectively. $[J]$, the Jacobian matrix, is a the matrix of partial derivatives.

The NR method is considered as a preferred technique for power flow analysis in transmission systems [38]. This is mainly due to its quadratic convergence characteristics [39], and its ability of solving highly meshed networks [40].

Although the advantages of applying the NR for solving transmission systems, the application of the NR method in distribution systems has two main limitations. First, the NR method has poor convergence characteristics in the case of distribution systems due to the high R/X ratio [38,41]. Second, distribution systems typically includes a large number of buses (with up to thousands of buses). The heavy computational burden of the NR method can therefore affect the DLF solution speed for distribution systems.

Despite the limitations of applying the standard NR method in distribution systems, some research has been carried out to develop the NR method for distribution systems using the sequence-component frame. This is because, compared to the standard NR method, using the sequence-component frame enables reducing the problem size and the computational burden as discussed in [35,42–44]. This approach was first presented in [42] by decomposing the DLF problem into three sub-problems in the three sequence networks. The positive sequence sub-problem is solved using the NR method. The negative and zero sequence sub-problems are formulated as two sets of linear simultaneous equations. The method presented in [42] assumed weak mutuality between the sub-problems. The mutuality was considered by including the three sub-problems into an iterative scheme.

This method was developed in [43] to include a decoupled sequence component model for transmission line.

The NR method with sequence-component frame is further developed in [44] by including models of electronically-coupled DG are included in the DLF problem. The method presented in [44] also tried to include single-phase laterals in the DLF problem. This is achieved by first separating the system into a three-phase part and single-phase laterals. Each single-phase lateral is then represented in the three-phase part by an equivalent single-phase load, whose value is calculated using a coincidence factor. This approach solves the DLF problem in the three-phase part with the use of the NR method in the sequence-component frame, and the DLF of each single-phase lateral is then solved using the forward/backward (F/B) method. Solving the DLF separately in the three-phase part and in the single-phase laterals fails to take into account the impracticality of a complete decoupling of the three-phase and single-phase sections in distribution systems. Another limitation of this approach is that the sequence admittance matrices must be updated for any change in the topology of the distribution system. The construction and factorization time required for updating the sequence admittance matrices can effectively increase the DLF solution time. This can affect the ability of this method to interact with changes of loads and/or network topology in smart grids.

2.4.2 Forward/Backward (F/B) Method

The second category of DLF techniques is the forward/backward (F/B) method. It is based on the ladder network theory, which was first applied in DLF by Kersting and Mendive in [45,46]. The F/B method is based on two simple steps, the backward sweep, in which the branch line currents, or powers, are calculated using Kirchhoff's current law (KCL) from the far ends of the system to the source node, and the forward sweep, where the source node voltage and the calculated branch currents are used to calculate the node voltages using Kirchhoff's voltage law (KVL). This iterative process is repeated until a convergence criterion is satisfied. Figure 2.1 shows the flowchart of the F/B method.

Figure 2.2 shows a line section in a ladder network. The KVL and KCL equations for the forward sweep and backward sweep of this portion are shown below in (2.2) and (2.3) respectively.

$$V_2 = V_1 - Z_{12} I_{12} \tag{2.2}$$

$$I_{12} = I_{load_2} + I_{23} \tag{2.3}$$

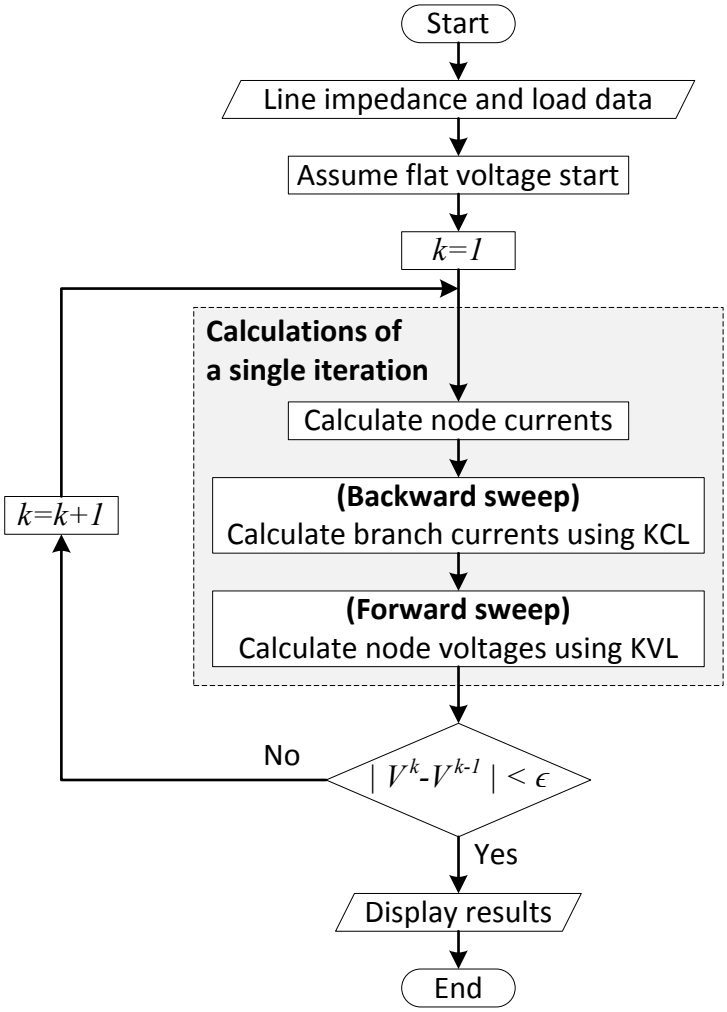

Figure 2.1: Flow chart of the forward/backward DLF method

where V_1 and V_2 are the voltages of nodes 1 and 2 respectively, I_{12} and I_{23} are the branch currents of the lines connecting nodes 1-2 and 2-3 respectively. Z_{12} is the impedance of the line connecting nodes 1-2, and I_{load_2} is the drawn current of the loads connected at node 2. Modeling line impedances and load currents is presented in Section 2.5.1 and Section 2.5.2.

The F/B method is characterized by its fast and robust performance in addition to simple calculation steps. In addition, the F/B method is suitable for distribution system characteristics such as radial topology; unbalanced loading and line configuration; and high R/X ratio [33, 47]. The F/B method also enables the DLF problem to be solved

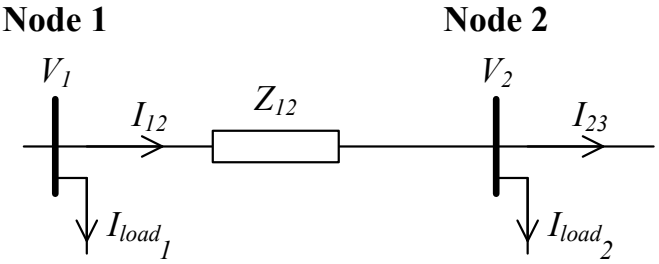

Figure 2.2: Line section in a ladder network

for the whole distribution system including the single-phase sections efficiently, unlike the NR-based DLF methods.

The F/B method has been extensively developed in the literature [36,47,48]. In [41,49], a matrix formulation of the F/B method was presented as a way to improve the performance of the F/B method in large distribution systems. In [49], a matrix formulation of the F/B method was presented and shown to be advantageous in terms of DLF solution time. The presented method depends on two matrices: the bus-injection to branch-current ($BIBC$) matrix and the branch-current to bus-voltage ($BCBV$) matrix. The $BIBC$ matrix describes the relationship between the bus current injections and the branch currents; this matrix is constructed by applying KCL in the distribution network. The branch currents $[I_{br}]$ can be written as a function of the bus-injection currents $[I_{bus}]$ as follows:

$$[I_{br}] = [BIBC]\ [I_{bus}] \tag{2.4}$$

The $BCBV$ matrix is constructed by applying KVL in the distribution system. This matrix relates the branch currents $[I_{br}]$ to the bus voltage drops $[\Delta V]$ as follows:

$$[\Delta V] = [BCBV]\ [I_{br}] \tag{2.5}$$

Substituting (2.4) into (2.5), the bus voltage drops can be given by

$$[\Delta V] = [BCBV][BIBC]\ [I_{bus}] \tag{2.6}$$

The bus voltage drops can then be calculated by solving (2.6) iteratively until convergence is reached.

The $BIBC$ and $BCBV$ are constant matrices that depend on distribution system topology. Any change in distribution system topology requires reconstructing both matrices. However, the building algorithm given in [49] of the $BIBC$ and the $BCBV$ matrices

is non-automated, which means that any changes to the network topology must be analyzed offline: a substantial barrier to the implementation of this method in a smart grid environment.

Another F/B matrix formulation, presented in [41], included an automated building algorithm of the F/B matrix formulation that involves a matrix inversion operation. Implementing such a building algorithm for online applications could be computationally expensive for large distribution systems, especially if network topology changes are taken into consideration.

Despite the large body of literature on the F/B method [36,47,48], all the previous work fall short in terms of the implementation of the F/B method in a smart grid environment. This is due to the following factors:

1. A major drawback of the F/B method as introduced in the literature is the need for the system nodes and/or branches to be numbered as in [41, 50–59]. Numbering schemes are used as a means of representing the connection between the system nodes, and hence, the correct order of the F/B calculations. However, solving the DLF problem by assigning numbering schemes to the system buses and/or branches reduces the flexibility of the DLF method and thus affects its ability to accommodate changes in topology of the distribution system.

2. Another problem with the F/B methods introduced in the literature is that the DLF solution time is affected by the number of system buses. The effect of the system size on the DLF solution time could thus become significant for the solution of real distribution systems with up to thousands of buses. Providing DLF results in a timely manner is of a particular importance to ensure proper operation of smart grid control systems.

2.5 Distribution System Modeling for DLF Analysis

This section discusses the modeling of distribution system lines, loads, and DG sources in distribution systems. The presented models are in accordance to the IEEE Std 1547 series bundle for interconnecting distributed resources with electric power systems. These models are employed in the proposed DLF algorithm, presented in Chapter 4.

2.5.1 Line Modeling

Distribution systems include three-phase, untransposed lines in addition to double-phase and single-phase lines. Figure 2.3 shows a section of a three-phase four-wire line with a grounded neutral. The primitive impedance matrix of this line is expressed by a 4×4 matrix [33,60]. The Kron's reduction method can be applied to reduce the phase impedance matrix of the line to a 3×3 matrix while considering the effect of the grounded neutral wire [33, 60]. The reduced phase impedance matrix of the line can be expressed as

$$Z_{line} = \begin{bmatrix} Z_{aa} & Z_{ab} & Z_{ac} \\ Z_{ba} & Z_{bb} & Z_{bc} \\ Z_{ca} & Z_{cb} & Z_{cc} \end{bmatrix} \tag{2.7}$$

where the diagonal elements represent the self-impedances of the line and the off-diagonal elements represent the mutual-impedances of the line. In the case of single-phase and double-phase line configurations, values of missing phases are replaced by zero entries.

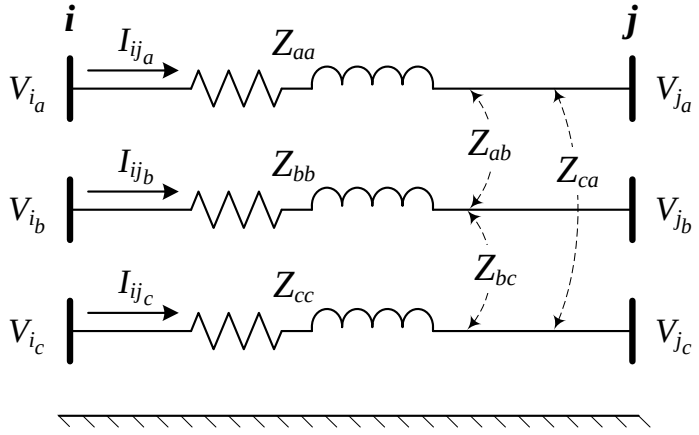

Figure 2.3: Three-phase line model

The relation between the three-phase voltages of buses i and j and three-phase feeder currents for the line section shown in Figure 2.3 is given by

$$\begin{bmatrix} V_{i_a} \\ V_{i_b} \\ V_{i_c} \end{bmatrix} = \begin{bmatrix} V_{j_a} \\ V_{j_b} \\ V_{j_c} \end{bmatrix} - \begin{bmatrix} Z_{aa} & Z_{ab} & Z_{ac} \\ Z_{ba} & Z_{bb} & Z_{bc} \\ Z_{ca} & Z_{cb} & Z_{cc} \end{bmatrix} \begin{bmatrix} I_{ij_a} \\ I_{ij_b} \\ I_{ij_c} \end{bmatrix} \tag{2.8}$$

2.5.2 Load Modeling

In accordance with the IEEE Std 1547.7-2013 for conducting impact studies for DG source interconnection [9], different types of loads models can be considered in the DG connection impact analysis. These types include constant power, constant current, and constant impedance load models. These models can be mathematically represented as given in [61] by the following relation:

$$S = S_0 \left(\frac{V}{V_0} \right)^{\alpha} \tag{2.9}$$

where S_0 is the load power consumed at the rated voltage, V_0 is the load rated voltage, and V is the bus voltage. The value of the parameter α determines the load model (0 for constant power, 1 for constant current, and 2 for constant impedance).

A distribution system can also include more than one load type connected at the same bus. In this case, the load is modeled as a polynomial load. The polynomial load is the summation of the constant power, constant current, and constant impedance loads.

2.5.3 DG Modeling

The IEEE Std 1547.7-2013 provides guidelines for conducting impact studies for DG source interconnection [9]. According to this standard, DG sources can be modeled for load flow analysis using one of the following models:

1. A fixed real and reactive power source.
2. A fixed real power source with a fixed power factor.
3. A fixed real power source with bus voltage control (with limits on reactive power output).
4. A swing generator in a stand-alone power system, including control of bus voltage, frequency, and phase angle (with limits on reactive power output).

The first and second models are equivalent to DG sources modeled as PQ buses. The third model is equivalent to DG sources modeled as PV buses. The fourth model is suitable for modeling DG sources in microgrids and islanded power systems.

In this research, only the first and second models are considered for modeling DG sources for connection impact assessment studies. The third and fourth model are not considered due to the following:

1. In accordance with the IEEE Std 1547-2003, for interconnecting DG sources with electric power systems [31], DG sources are not permitted to actively regulate the voltage at the point of common coupling. This rule prevents any possible opposition between the DG voltage regulation controller and the regulation equipment installed in the distribution system.

2. According the IEEE Std 1547.6-2011 for interconnecting DG sources with secondary distribution networks [62], DG sources are not allowed to cause an islanding condition. This rule is to avoid the adverse impacts caused by DG islanding such as abnormal voltage and frequency values and interference with the restoration process of the utility's normal supply [12].

2.6 Summary

This chapter presents a literature review on the technical requirements for installing small-scale renewable DG sources under the microFIT program. In addition, different potential solutions have been discussed for increasing renewable DG installed capacity in distribution systems. The review shows that DG power curtailment can provide an effective means of accommodating high renewable DG penetration in distribution systems. However, existing literature falls short in two critical dimensions. First, there is a need for considering the economic aspect of DG power curtailment in order to ensure adequate profit for DG investors. To fill this gap in the literature, Chapter 3 presents a techno-economic planning model. This model increases the installed renewable DG capacity and guarantees an adequate profit for DG investors when a curtailment method is in place. Second, there is a need for employing DG power curtailment for solving other problems, besides overvoltage, caused by increasing renewable DG capacity, such as voltage unbalance and reverse power flow. In order to address these problems, DG power curtailment should be based on fast and accurate DLF results. This chapter has therefore presented a critical review of DLF techniques. The review shows that there is a lack of a fast DLF technique with the ability to interact with continual changes in loads and network topology of smart grids. To fill this gap in the literature, Chapter 5 proposes a management scheme for DG connection online assessment. The proposed management scheme controls DG curtailment to mitigate overvoltage, voltage unbalance, and reverse power flow. The proposed management scheme is based on a novel "zooming" DLF algorithm that enables accommodating changes in network topology and loading. The zooming DLF algorithm is presented in Chapter 4.

Chapter 3

A Techno-Economic Planning Model for Increasing the Connectivity of Small-Scale Renewable DG in Distribution Systems

3.1 Introduction

This chapter presents a techno-economic planning model for increasing the capacity of small-scale renewable DG sources while a curtailment method is in place. The proposed techno-economic planning model represents the main framework on which the DG connection online assessment, presented in Chapter 5, is based. In this framework, the output power of each DG unit is divided into two components: unconditional and conditional. The unconditional DG component is not susceptible to curtailment. Conversely, the conditional DG component is subject to curtailment according to an online assessment of the DG connection in the distribution system.

The proposed planning model is called techno-economic since it includes two parts: an economic assessment and a technical assessment of the DG project. In the first part, the objective of the economic assessment is to calculate the unconditional and conditional components for renewable DG sources connected under FIT programs. An economic model is first presented to calculate the rate of return for DG projects. The calculated rate of return is then compared to a selected minimum attractive rate of return ($MARR$). The $MARR$ is defined as the minimum rate of return that is considered acceptable before

starting a project [63, 64]. If the rate of return of a DG project is less than or equal to the $MARR$, the output power of this DG project is not subject to curtailment. On the other hand, If the rate of return of a DG project is higher than the $MARR$, the output power of this DG project will be divided into two components: unconditional and conditional. The unconditional component is the portion of the DG output power that is not subject to curtailment; this component yields a rate of return equal to the $MARR$. Conversely, the conditional DG component is subject to curtailment based on the online condition of the system.

In the second part of the proposed planning model, the objective of the technical assessment is to increase the connectivity of renewable DG units with conditional/unconditional components in distribution systems. The technical assessment part is based on an optimization model to maximize the number of installed DG source in the system. An economic constraint is added to the optimization model; this constraint is based on the economic assessment of the DG project, conducted in the first part. The economic constraint is added for two purposes. First, a DG unit with a rate of return less than or equal to $MARR$ is granted permission to inject power into the system without curtailment for all online conditions of the distribution system. Second, the curtailment of a DG unit, with a rate of return higher than $MARR$, is limited to the value of it conditional component. Achieving these two purposes guarantees that the economic feasibility of a DG project is not affected when curtailment is in place.

This chapter is organized as follows. Section 3.2 presents an economic assessment model for renewable DG project for calculating the unconditional and conditional components. Section 3.3 introduces the techno-economic planning model for increasing the integration of renewable DG sources in distribution systems. The simulation results are presented Section 3.4. Finally, A summary is presented in Section 3.5.

3.2 Economic Assessment of Renewable DG Investments for Calculating the Unconditional and Conditional Components

The goal of the economic assessment of a DG project is to ensure that the anticipated economic benefits will surpass the associated costs. This section provides an economic model for evaluating renewable DG projects. The analysis presented in this section is employed for calculating the unconditional and conditional DG components.

The next subsections present the basics for decision making among a set of investment alternatives. The first subsection introduces the classification of investment alternatives into dependent and independent. The second subsection discusses the criteria of evaluating a set of mutually exclusive investment alternatives. The third subsection presents the basics of calculating after-tax cash flows for renewable DG projects. Finally, the fourth subsection presents the calculation of unconditional and conditional DG components.

3.2.1 Classification of Investment Alternatives

A set of investment alternatives can be classified as independent and dependent. Selecting the DG unit capacity from a set of candidate capacities depends on whether the candidate DG capacities form a set of independent investment alternatives or dependent investment alternatives.

In the first category, independent projects usually have unrelated purposes and natures. A set of projects is independent if, in the set, the acceptance of one project has no effect on the acceptance or rejection of other projects [63–66].

For the second category, a set of projects is dependent if, in the set, the acceptance of one project will affect the accept-reject decision of the other projects. Dependency relationships between projects have two types. The first one is the contingent relationship. A project is considered contingent if its acceptance depends on the acceptance of another project [63]. In other words, the acceptance of one project entails the acceptance of one or more other projects. The second type of dependency between projects is the mutual exclusive relationship. A set of projects is mutually exclusive if the acceptance of one project precludes the acceptance of other projects in the set [63–66]. An example is a set of projects that substitute each other in achieving a given purpose.

According to the guidelines of the microFIT program in Ontario, investors are prohibited from installing more than one DG project of the same renewable fuel on the same property [67, 68]. Therefore, based on the aforementioned classification, selecting a DG capacity to be installed in a given location from a set of DG candidate capacities is equivalent to selecting a project from a set of mutually exclusive investment alternatives. The next subsection discusses the criteria of evaluating a set of mutually exclusive investment alternatives.

3.2.2 Selecting the Best Project among Mutually Exclusive Investment Alternatives

The minimum attractive rate of return ($MARR$) or hurdle rate is used as a basis of comparing mutually exclusive investment alternatives [63,64]. As the name implies, the minimum attractive rate of return is defined as the minimum rate of return that is considered acceptable before starting a project [63, 64].

The $MARR$ is considered as a cut-off rate to screen the candidate investment alternatives. A project is considered profitable if its internal rate of return (IRR) is higher than the $MARR$. The IRR of a project is the rate of return that yields a zero present worth value of the cash flow of the project [63].

The value of the $MARR$ directly influences the accept-reject decision of a project. The improper selection of the $MARR$ can lead to wrong investment decisions. A very high $MARR$ can result in rejecting good investments, while a very low $MARR$ can result in accepting investments that are not economically viable.

To date, there has been little agreement on a reliable method for selecting the $MARR$ [63]. $MARR$ values in renewable DG projects depend on project size and type of technology applied. The $MARR$ values for different renewable DG projects given in [69] are used in the analysis presented in this thesis.

3.2.3 After-Tax Cash Flow for Renewable DG Projects

As discussed in the previous subsection, the evaluation of a set of mutually exclusive projects is achieved by comparing their internal rate of return (IRR) values with the selected $MARR$ value. As stated previously, the IRR of a project is the rate of return that yields a zero present worth value of the cash flow of the project [63]. The IRR is the rate of return that satisfies the following equation [63]:

$$0 = PW(IRR) = \sum_{t=0}^{N} \frac{C_t}{(1 + IRR)^t} \tag{3.1}$$

where PW is the present worth value of the project, N is the project lifetime, and C_t is the cash flow at the period t.

The IRR should be calculated using an after-tax cash flow. An after-tax cash flow is a measure of the ability of a project to generate positive cash flow after deducting taxes. The

after-tax cash flow considers the effect of income tax and depreciation in the investment evaluation process. The after-tax cash flow should cover the estimated lifetime of the project. Moreover, the effect of inflation should be considered in the investment evaluation process in order to calculate a real IRR that better represents what an investor will receive.

An after-tax cash flow is calculated for each project using the tabular calculation procedure presented in [63]. As an example to illustrate the after-tax cash flow analysis, the economic parameters of a renewable energy DG project are listed in Table 3.1. The after-tax cash flow of this DG project example is given in Table 3.2. The following paragraphs discuss the steps for calculating the after-tax cash flow using the tabular calculation procedure.

Table 3.1: Economic parameters of a renewable energy DG project

Parameter	Value
DG capacity	10 kW
DG capital cost	\$3 W^{-1}
DG investment lifetime	20 yr
PV DG Feed-in-tariff	\$0.4 kWh^{-1}
Feed-in-tariff escalation percentage	0 %
DG potential generated energy	1000 kWh kW^{-1} yr^{-1}
Fixed operation and maintenance cost	\$10 kW^{-1} yr^{-1}
Variable operation and maintenance cost	\$0 kWh^{-1} yr^{-1}
Depreciation rate	80 %
Income tax rate	30 %
Inflation rate	2 %

As shown in the cash flow presented in Table 3.2, the columns of the cash flow table are labelled from A to H. The cash flow is calculated for the project lifetime (20 years) as indicated by column A. In the cash flow, revenues and expenses of the cash flow are assigned positive and negative values, respectively. Column B presents the net annual income of the project, which is the before-tax cash flow. The first value of column B (at year 0) shows the capital cost of the project. The annual income for each year equals the revenue of the generated energy minus the operation and maintenance cost. The capital cost and the annual income of a DG project for the year y are calculated using (3.2) and (3.3), respectively, as follows:

Table 3.2: After-tax cash flow for the DG project example given in Table 3.1

End of year	Before-tax cash flow	Depreciation charges	Taxable income	Taxes	After-tax cash flow	Inflation index	After-tax cash flow with inflation
			B + C	*-0.3 × D*	*B + E*		*F / G*
A	*B*	*C*	*D*	*E*	*F*	*G*	*H*
0	-30000				-30000	1	-30000
1	3900.00	-24000.00	-20100.00	6030.00	9930.00	1.02	9735.29
2	3900.00	-4800.00	-900.00	270.00	4170.00	1.04	4008.07
3	3900.00	-960.00	2940.00	-882.00	3018.00	1.06	2843.93
4	3900.00	-192.00	3708.00	-1112.40	2787.60	1.08	2575.31
5	3900.00	-38.40	3861.60	-1158.48	2741.52	1.10	2483.08
6	3900.00	-7.68	3892.32	-1167.70	2732.30	1.13	2426.21
7	3900.00	-1.54	3898.46	-1169.54	2730.46	1.15	2377.03
8	3900.00	-0.31	3899.69	-1169.91	2730.09	1.17	2330.11
9	3900.00	-0.06	3899.94	-1169.98	2730.02	1.20	2284.36
10	3900.00	-0.01	3899.99	-1170.00	2730.00	1.22	2239.55
11	3900.00	0.00	3900.00	-1170.00	2730.00	1.24	2195.64
12	3900.00	0.00	3900.00	-1170.00	2730.00	1.27	2152.59
13	3900.00	0.00	3900.00	-1170.00	2730.00	1.29	2110.38
14	3900.00	0.00	3900.00	-1170.00	2730.00	1.32	2069.00
15	3900.00	0.00	3900.00	-1170.00	2730.00	1.35	2028.43
16	3900.00	0.00	3900.00	-1170.00	2730.00	1.37	1988.66
17	3900.00	0.00	3900.00	-1170.00	2730.00	1.40	1949.66
18	3900.00	0.00	3900.00	-1170.00	2730.00	1.43	1911.44
19	3900.00	0.00	3900.00	-1170.00	2730.00	1.46	1873.96
20	3900.00	0.00	3900.00	-1170.00	2730.00	1.49	1837.21

$$\text{capital cost} = \text{DG capacity} \times \text{DG capital cost per kW capacity} \tag{3.2}$$

$$\text{income}_y = \text{generated energy}_y \times \text{feed-in-tariff} \times (1+\text{feed-in-tariff escalation } \%)^y \tag{3.3}$$

Column C shows the depreciation charges; they are calculated using the declining basis method [63]. According to this method, the depreciation charges for the year y are

calculated by multiplying the depreciation rate by the book value of the project at the start of the year as follows:

$$\text{dep. charges}_y = \text{dep. rate} \times \left\{ \text{capital cost} - \sum_{0}^{y-1} \text{dep. charges}_y \right\} \tag{3.4}$$

The depreciation charges are used in calculating the taxable income displayed in Column D. The taxable income for the year y is calculated by adding the before-tax cash flow (column B) and the depreciation charges (column C) as in the following equation:

$$\text{taxable income}_y = \text{before-tax cash flow}_y - \text{dep charges}_y \tag{3.5}$$

The taxes for the year y are then calculated in column E by multiplying the taxable income (column D) by the income tax rate as in following equation:

$$\text{taxes}_y = \text{income tax rate}_y \times \text{taxable income}_y \tag{3.6}$$

The after-tax cash flow for the year y is calculated in column F by adding the before-tax cash flow (column B) and the taxes (column E) as in the following equation:

$$\text{after-tax cash flow}_y = \text{before-tax cash-flow}_y - \text{taxes}_y \tag{3.7}$$

The effect of the inflation rate on the after-tax cash flow is considered by calculating the inflation index in column G. The inflation index equals one at the start of the project. This index is multiplied each year by the inflation rate. The inflation adjusted after-tax cash flow for the year y is calculated in column H by dividing the after-tax cash flow (column F) by the inflation index (column G) as in the following equation:

$$\text{inflation-adjusted after-tax cash flow}_y = \frac{\text{after-tax cash-flow}_y}{(1 + \text{inflation index})^y} \tag{3.8}$$

Table 3.3 lists the calculated IRR for the three cash flows: before-tax (column B), after-tax (column F), and after-tax with inflation (column H). The IRR values are calculated for the three cash flows using 3.1. As shown in Table 3.3, the IRR equals 11.536 % before considering the effect of taxes and inflation. Considering the effect of taxes results in reducing the IRR value to 10.772 %. The IRR value further drops to 8.6 % by considering the effect of taxes and inflation. These results show that failure to consider the effect of

tax and inflation rates can lead to overrated IRR values, which can result in inaccurate investment evaluation. Therefore, the after-tax inflation-adjusted IRR is considered in calculating the unconditional and conditional DG components as illustrated in the next subsection.

Table 3.3: Calculated IRR values for the DG project example given in Table 3.1

Cash flow	IRR
Before-tax (column B)	11.536 %
After-tax (column F)	10.772 %
After-tax with inflation (column H)	8.6 %

3.2.4 Calculation of Unconditional and Conditional DG Components

The $MARR$ is used as a basis of calculating the unconditional and conditional component of a DG project. The unconditional DG component can be defined as the portion of DG output power that yields an internal rate of return (IRR) equals the $MARR$.

The IRR of a DG project and the selected $MARR$ have a direct effect on the values of the conditional and unconditional DG components. If the IRR of a DG project is less than or equal to the $MARR$, then the unconditional DG component is 100 % of the DG output power, and the conditional component is zero. On the other hand, if the IRR of a DG project is higher than the $MARR$, then the DG output power is divided into unconditional and conditional.

In order to determine the unconditional component (β) of the candidate DG capacity, (3.3) is replaced by the following equation:

$$\text{income}_y = \beta \times \text{generated energy}_y \times \text{feed-in-tariff} \times (1+\text{feed-in-tariff escalation \%})^y \quad (3.9)$$

where β is the percentage portion of the DG output power which is not subject to curtailment. Then, β can be found by setting the IRR equal to the $MARR$ in the after-tax inflation-adjusted cash flow. The conditional component of the DG candidate equals $(100\ \% - \beta)$.

In the example presented in the previous subsection, the after-tax inflation-adjusted IRR of a 10 kW DG unit is 8.6 %. If the $MARR$ is 9 %, then the unconditional component equals 100 % and the conditional component is zero. On the other hand, if the $MARR$ is 7 %, then the unconditional component equals 89 % and the conditional component equals to 11 %. These two examples show the direct effect of the $MARR$ and the IRR on the unconditional and conditional component.

As discussed earlier in Section 3.2.2, there has been little agreement on a reliable method for selecting the $MARR$ [63]. $MARR$ values in renewable DG projects depend on project size and type of technology applied. The $MARR$ values for different renewable DG sizes and technologies given in [69] are used in the analysis presented in this thesis.

The IRR of a renewable DG projects depends on the potential DG energy generated per year. A higher rate of potentially generated DG energy will yield higher IRR rates, which will, in turn, reduce the unconditional DG component. The variability of renewable energy sources like solar and wind can be considered in calculating the potential DG energy generated per year by using probabilistic models for renewable energy sources as discussed in [70]. Alternatively, wind and solar maps can be used to estimate the potential DG energy generated per year for solar and wind sources. For example, National Resources Canada (NRCan) provides online data for the photovoltaic potential energy and solar resource maps of Canada [71]. Also, Environment Canada provides an online wind atlas for wind energy industry in Canada [72]. Similarly, the US Department of Energy provides online wind and solar maps using a Geographical Information System (GIS) [73, 74].

3.3 Techno-Economic Planning Model for Increasing the Connectivity of Renewable Energy Sources in Distribution Systems

The proposed techno-economic planning model provides the distribution network operator (DNO) with the maximum number of units a given candidate DG capacity that can be connected per distribution transformer in a given distribution system. The optimization problem is formulated as a nonlinear integer problem. This is due to the nonlinearity of the load flow constraints and the integer constraint with respect to the number of DG units that can be installed. The problem is solved at the primary distribution system level; loads and DG units connected to the secondary sides of the distribution transformers are represented as lump sum loads in the primary distribution system. The problem is solved

by employing genetic algorithm (GA). The problem formulation is as follows:

Objective function:

$$\max \sum_{dt} N_{DG_{dt}}, \quad \forall dt \in DT \tag{3.10}$$

where $N_{DG_{dt}}$ is the number of DG units to be connected to distribution transformer dt, and DT is the set of distribution transformers in the distribution system.

Subject to:

1- Decision Variable Constraints

The decision variables of the problem are the numbers of DG units installed per distribution transformer. These numbers are non-negative integers constrained by maximum and minimum values. With consideration of the minimum load of the distribution transformer, the maximum values are set to limit the summation of the unconditional components of the DG units connected to a distribution transformer to a percentage of the capacity of the distribution transformer. This percentage value should be set by the DNO. In the presented analysis, this percentage value was set to 80 %. The minimum values of the DG units per distribution transformer are set by the DNO to be either zero or a non-negative integer less than the maximum values. The constraints on the decision variables are given by the following:

$$N_{DG_{dt}} \in \mathbb{Z}_{\geq 0}, \quad \forall dt \in DT \tag{3.11}$$

$$N_{DG_{dt_{min}}} \leq N_{DG_{dt}} \leq \text{floor}\left(\frac{0.8\,(S_{cap_{dt}} + S_{min_{dt}})}{\beta P_{DG_{cap}}}\right), \quad \forall dt \in DT \tag{3.12}$$

where $N_{DG_{dt_{min}}}$ is the minimum number of DG units per distribution transformer dt, $S_{cap_{dt}}$ is the capacity of distribution transformer dt, $S_{min_{dt}}$ is the minimum load of distribution transformer dt, β is the conditional component of the DG output power, and $P_{DG_{cap}}$ is the DG capacity.

2- Economic Constraints

$$P_{dg} = \begin{cases} P_{DG_{cap}} & \text{if } IRR \leq MARR \\ \beta P_{DG_{cap}} & \text{if } IRR > MARR \end{cases} \qquad \forall dg \in DG \tag{3.13}$$

where P_{dg} is the output active power of DG unit dg.

This constraint is based on the value of IRR, calculated from the economic assessment of the DG project as discussed in Section 3.2.4. This economic constraint ensures satisfying two conditions. First, a DG unit with an IRR less than or equal to $MARR$ is granted permission to inject power into the system without curtailment for all online conditions of the distribution system. Second, the curtailment of a DG unit, with an IRR higher than $MARR$, is limited to the value of it conditional component. Satisfying these two conditions guarantees that the economic feasibility of a DG project is not affected when curtailment is in place.

3- Load Flow and Voltage Regulator Constraints

The load flow constraints include the Kirchhoff's current law (KCL) and the Kirchhoff's voltage law (KVL) equations for the distribution system. A F/B DLF algorithm is utilized as a means of including consideration of these constraints in the optimization model [33]. The F/B DLF algorithm is chosen since it is suitable for distribution systems, which are characterized by radial topologies and high R/X ratios [47].

The F/B DLF algorithm is employed in order to obtain the DLF solution for the entire population of each GA offspring. The DLF solution is then used for evaluating the remainder of the constraints in the optimization problem. These constraints are the voltage constraints, expressed in (3.14), and the voltage unbalance constraints, expressed in (3.15).

In the F/B DLF algorithm, system loads are modeled using the constant power load model, the constant current load model, the constant impedance load model, or the polynomial load model [61], and voltage regulators are modeled using the models described in [33]. The F/B DLF algorithm calculates the voltage regulator tap settings according to the voltage level, the bandwidth, and the R and X settings of the voltage regulator. The maximum and minimum limits of the voltage regulator taps are inherently included in the F/B DLF algorithm.

4- Voltage Constraints

$$V_{min} \leq |V_{i_x}| \leq V_{max}, \quad \forall i \in B \tag{3.14}$$

where V_{i_x} is the voltage of phase x at bus i, $x \in \{a, b, c\}$; V_{min} and V_{max} are the minimum and maximum allowable system voltages, respectively; and B is the set of buses in the distribution system.

5- Voltage Unbalance Constraints

$$UB_i < UB_{max}, \quad \forall i \in B_{3ph} \mid B_{3ph} \subset B \tag{3.15}$$

where UB_i is the voltage unbalance index of bus i, UB_{max} is the maximum allowable voltage unbalance index, and B_{3ph} is the set of 3-phase buses in the distribution system. The voltage unbalance index at any bus i is calculated as given be [75] by

$$UB_i = \frac{\max\limits_{x} \left\{ \left| |V_{i_x}| - V_{i_{avg}} \right| \right\}}{V_{i_{avg}}} \tag{3.16}$$

where $V_{i_{avg}}$ is the average voltage at bus i given by

$$V_{i_{avg}} = \tfrac{1}{3} \sum_{x} |V_{i_x}| \tag{3.17}$$

The proposed planning model utilizes GA to find the maximum number of DG units in the system. The selection of GA, or any other meta-heuristic optimization technique, enables considering the load flow constraints by utilizing a F/B DLF algorithm. This approach has two advantages: 1) Utilizing a F/B DLF algorithm avoids the need for including the load flow constraints as equality constraints in the optimization model, hence reducing the complexity of the problem. 2) The F/B DLF algorithm is the most suitable DLF method for distribution systems, as discussed in the literature in Section 2.4.2.

It is important to note that the proposed planning model does not consider constraints related to the protection scheme of the system. Under the microFIT program, over 99 % of the DG units photovoltaic (PV) inverter-based DG [14]. The capacity of a DG unit is less than the capacity of a distribution transformer, which is typically 50 kVA. Connecting these small-scale inverter-based DG units will have insignificant effect on the protective scheme of the system due to the following reasons. First, an inverter-based DG has a fault current contribution that is less than 125 % its rated current [62]. Since the DG units

have small capacities, their fault contribution is minimal. Second, inverter-based DG units have short disconnecting times in the event of a fault. They can be programmed to shut down in less than a cycle after receiving a control signal indicating a network fault [62]. Third, inverters compliant with the IEEE Std 1547-2003 shut down in the case of loss of voltage and cease to reconnect until the voltage has been steadily restored for a preset time period [62]; this feature prevents network islanding conditions.

System loads are modeled deterministically in the proposed techno-economic planning model. Load profiles for the four seasons are divided into states. For each load state, the techno-economic optimization model determines the maximum number of DG units ($N_{DG_{dt}}$) to be connected to each distribution transformer dt in the system. Then, for each distribution transformer dt, the minimum calculated $N_{DG_{dt}}$ in all the load states is considered in the final output of the planning model.

The proposed planning model ensures that any DG unit, that is subject to curtailment, yields an IRR higher than the $MARR$. However, this planning model does not provide the IRR of the DG project after curtailment. Calculating the IRR of the DG project requires modeling the system loads and the DG generation probabilistically, which is out of the scope of this research.

3.4 Simulation Results

The IEEE 123-bus system was used for the evaluation of the proposed planning model. The data for this system are available in [76]. The single-line diagram of the system is shown in Figure 3.1. The system has 77 Y-connected single-phase loads rated at (40 kW + 20 kVAR) and (20 kW + 10 kVAR). The system was modified by replacing these 77 loads with 240-120 V single-phase secondary-distribution residential networks. The layout of a 240-120 V single-phase secondary-distribution residential network is shown in Figure 3.2. Each network is supplied by a 50 kVA single-phase pole-mounted distribution transformer with a 1.9 % impedance. The locations of the 77 single-phase secondary-distribution residential networks in the IEEE 123-bus are indicated in Figure 3.1. The 77 single-phase secondary-distribution residential networks are connected to the same phases and at the same buses as the 77 loads, as indicated in [76]. Each network feeds 12 houses using 1/0 AWG ACSR overhead distribution feeders. The residential loads are assumed to follow the four-season daily load profiles given in [77] for a house in Canada and to have a lagging power factor of 0.9. These daily residential load profiles are displayed in Figure 3.3.

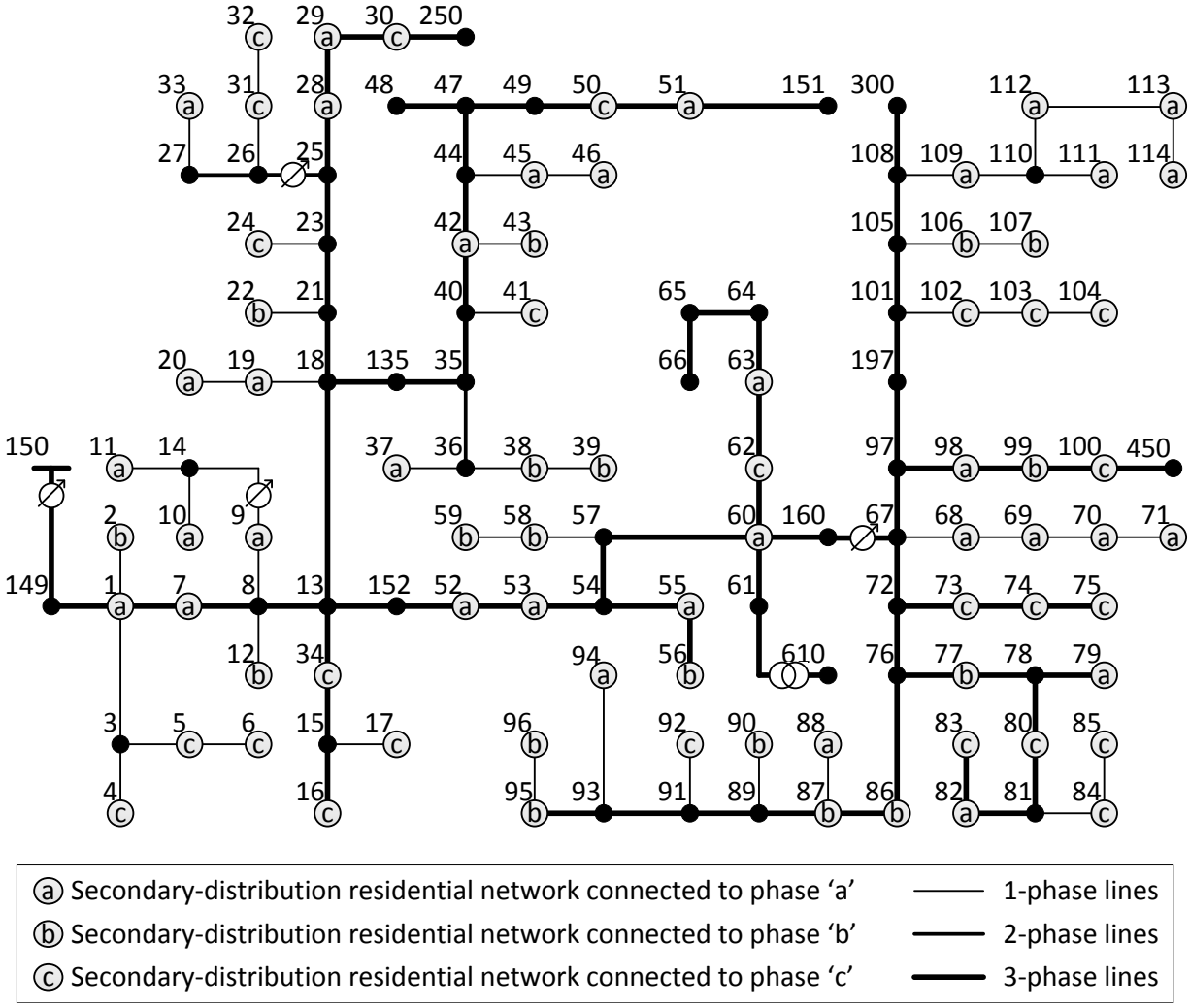

Figure 3.1: Single-line diagram of the modified IEEE 123-bus system, indicating the locations and phases of the 77 secondary-distribution residential networks

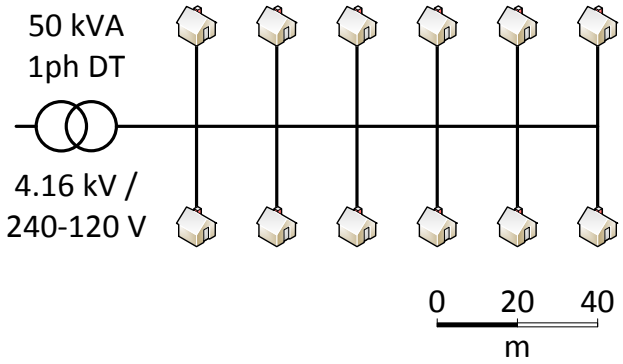

Figure 3.2: Configuration of a 240-120 V secondary-distribution residential network

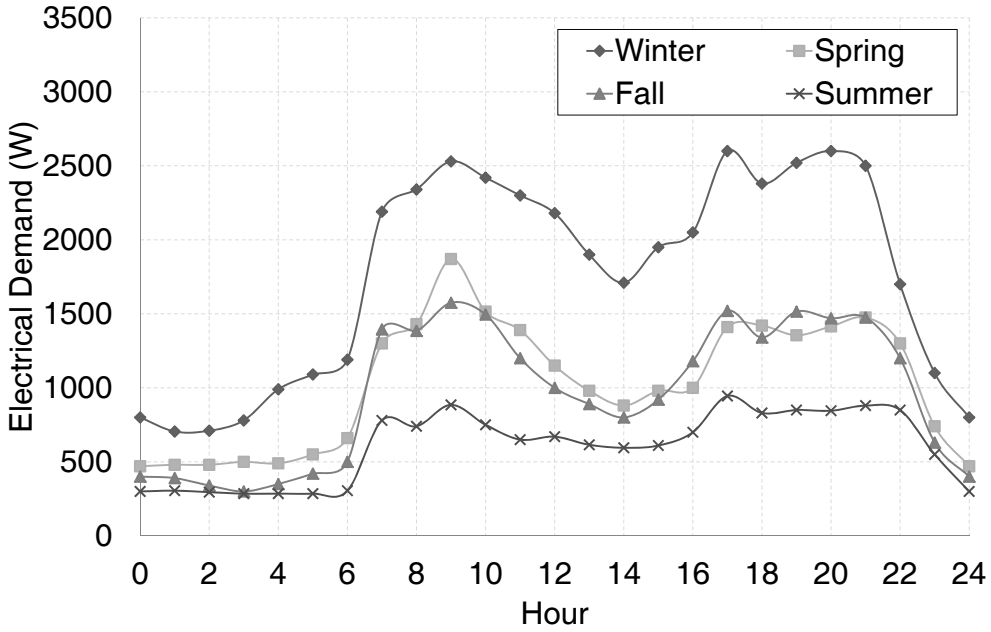

Figure 3.3: Four-season daily residential load profiles given in [77] for a house in Canada

Of the renewable energy technologies included in the microFIT program, PV DG is by far the most attractive option for DG investors. PV DG represents over 99 % of total microFIT program applications [14]. Therefore, all of the DG units in the system under study are assumed to be single-phase rooftop PV DG units installed in the secondary-distribution residential networks. The PV DG units are modeled as PQ buses, as discussed in Section 2.5.3. The PV DG units are assumed to operate with unity power factor. The distribution system under study is assumed to be located in Mississauga, Ontario, Canada.

The simulation results of the proposed techno-economic planning model are organized as follows. Section 3.4.1 presents the results for calculating the unconditional and conditional DG components for a set of rooftop PV DG candidate capacities. Then, Section 3.4.2 presents a comparison between two maximum renewable DG capacities - that which can be installed according to the current FIT rules in Ontario and that which can be installed by implementing the proposed planning model.

3.4.1 Calculation of the Unconditional and Conditional DG Components

As presented in Section 3.2.4, the unconditional DG component is the portion of DG output power that yields an IRR equal to the $MARR$. The first step in the selection of the unconditional DG component is therefore to set the value of the $MARR$. This value is then applied in order to evaluate the IRR values of the candidate DG capacities. The IRR values are calculated based on an after-tax inflation-adjusted economic analysis of the candidate DG capacities.

The choice of $MARR$ is crucial for the evaluation of mutually exclusive investments. In fact, to date little agreement has been established with respect to a reliable method of selecting the $MARR$ [63]. A high $MARR$ may lead to the rejection of economically viable investments, while a low $MARR$ may result in the acceptance of unprofitable investments. In this analysis, the $MARR$ (after-tax with inflation) for PV DG projects was set at 7.5 %. This value is within the range of the hurdle rate for solar renewable energy projects, as given in [69].

The parameters of the economic model used for calculating the IRR are listed in Table 3.4. The DG capital cost for rooftop PV systems, including the installation cost, is shown in Table 3.5. The DG capital cost was obtained based on Ontario market prices [78]. Because PV DG unit owners who are Ontario microFIT participants are eligible to recover any harmonized sales tax (HST) paid [79], the HST was excluded from the analysis.

The project lifetime was set to 20 years, which is equal to the microFIT contract period [11]. The price of the feed-in energy for rooftop PV DG and the escalation percentage of this price were set in accordance with the latest price schedule issued by the Ontario Power Authority, as given in [80]. The potential PV DG energy generated per year in the Mississauga area for solar modules facing south (tilt = latitude-15°) is 1166 kWh kW^{-1} yr^{-1} [81]. The capital cost of renewable DG projects in Ontario is eligible for accelerated capital cost allowances (CCA) under Classes 43.1 and 43.2 [82, 83], which provide an additional incentive for the development of alternative renewable energy sources in Ontario. The CCA rates for Classes 43.1 and 43.2 are 30 % and 50 % per year, respectively. The depreciation rate was therefore set to 80 %, computed on a declining-balance basis. The half-year rule is considered in calculating the depreciation. According to this rule, only half of the CCA rate is applied in the year the renewable energy source is installed (the first year of the project) [82, 83]. The income tax return was set to 30 %, and the inflation rate is assumed to be 2 % per year.

Table 3.4: Economic model parameters

Parameter	Value
$MARR$ [69]	7.5 %
PV DG capital cost	see Table 3.5
PV DG investment lifetime [80]	20 yr
PV DG Feed-in-tariff [80]	\$0.396 kWh^{-1}
Feed-in-tariff escalation percentage [80]	0 %
PV DG potential generated energy [81]	1166 kWh kW^{-1} yr^{-1}
Fixed operation and maintenance cost	\$10 kW^{-1} yr^{-1}
Variable operation and maintenance cost	\$0 kWh^{-1} yr^{-1}
Depreciation rate [82]	80 %
Income tax rate	30 %
Inflation rate	2 %

The candidate DG capacities in kW are $\{2, 3, 4, 5, 7, 10\}$. The cash flows for each DG capacity are given in details in Appendix A; they are calculated as described in Section 3.2.3. Table 3.5 indicates the capital cost and IRR for each candidate capacity and Table 3.6 lists the calculated conditional and unconditional components for each candidate capacity.

The results in Table 3.5 show that raising the DG capacity results in increases in the IRR. This effect was expected since the capital cost of DG decreases as the DG capacity

increases. Table 3.5 shows that DG units with less than 7 kW yield an IRR less than the $MARR$. Therefore, as shown in Table 3.6, the unconditional components of these DG units equals 100 %, and the conditional components of these DG units is zero.

Table 3.6 shows that the conditional component of a 7 kW DG unit is very small. This small value is because the IRR of the 7 kW DG capacity is very close to the $MARR$, as shown in Table 3.5. Conversely, the conditional component of the 10 kW DG unit is relatively high (15 %). The 10 kW DG capacity is therefore considered in evaluating the performance of the management scheme for DG connection online assessment, presented in Chapter 5.

Table 3.5: Capital cost and IRR for the candidate DG capacities

DG capacity (kW)	Capital cost ($/W) [78]	IRR (%)
2	6.23	1.526
3	4.87	4.166
4	4.24	5.797
5	3.85	7.005
7	**3.5**	**8.265**
10	3.14	9.787

Table 3.6: Unconditional and conditional DG components for the output power of the candidate DG capacities

DG capacity (kW)	Unconditional component (%) β	Conditional component (%) (100 % $-$ β)
2	100	0
3	100	0
4	100	0
5	100	0
7	94.6	5.4
10	85	15

3.4.2 Calculation of the Maximum DG Capacity to be Installed in the System

The maximum number of DG units that can be installed in the system under study was calculated in three different scenarios. In Scenario #1, the current microFIT regulations were implemented for the calculation of the maximum DG capacity in the system. In Scenario #2 and Scenario #3, the proposed techno-economic planning model, presented in Section 3.3, was applied in order to calculate the maximum number of DG units. It was assumed that all DG units installed have a 7 kW capacity and 10 kW capacity in Scenario #2 and Scenario #3, respectively.

Scenario #1

As discussed in Section 2.2, the microFIT technical interconnection requirements (TIR) limit the total interconnected generation 7 % of the annual line section peak load [13]. The annual peak load of the system under study without the installation of PV DG units is 3759.4 kVA. The maximum PV DG capacity that can be installed is thus limited to 263.15 kW. This capacity is equal to 26 rooftop PV DG units at 10 kW each. The system under study includes 924 houses. Consequently, only 2.8 % of the home owners will be permitted to install rooftop PV DG units in the system under study.

Scenario #2

In this scenario, all PV DG units were assumed to have a capacity of 7 kW. Table 3.6 shows that the conditional component of a 7 kW DG unit is very small. Therefore, the unconditional component was assumed in this scenario to be 100 % and the conditional DG component was assumed to be zero. In other words, the 7 kW DG units will not be subject to curtailment.

The planning model described in Section 3.3 was applied for calculating the maximum number of PV DG units in the system under study. In (3.12), the minimum number of DG units per distribution transformer ($N_{DG_{dt_{min}}}$) was set to zero. The value of $N_{DG_{dt_{min}}}$ should be selected by the DNO and can be set to a non-zero value, as indicated in Section 3.3. The values of V_{max} and V_{min} were set to be equal to the limits of the normal operating conditions of the voltage given in the microFIT TIR [13]. The value of UB_{max} was set to 2 %, based on the microFIT TIR [13].

The maximum number of PV DG units in Scenario #2 is 330. This number is equivalent to a 2310 kW PV DG capacity. For the system under study, applying the proposed techno-economic planning model without curtailment therefore enables 35.71 % of home owners to install rooftop PV DG units.

Table 3.7 lists the locations of the distribution transformers where the 330 DG units are connected. The locations are identified by the bus number and phase index. For each distribution transformer, a DG unit is installed on the rooftop of any of the 12 houses in the 240-120 V secondary-distribution residential networks, shown in Figure 3.2. The DG units are assumed to be randomly located in the 240-120 V secondary-distribution residential network.

Table 3.7: Number of installed DG units in Scenario #2 (7 kW capacity) per distribution transformer in the modified IEEE 123-bus system

DGs per DT	DT locations					
6	{2b,	4c,	5c,	7a,	12b,	16c,
	17c,	19a,	22b,	24c,	30c,	31c,
	33a,	34c,	37a,	38b,	39b,	41c,
	42a,	46a,	50c,	51a,	52a,	53a,
	56b,	59b,	60a,	62c,	73c,	75c,
	77b,	79a,	80b,	83c,	84c,	85c,
	86b,	87b,	90b,	92c,	95b,	99b,
	100c,	102c,	103c,	104c,	106b,	112a}
5	{11a,	109a,	111a}			
4	{43b,	55a,	58b,	63a}		
3	{9a,	98a,	114a}			
2	{94a}					
0	{1a,	6c,	10a,	20a,	28a,	29a,
	32c,	45a,	68a,	69a,	70a,	71a,
	74c,	82a,	88a,	96b,	107b,	113a}

Scenario #3

In this scenario, the planning model described in Section 3.3 was applied for the calculation of the maximum number of the 10 kW PV DG units. As with Scenario #2, $N_{DG_{dt_{min}}}$ was set to zero and the values of V_{max}, V_{min}, and UB_{max} ware set according to the microFIT TIR [13].

In contrast to the previous scenario, DG units in this scenario are subject to curtailment. As shown in Table 3.6, the unconditional component for the 10 kW DG unit equals 85 %, and the conditional DG component equals 15 %. So the output power of the 10 kW PV DG unit can curtailed by a maximum value of 15 %. DG curtailment is controlled by the proposed management scheme for DG connection online assessment, presented in Chapter 5.

The maximum number of PV DG units that can be installed in this scenario is 286. This number corresponds to a total PV DG capacity of 2860 kW. Calculating the maximum number of DG units using the 10 kW DG capacity therefore enables the installation of rooftop PV DG units on 30.95 % of the houses in the system under study.

Table 3.8 lists the locations of the distribution transformers where the 286 DG units are connected. The locations are identified by the bus number and phase index. As in Scenario #2, for each distribution transformer, a DG unit is installed on the rooftop of any

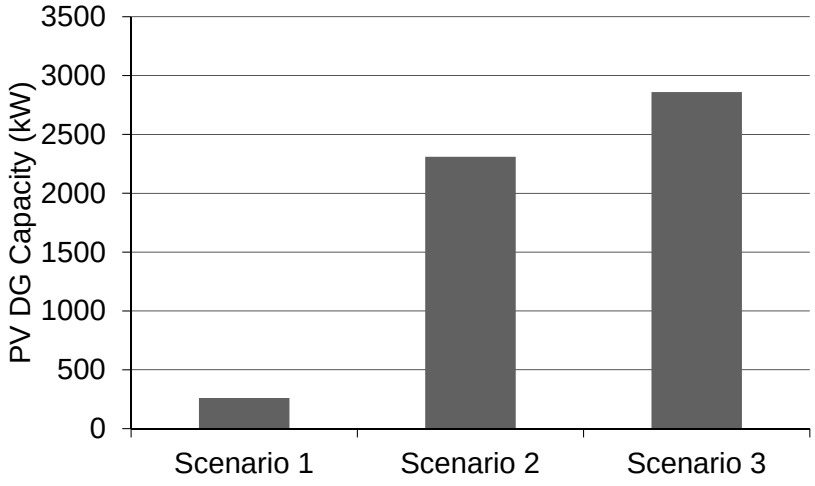

Figure 3.4: Maximum PV DG capacity for the three scenarios examined for the distribution system under study

of the 12 houses in the 240-120 V secondary-distribution residential networks, shown in Figure 3.2. The DG units are assumed to be randomly located in the 240-120 V secondary-distribution residential network. Scenario #3 is considered in evaluating the performance of the management scheme for DG connection online assessment, as presented in Chapter 5.

Table 3.8: Number of installed DG units in Scenario #3 (10 kW capacity) per distribution transformer in the modified IEEE 123-bus system

DGs per DT	DT locations					
5	{4c, 12b, 28a, 37a, 50c, 73c, 84c, 95b, 106b,	5c, 16c, 29a, 38b, 52a, 74c, 85c, 96b, 107b,	6c, 17c, 30c, 39b, 56b, 75c, 86b, 99b, 111a,	7a, 20a, 31c, 41c, 58b, 77b, 87b, 100c, 113a,	10a, 22b, 32c, 43b, 59b, 80b, 90b, 102c, 114a}	11a, 24c, 34c, 46a, 62c, 83c, 92c, 104c,
4	{33a,	55a,	79a,	109a}		
3	{88a}					
2	{69a}					
0	{1a, 51a, 71a,	2b, 53a, 82a,	9a, 60a, 94a,	19a, 63a, 98a,	42a, 68a, 103c,	45a, 70a, 112a}

Figure 3.4 displays the maximum PV DG capacity that can be installed for the three scenarios in the distribution system under study. As shown in Figure 3.4, the proposed planning model, which is applied in Scenario #2 and Scenario #3, can significantly increase the PV DG penetration level in the system under study compared to Scenario #1, which follows the 7 % capacity limit imposed by the microFIT TIR. Compared to Scenario #1, the PV DG capacity that can be installed in the system under study is 8.8 times higher in Scenario #2 and 10.9 times higher in Scenario #3.

The total DG capacity in Scenario #3 is higher than the total DG capacity in Scenario #2 by 550 kW. This increased capacity is equivalent to 23.81 % of the total DG

capacity in Scenario #2. The significant increase in the total DG capacity in Scenario #3 compared to Scenario #2 demonstrates the advantage of applying active power curtailment. The curtailment of the DG conditional capacity is controlled by the management scheme for DG connection online assessment, presented in Chapter 5.

3.5 Summary

This chapter introduces a techno-economic planning model for small-scale renewable DG resources connected under FIT programs. The proposed planning model represents the main framework of the DG connection online assessment, presented in Chapter 5. The output power of each installed DG unit is divided into two components: 1) an unconditional component that ensures an adequate profit for the DG owner when curtailment is in place, and 2) a conditional component that can be curtailed based on a management scheme, presented in Chapter 5. The simulation results show that applying the proposed techno-economic planning model ensures that a significantly higher PV DG capacity can be connected to the system than would be permitted according to current microFIT program regulations. In addition, the results show that the addition of conditional DG component, that is subject to curtailment, can significantly increase the penetration level of renewable DG sources. The curtailment of the conditional DG component is controlled by the management scheme for DG connection online assessment, presented in Chapter 5. The management of the unconditional DG components depends on the availability of up-to-date DLF results that reflects the actual conditions of the system, such as loads and network topology. These conditions are subject to continual changes especially in the context of smart grid. The next chapter presents a novel "zooming" DLF algorithm for smart grids. The zooming DLF algorithm is employed in the online management scheme, in Chapter 5, to control the curtailment of the conditional DG components in the system.

Chapter 4

A "Zooming" Algorithm for Distribution Load Flow Analysis in Smart Grids

4.1 Introduction

The main objective of the online assessment of DG connection is increasing the connectivity of renewable DG sources while preserving the system within its operating constrains. Achieving this objective depends on the availability of up-to-date DLF results that reflect the actual load flow conditions of the systems. Providing fast and accurate DLF results is necessary to identify any violations in the system operating constraints, such as overvoltage, voltage unbalance, and reverse power flow. However, as discussed earlier in Chapter 2, current DLF techniques are unsuitable for online interaction with continual changes in loads, renewable DG sources, and network topology. Addressing this problem is of a particular importance especially in the context of smart grid.

This chapter presents a novel algorithm for determining the distribution load flow (DLF) in smart grids.This algorithm has the advantage, with respect to smart grids, of solving the DLF problem for systems with flexible network topologies. The proposed algorithm can be called a "zooming" algorithm because it can solve the DLF problem in a specific area of interest in the distribution system without necessitating the inclusion of all of the system buses. The area of interest is established based on a user-input bus, called the zoom-in bus. The area of interest includes only the buses that connect the source bus to the zoom-in bus. Focusing on the area of interest enables the DLF problem size to be reduced, hence

decreasing the solution time. In order to focus on the area of interest while considering the effect of all the buses in the distribution system, other parts of the distribution system are replaced by their equivalent power. This is achieved through the use of a proposed system lumping technique also explained in this chapter.

The zooming DLF algorithm is a main component in the online assessment scheme, presented in Chapter 5. The zooming DLF algorithm enables solving the DLF in a specific area of interest. This feature is utilized in the online assessment scheme to manage the curtailment of DG sources located in a specific area of interest without considering all the DG sources in the system. This area of interest is determined based on the location of buses and/or lines which suffer from violations to the system constraints, such as overvoltage, voltage unbalance, and reverse power flow. The significant reduction of the DLF solution time offered by the zooming DLF algorithm enables the online operation of the proposed DG connection online assessment scheme, as discussed in Chapter 5.

The DLF zooming algorithm modifies the F/B matrix formulation introduced in [49] and described in Section 2.4.2, by automating the matrix-building algorithm through a novel recursive process. Constructing the DLF problem with this process enables the online processing of the continual changes that take place in the network topology of a smart grid. This automated feature offered by the zooming algorithm also facilitates the integration of DLF analysis in a variety of smart grid applications, especially in ones that require repeated DLF analysis, such as optimal network reconfiguration.

To validate the accuracy of the DLF zooming method, the results were compared to the DLF results obtained with the F/B method presented in [49] and described in Section 2.4.2. A variety of scenarios that correspond to smart grid conditions such as flexible network topology were also examined as a means of evaluating the performance of the DLF zooming method in a smart grid environment.

The remainder of this chapter is organized as follows. In Section 4.2, the proposed system lumping technique is presented. In Section 4.3, the system configuration modeling is described. Section 4.4 presents the proposed DLF zooming algorithm. The results of the accuracy validation and the evaluation for smart grid operation are given in Section 4.5.1 and Section 4.5, respectively. A summary is presented in Section 4.6.

4.2 Proposed System Lumping Technique

The total power supplied to any lateral feeder can be divided into two components: the summation of the lateral supplied loads and the total active and reactive power losses of

the laterals. The proposed system lumping technique enables the calculation of the approximate equivalent power supplied to any part of the distribution system; this equivalent power is calculated without the necessity of performing detailed load flow calculations for the lumped portion.

In a hypothetical three-phase lateral feeder f in a radial distribution system, if the number of buses of the lateral f including its sublaterals for phase x is n_x, where $x \in \{a, b, c\}$, then the total number of sections per phase is $(n_x - 1)$. The p.u. active and reactive power losses of phase x of any feeder section s can be given by

$$P_{loss_{s_x}} = \frac{{P_{load_{s_x}}}^2 + {Q_{load_{s_x}}}^2}{V_{s_x}} \, R_{s_x} \tag{4.1}$$

$$Q_{loss_{s_x}} = \frac{{P_{load_{s_x}}}^2 + {Q_{load_{s_x}}}^2}{V_{s_x}} \, X_{s_x} \tag{4.2}$$

where V_{s_x} is the p.u. voltage of phase x at the connection bus of the feeder section s. V_{s_x} is assumed to be unity as a first approximation. If necessary, to increase the accuracy of the DLF solution, the value of V_{s_x} can be iteratively updated after the DLF problem is solved. R_{s_x} and X_{s_x} represent the p.u. resistance and reactance of phase x of the feeder section s, respectively.

In [84], an equivalent base resistance concept was proposed for transforming non-uniform feeders into equivalent uniform feeders. This concept is applied here for calculating the equivalent base resistance and reactance values for phase x of the lateral f, as follows:

$$R_{base_{f_x}} = \frac{\sum_{s=1}^{n_x-1} P_{loss_{s_x}}}{\left(P_{load_{f_x}}\right)^2 + \left(Q_{load_{f_x}}\right)^2} \tag{4.3}$$

$$X_{base_{f_x}} = \frac{\sum_{s=1}^{n_x-1} Q_{loss_{s_x}}}{\left(P_{load_{f_x}}\right)^2 + \left(Q_{load_{f_x}}\right)^2} \tag{4.4}$$

where $P_{load_{f_x}}$ and $Q_{load_{f_x}}$ are the total p.u. active and reactive loads, respectively, of phase x fed from the lateral f. The values of $R_{base_{f_x}}$ and $X_{base_{f_x}}$ can be used for calculating the

total active and reactive power losses of the lateral feeder f, as in (4.5) and (4.6):

$$P_{loss_{f_x}} = R_{base_{f_x}} \left| \frac{P_{load_{f_x}} + jQ_{load_{f_x}}}{V_{f_x}} \right|^2 \tag{4.5}$$

$$Q_{loss_{f_x}} = X_{base_{f_x}} \left| \frac{P_{load_{f_x}} + jQ_{load_{f_x}}}{V_{f_x}} \right|^2 \tag{4.6}$$

where V_{f_x} is the p.u. voltage of phase x of the connection bus of the lateral f.

The equivalent load of the lateral f, including its sublaterals, is given by

$$S_{f_x} = \left(P_{load_{f_x}} + P_{loss_{f_x}}\right) + j\left(Q_{load_{f_x}} + Q_{loss_{f_x}}\right) \tag{4.7}$$

An equivalent load is calculated for each lumped lateral in each iteration of the DLF solution using (4.7) and is then added as a spot load to the connection bus of the lumped lateral.

4.3 System Configuration Modeling

The distribution system configuration is modeled using the bus-injection to branch-current ($BIBC$) matrix presented in [49] and described in Section 2.4.2. This matrix, named here the physical connection (PC) matrix, is utilized in the proposed DLF zooming algorithm. The following subsections highlight the characteristics of the PC matrix and present the PC matrix building algorithm.

4.3.1 PC Matrix Characteristics

The IEEE 13-bus system, displayed in Figure 4.1, is used as an example to demonstrate the characteristics of the PC matrix. The configuration of the IEEE 13-bus system is given in [85]. The PC_{13} matrix of the system is shown in Figure 4.2. The matrix columns refer to the bus names, and the rows indicate the network branches. The network branches are identified by the name of the branch-end bus.

The PC matrix is used for modeling the network configuration for the DLF zooming algorithm. For any bus in the network, the PC matrix is utilized as the identifier of two sets of buses: upstream and downstream. The upstream set for a given bus is the group of system buses connecting this bus to the source bus. The downstream set for a given

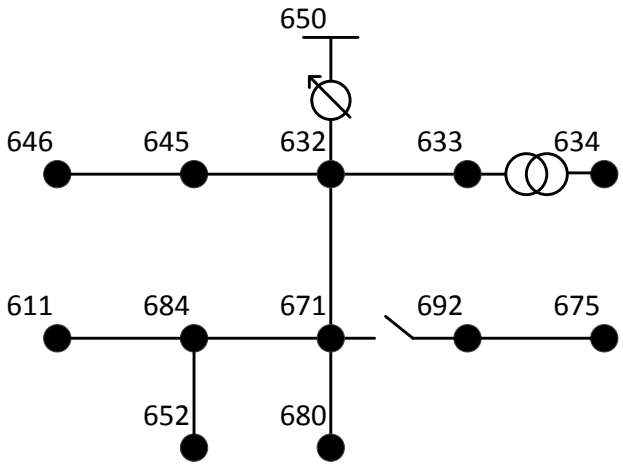

Figure 4.1: The IEEE 13-bus system

bus is the group of system buses fed by this bus. The upstream and downstream sets for any given bus are identified by the unity entries of the corresponding column and row, respectively, for the given bus in the PC matrix. For example, Figure 4.1 shows that the upstream set for bus 684 is $\{632, 671\}$. An examination of PC_{13} in Figure 4.2 reveals that the corresponding column for bus 684 has two unity entries that refer to buses 632 and 671. The downstream set can be determined in the same way using the corresponding row for bus 684.

The characteristics of the PC matrix are exploited in the zooming algorithm, in which the matrix is used for identifying the downstream buses of any lumped parts, as explained in Section 4.4.

4.3.2 PC Matrix Building Algorithm

The proposed PC matrix building algorithm is based on the use of a recursive process for the exploration of the connections between system buses. This type of process enables system configuration changes to be accommodated quickly and accelerates the construction of the PC matrix.

Figure 4.3 displays the flowchart for the proposed PC matrix building algorithm. The IEEE 13-bus system, shown in Figure 4.1, is used as an example that illustrates the proposed algorithm. The algorithm starts by reading the system bus incidence (BI) matrix. The system is modelled as an undirected graph: each bus is represented by a column and

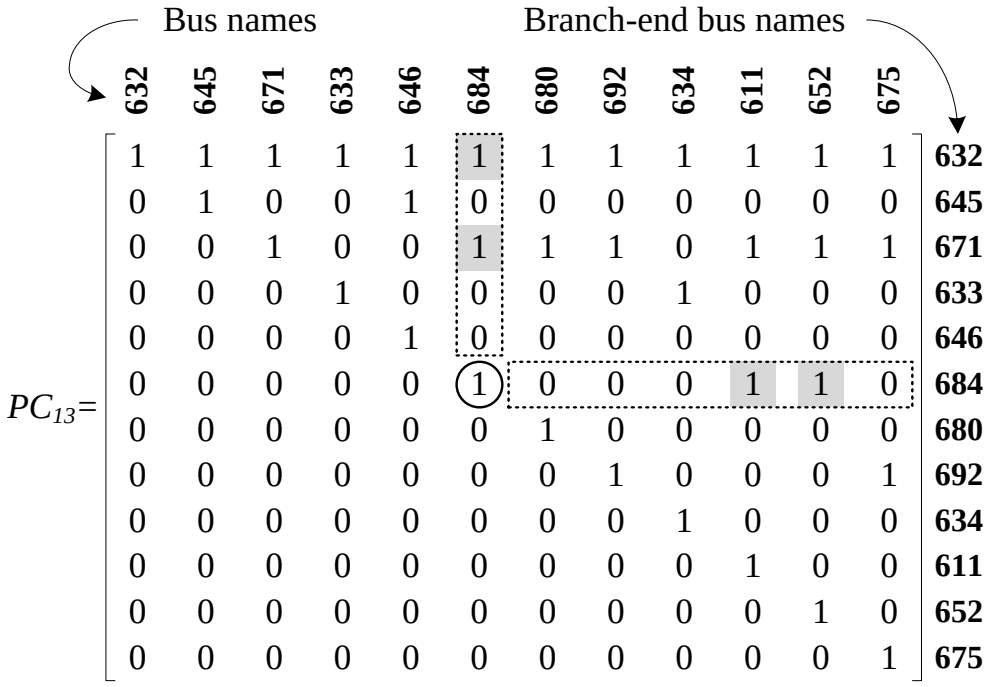

Figure 4.2: PC_{13} matrix of the IEEE 13-bus system

each branch is represented by a row. The BI matrix element a_{ij} of row i and column j is given by [86]

$$a_{ij} = \begin{cases} 0 & \text{if branch } i \text{ is not connected to bus } j \\ 1 & \text{if branch } i \text{ is connected to bus } j \end{cases} \tag{4.8}$$

The building algorithm then reads the name of the reference bus {650}. For multiple-source distribution systems, the system slack bus is used as the reference bus in the building algorithm. Next, the system buses are ordered in a breadth-first sequence, starting from the reference bus [87]. This bus sequence is applied as a means of ordering the columns of the BI matrix. The ordered BI_{13} matrix of the IEEE 13-bus system is displayed in Figure 4.4 without the column of the reference bus. This order scheme generates a lower triangular BI matrix with unity-diagonal elements. In the following analysis, the rows of the BI matrix are therefore referred to using the bus names of their corresponding columns.

The recursive process starts after the ordering of the system BI matrix; the process is indicated inside the dashed block in Figure 4.3. In the recursive process, a subroutine calls itself until a termination condition is satisfied. The recursion control flow has two paths:

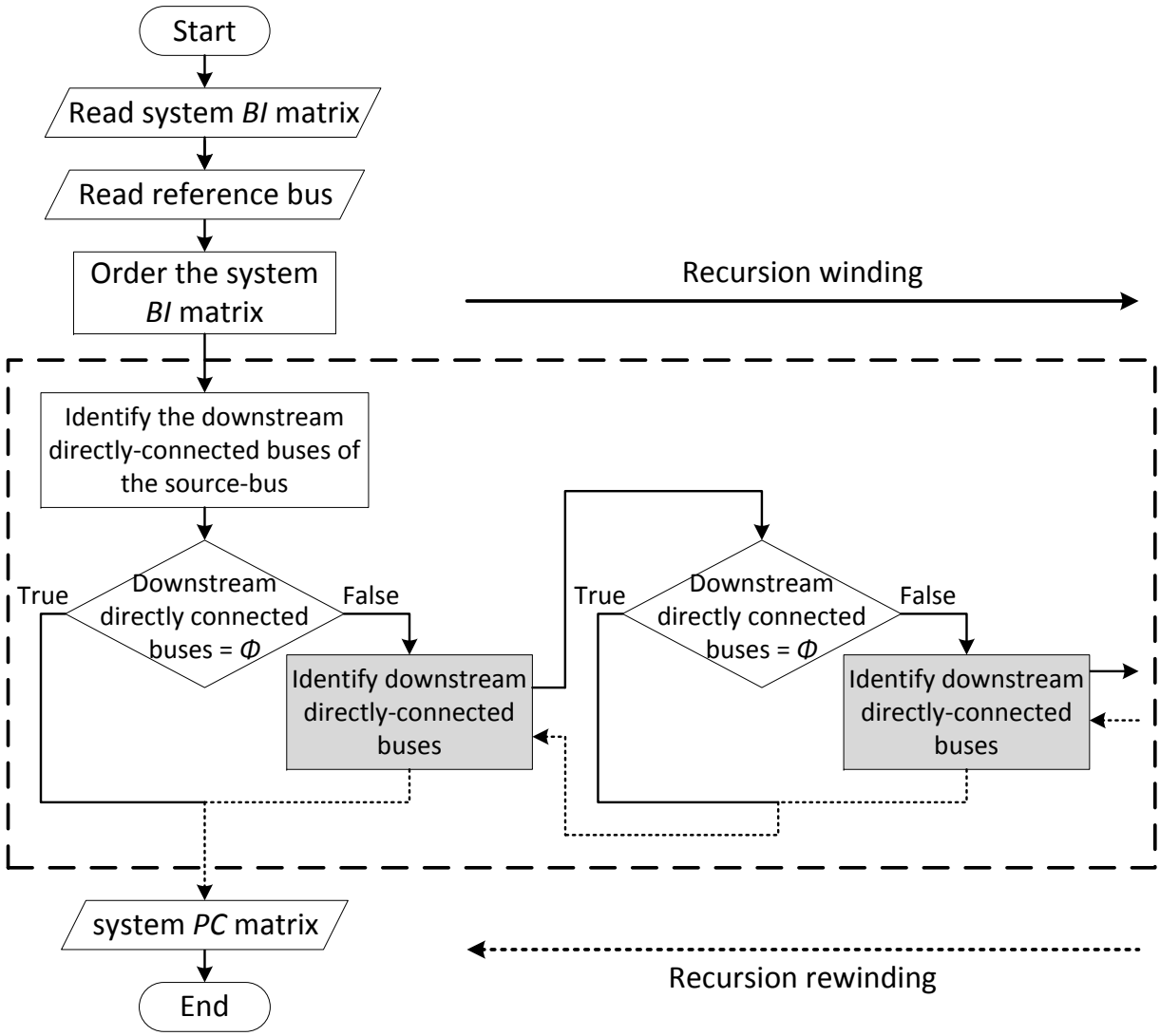

Figure 4.3: Flowchart of the PC matrix building algorithm

recursion winding and rewinding. The recursion winding path, shown as solid lines, occurs before the termination condition is satisfied. Conversely, the recursion rewinding path, shown as dotted lines, occurs after the termination condition is satisfied and returns back

$$BI_{13} = \begin{array}{c} \begin{array}{cccccccccccc} \mathbf{632} & \mathbf{645} & \mathbf{671} & \mathbf{633} & \mathbf{646} & \mathbf{684} & \mathbf{680} & \mathbf{692} & \mathbf{634} & \mathbf{611} & \mathbf{652} & \mathbf{675} \end{array} \\ \left[\begin{array}{cccccccccccc} 1 & 0 & 0 & 0 & 0 & 0 & 0 & 0 & 0 & 0 & 0 & 0 \\ 1 & 1 & 0 & 0 & 0 & 0 & 0 & 0 & 0 & 0 & 0 & 0 \\ 1 & 0 & 1 & 0 & 0 & 0 & 0 & 0 & 0 & 0 & 0 & 0 \\ 1 & 0 & 0 & 1 & 0 & 0 & 0 & 0 & 0 & 0 & 0 & 0 \\ 0 & 1 & 0 & 0 & 1 & 0 & 0 & 0 & 0 & 0 & 0 & 0 \\ 0 & 0 & 1 & 0 & 0 & 1 & 0 & 0 & 0 & 0 & 0 & 0 \\ 0 & 0 & 1 & 0 & 0 & 0 & 1 & 0 & 0 & 0 & 0 & 0 \\ 0 & 0 & 1 & 0 & 0 & 0 & 0 & 1 & 0 & 0 & 0 & 0 \\ 0 & 0 & 0 & 1 & 0 & 0 & 0 & 0 & 1 & 0 & 0 & 0 \\ 0 & 0 & 0 & 0 & 0 & 1 & 0 & 0 & 0 & 1 & 0 & 0 \\ 0 & 0 & 0 & 0 & 0 & 1 & 0 & 0 & 0 & 0 & 1 & 0 \\ 0 & 0 & 0 & 0 & 0 & 0 & 0 & 1 & 0 & 0 & 0 & 1 \end{array}\right] \end{array} \begin{array}{c} \\ \mathbf{632} \\ \mathbf{645} \\ \mathbf{671} \\ \mathbf{633} \\ \mathbf{646} \\ \mathbf{684} \\ \mathbf{680} \\ \mathbf{692} \\ \mathbf{634} \\ \mathbf{611} \\ \mathbf{652} \\ \mathbf{675} \end{array}$$

Figure 4.4: Ordered BI matrix of the IEEE 13-bus system

to the first subroutine call. It is important to note that the number of recursive iterations depends on the complexity of the network configuration rather than on the number of system buses.

The function of the subroutine is to use the ordered BI matrix to identify the set of directly connected downstream buses for a given input bus. This task is accomplished through the location of the unity entries from the input bus column and the exclusion of the diagonal unity entry. The rows of the located unity entries correspond to the names of the directly connected downstream buses for the input bus.

With respect to the IEEE 13-bus system, the recursive process is described as follows:

1. The algorithm identifies the set of downstream buses connected directly to the source bus. Any such bus has a single unity entry in its row. For the IEEE 13-bus system, the set of downstream buses connected directly to the source bus is $\{632\}$, so bus 632 becomes the input for the first subroutine call.

2. The first output of the subroutine is $\{645, 671, 633\}$, which is the set of directly connected downstream buses for bus 632.

3. The subroutine then calls itself for each element of the first output set. The process continues in the recursion winding direction until the entire output of the recursive subroutines is equal to ϕ (a set with zero elements).

4. In the recursion rewinding direction, the sets of directly connected downstream buses for each bus are collected in order to determine the set of all downstream buses for each system bus. Table 4.1 shows the final output of the recursive process for the IEEE 13-bus system.

The final output of the recursive process is then used for finding the off-diagonal unity entries of the PC matrix. For each row in the PC matrix, the set of downstream buses indicates the names of the buses that have unity entries. A comparison of the PC_{13} matrix of the IEEE 13-bus system, displayed in Figure 4.2, with the recursive process output, presented in Table 4.1, provides an understanding of this step. For example, as with the selection of the set of downstream buses for the sixth bus in the recursive process output, the off-diagonal unity entries of the sixth row of PC_{13} correspond to buses 611 and 652. In the case of three-phase networks, the unity entries of the PC matrix are replaced by (3×3) identity matrices, in a process similar to that employed in [49]. In the case of a single-line or double-line feeder section, the unity entries of the missing phases are replaced by zeros in the identity matrix.

It should be emphasized that the proposed building algorithm requires no matrix operations, especially matrix inversion: a feature that guarantees fast execution for large-scale distribution systems.

4.4 Proposed DLF Zooming Algorithm

The flowchart of the proposed DLF zooming algorithm is shown in Figure 4.5. The algorithm starts with the construction of the system PC matrix, as explained in Section 4.3.2. The algorithm next reads the name of the zoom-in bus at the location where it is required to zoom in for the DLF solution. The system loading data are then updated; the data include the output power of the DG sources in the system and the system loads. In this work, it is assumed that DG sources and loads are equipped with smart automatic meter reading (AMR) devices. DG sources are modeled as PQ-buses as discussed in Section 2.5.3, and loads are modeled using the following equation as discussed in Section 2.5.2:

$$S = S_0 \left(\frac{V}{V_0} \right)^{\alpha} \tag{4.9}$$

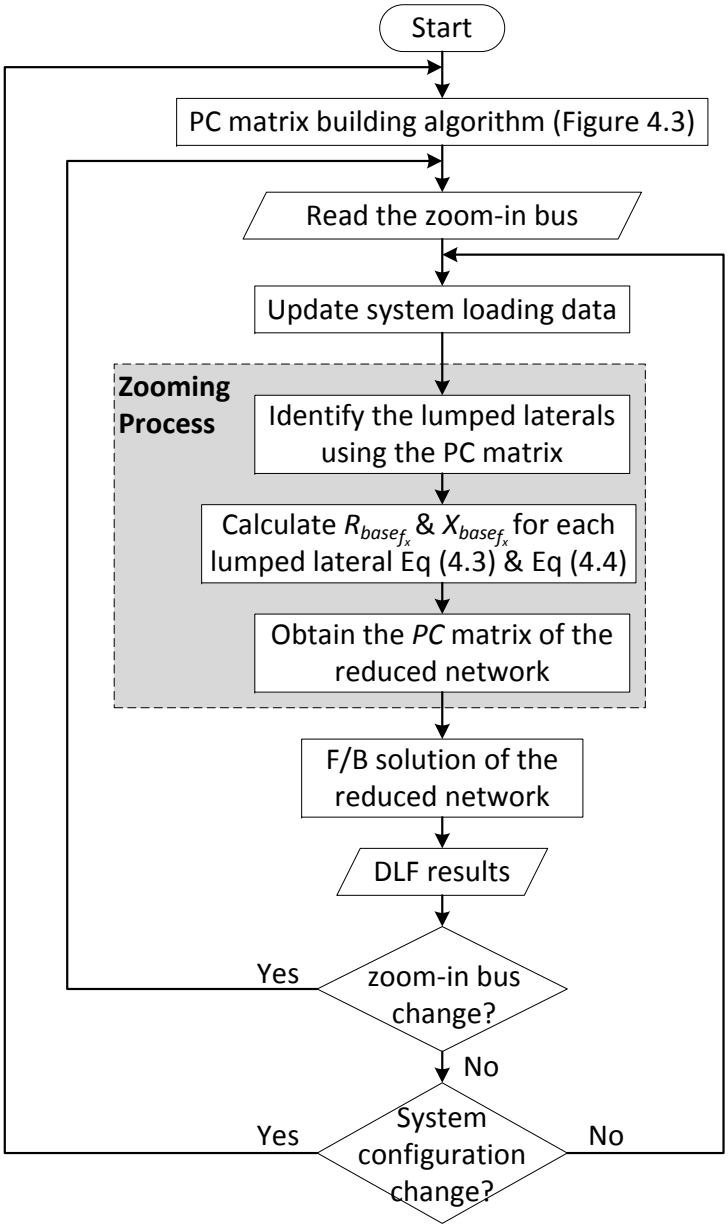

Figure 4.5: Flowchart of the proposed DLF zooming algorithm

Table 4.1: Recursive process output for the IEEE 13-bus system

Bus	Set of downstream buses
632	$\{645, 671, 633, 646, 684, 680, 692, 634, 611, 652, 675\}$
645	$\{646\}$
671	$\{684, 680, 692, 611, 652, 675\}$
633	$\{634\}$
646	ϕ
684	$\{611, 652\}$
680	ϕ
692	$\{675\}$
634	ϕ
611	ϕ
652	ϕ
675	ϕ

where S_0 is the load power consumed at the rated voltage, V_0 is the load rated voltage, and V is the bus voltage. The value of the parameter α determines the load model (0 for constant power, 1 for constant current, and 2 for constant impedance).

The zooming process is performed after the system loading data have been updated and consists of the following three steps:

1. Identify the lumped laterals using the PC matrix: This step is executed by acquiring the upstream set for the zoom-in bus, following which, for each bus of the upstream set, the downstream set is determined. These downstream sets contain the bus names of the lumped laterals.

2. Calculate $R_{base_{fx}}$ and $X_{base_{fx}}$ for the lumped laterals using (4.3) and (4.4), respectively.

3. Obtain the PC matrix of the zone of interest by excluding the rows and columns of the lumped parts.

The DLF solution for the zone of interest is then calculated using the method described in [49], which is described in Section 2.4.2. In each iteration of the DLF solution, the

equivalent load of each lumped lateral is calculated using (4.7) and is then added as a spot load to the connection bus of the lumped lateral.

As shown in Figure 4.5, the algorithm automatically repeats after the DLF solution of the zone of interest has been determined. This feature ensures the updating of the DLF solution in case any changes occur in the zoom-in bus, system configuration, output power of DG sources, or system loading. The input and the output of the algorithm are listed in Table 4.2.

Table 4.2: Input and output of the proposed DLF zooming algorithm

Input	System BI matrix Reference bus name Zoom-in bus name System loads System line impedances
Output	DLF solution of the zone of interest

4.5 Simulation Results

The management scheme for DG connection online assessment, presented in Chapter 5, depends on the availability of up-to-date DLF results that reflects the actual conditions of the system, such as loads and network topology. These conditions are subject to continual changes especially in the context of smart grid.

The zooming DLF algorithm is a main component of the proposed management scheme, presented in Chapter 5. The ability of the zooming algorithm to focus the DLF solution on the area of interest is utilized in the management scheme. The area of interest in the management scheme is determined based on the locations of buses and/or lines which suffer from violations to the system constraints, such as overvoltage, voltage unbalance, and reverse power flow. The determination of the area of interest for the management scheme is discussed in Section 5.2.1. The ability of management scheme to be implemented online therefore depends on the speed of the zooming DLF algorithm and the ability of the zooming DLF algorithm to interact with network topology changes online.

The following subsections demonstrate the effectiveness of the proposed DLF zooming algorithm for implementing the proposed DG connection online assessment for smart grid, presented in Chapter 5. The first subsection validates the accuracy of the zooming algorithm. In the second subsection, the speed of the DLF solution was investigated in order to assess the ability of the proposed algorithm to interact efficiently with smart grid control systems. In addition, the effect on the DLF solution time when the size of the system is increased was also examined. In the third subsection, the ability of the zooming algorithm to interact online with changes in network topology was evaluated. A number of case studies were conducted as a means of assessing the performance of the proposed algorithm in distribution systems that have a flexible network topology.

4.5.1 Accuracy Validation

The accuracy of the proposed DLF zooming algorithm was tested on the IEEE 37-bus and the IEEE 123-bus systems shown in Figure 4.6(a) and Figure 4.7(a), respectively.

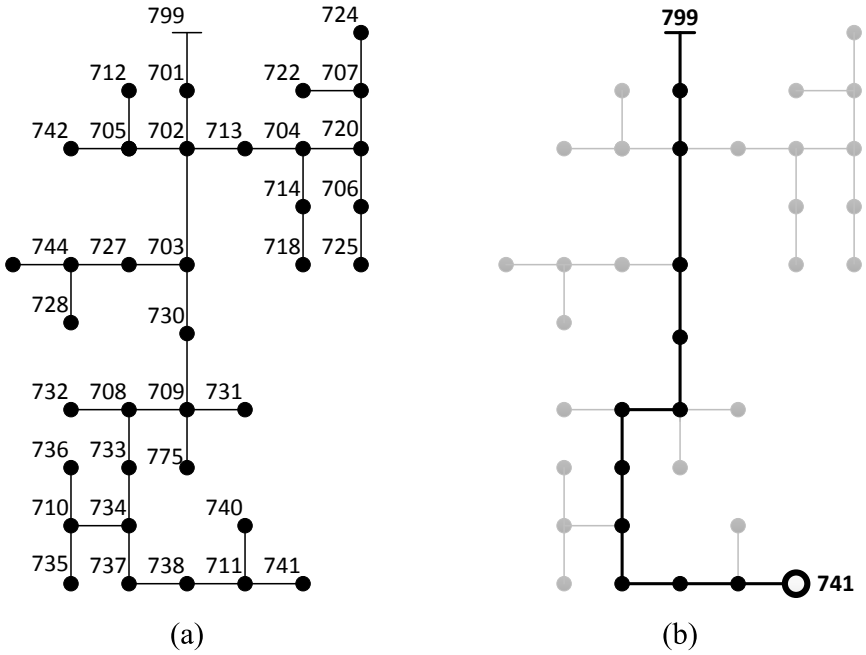

Figure 4.6: Configuration of the (a) IEEE 37-bus system and (b) the zone of interest of the IEEE 37-bus system, showing the zooming-in on bus 741. The greyed parts of the system represent the lumped laterals

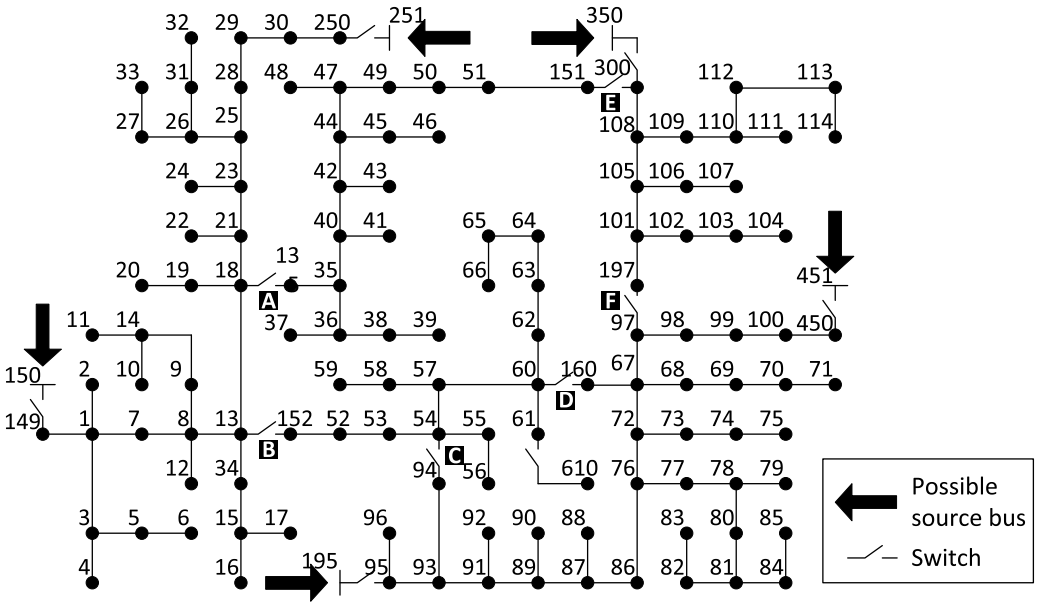

(a)

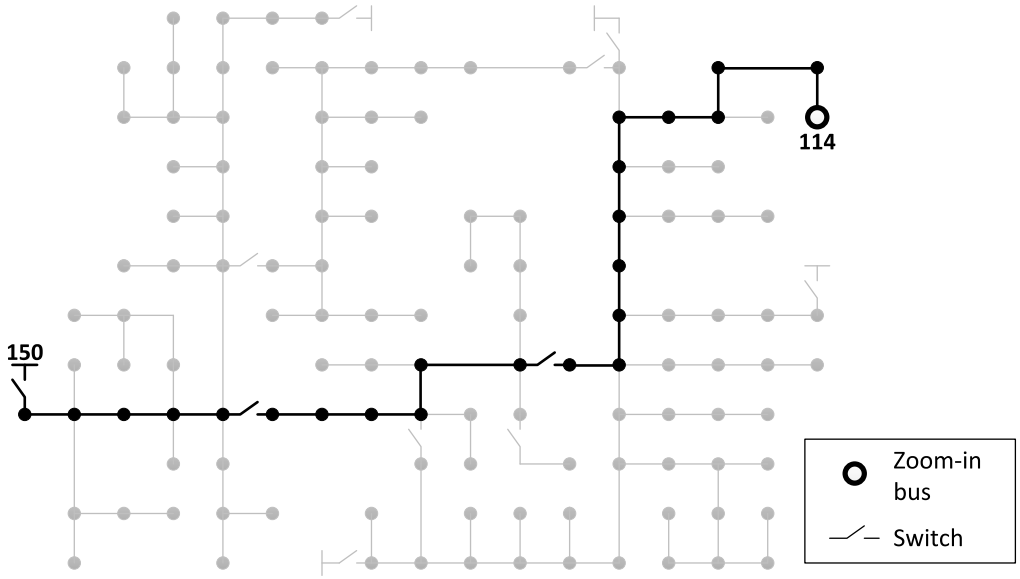

(b)

Figure 4.7: Configuration of the (a) IEEE 123-bus system and (b) the zone of interest of the IEEE 123-bus system, showing the zooming-in on bus 114. The greyed parts of the system represent the lumped laterals

The system parameters and load data of both systems are given in [76]. The proposed algorithm and the F/B method presented in [49] were each used to solve the DLF problem for the IEEE 37-bus and the IEEE 123-bus systems without voltage regulators. The results produced by the proposed algorithm were then compared to those obtained using the F/B method presented in [49].

Both methods were programmed in a MATLAB environment on a laptop with an Intel® Core™ i5 processor and 4GB of RAM. The DLF convergence tolerance was set to 10^{-4} p.u.

The IEEE 37-bus system source was bus 799; the zoom-in bus was set to bus 741 (the farthest bus). The proposed zooming algorithm includes in the DLF problem only buses in the zone of interest indicated in Figure 4.6(b). All of the system laterals extending from the zone of interest are lumped. On the other hand, the F/B method presented in [49] includes all of the system buses in the DLF problem. Figure 4.8(a) displays the DLF results for phase 'a' using the proposed algorithm and those using the F/B method presented in [49]. The maximum difference between the voltage magnitudes calculated for the buses of the zone of interest using the proposed algorithm and those computed with the F/B method presented in [49] is 0.000452 p.u. The DLF results of the zone of interest of the IEEE 37-bus system using the F/B method and the proposed zooming algorithm are given in details in Appendix B in Table B.1.

The IEEE 123-bus system was set to bus 150 and the zoom-in bus to bus 114 (the farthest bus). The zone of interest in the IEEE 123-bus system is shown in Figure 4.7(b). The DLF results for phase 'a' using the proposed DLF zooming algorithm and those using the F/B method presented in [49] were plotted as shown in Figure 4.8(b). The maximum difference between the voltage magnitudes calculated for the buses of the zone of interest using the proposed algorithm and those computed with the F/B method presented in [49] is 0.001977 p.u. The DLF results of the zone of interest of the IEEE 123-bus system using the F/B method and the proposed zooming algorithm are given in details in Appendix B in Table B.2.

For a 32-step voltage regulator with a range of ± 10 %, a one-step tap change of the regulator equals 0.006250 p.u. From a practical point of view, the resolution of the DLF solution should be less than this value. The maximum difference between the voltage magnitudes calculated by the proposed DLF zooming method and those computed by the F/B method presented in [49] is thus less than one tap change of the voltage regulator. The results produced by the proposed DLF zooming algorithm are therefore acceptable.

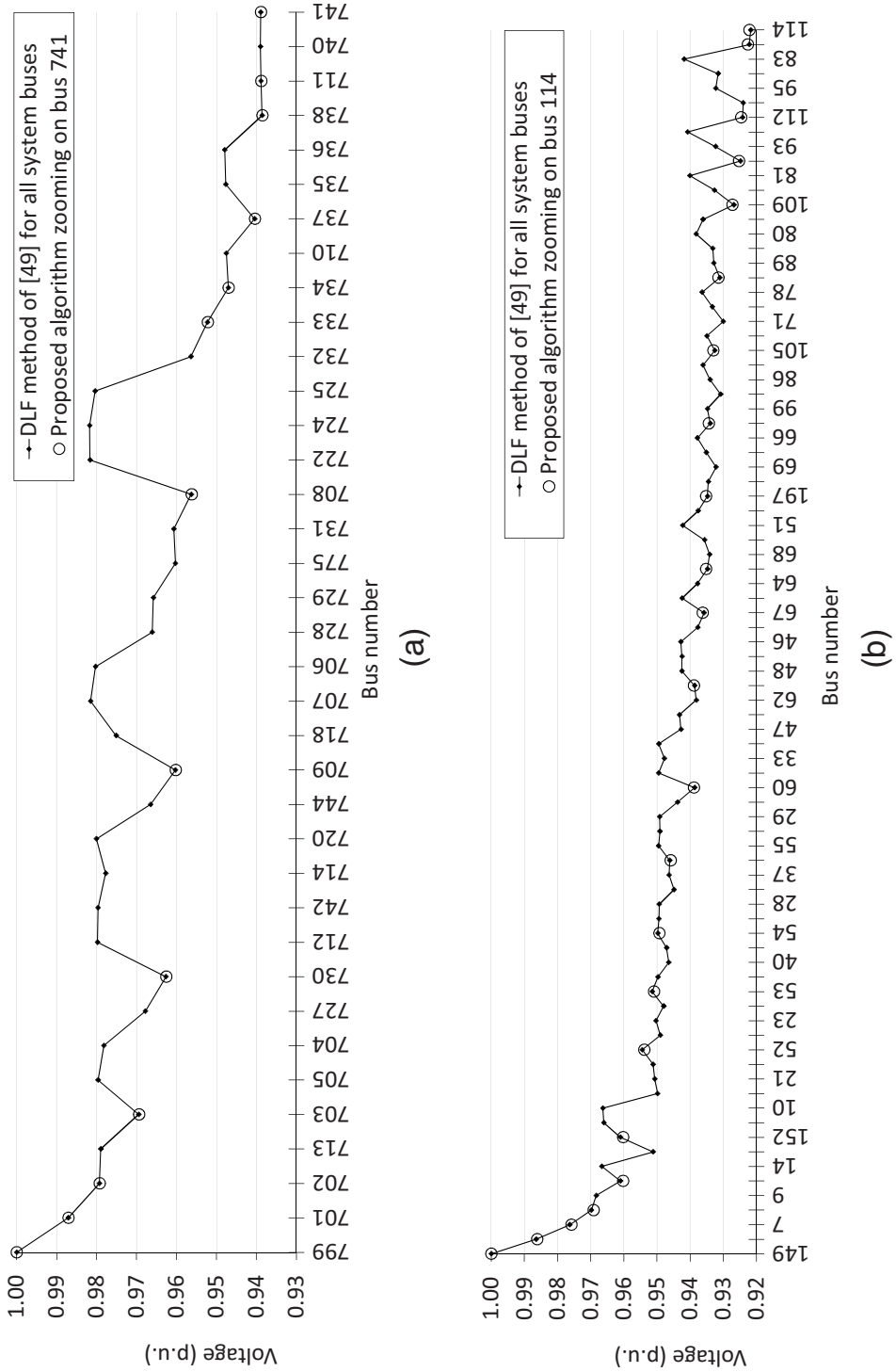

Figure 4.8: DLF results of phase 'a' using the method presented in [49] for all the system buses and using the proposed DLF zooming algorithm (zooming on the farthest bus). (a) The IEEE 37-bus system. (b) The IEEE 123-bus system

4.5.2 DLF Solution Speed Evaluation

The ability of the DLF algorithm for online implementations is dependent on the speed with which the DLF solution can be obtained. The primary advantage of the proposed algorithm is that it provides the DLF solution while reducing the problem size. The proposed algorithm thus minimizes the effect of system size on the time required for obtaining the DLF solution, which results in improved ability to interact with smart grid control systems.

Table 4.3 shows the effect of increasing the system size with respect to the number of iterations and the DLF solution time in the case of the proposed DLF zooming algorithm compared to those required with the F/B method presented in [49]. The source-buses of the IEEE 37-bus and 123-bus systems were set to buses 799 and 150, respectively. For the proposed algorithm, the zoom-in buses of the IEEE 37-bus and IEEE 123-bus systems were set to the farthest buses: 741 and 114, respectively. The reduced IEEE 37-bus and IEEE 123-bus systems are displayed in Figure 4.6(a) and Figure 4.7(a), respectively; the greyed portions represent the lumped laterals.

The results listed in Table 4.3 reveal that the number of iterations in the case of the F/B method presented in [49] is affected by increases in the system size. However, in the case of the proposed DLF zooming algorithm, the number of iterations remains the same. Expanded system size also creates a considerable increase in the solution time required for the F/B method presented in [49]. On the other hand, with the proposed algorithm, the increase in the solution time is insignificant. Compared to the F/B method presented in [49], the proposed method reduces the DLF solution time by 59.38 % in the case of the IEEE 37-bus system and by 94.5 % in the case of the IEEE 123-bus system. It can be observed that the percentage reduction in the DLF solution time increases as the number of

Table 4.3: Effect of increasing the system size on the results produced by the F/B method presented in [49] and the proposed zooming algorithm

	Number of iterations		DLF solution time (ms)	
System	[49]	Zooming	[49]	Zooming
IEEE-37	3	4	2.29	0.93
IEEE-123	4	4	22.20	1.22

system buses increases. This feature is of critical importance for integrating the zooming DLF algorithm in the management scheme for DG connection assessment, presented in Chapter 5, especially in distribution systems that involve a very large number of buses.

It should be emphasized that the results obtained with the proposed DLF zooming algorithm, as listed in Table 4.3, correspond to zooming in on the farthest bus. Zooming in on any other system bus results in a smaller DLF problem size and, consequently, a shorter solution time.

4.5.3 Network Topology Changes

Several factors can cause changes in the topology of a smart grid network, such as self-healing and optimal reconfiguration applications. The following case studies were designed for the investigation of the effect of changes in the network topology with respect to the time required for constructing the DLF problem using the proposed DLF zooming algorithm. The case studies were conducted on the IEEE 123-bus system. The system configuration is displayed in Figure 4.7(a); the system parameters and load profile are given in [76]. The topology of the IEEE 123-bus system is flexible due to two factors. First, the system is equipped with six switches that enable the network topology to be changed. Figure 4.7(a) indicates system switches numbered from A to F; these switches can be exploited to simulate the flexibility of a smart grid network topology. The second factor is the ability of the IEEE 123-bus system to be fed from one of five possible source buses. As indicated in Figure 4.7(a), the possible source buses are 150, 251, 350, 451, and 195. In a smart grid context, these possible sources could represent connections to renewable DG sources.

Case 1: System Reconfiguration

Table 4.4 shows the normal conditions and the reconfiguration conditions of the IEEE 123-bus system switches. The conditions of four switches were changed for the system reconfiguration. The time required for the proposed DLF zooming algorithm to build the PC matrix of the reconfigured system is only 72.9 ms.

Case 2: Zoom-in Bus or Source-Bus Changes

The effect of changing the zoom-in bus with respect to the time required for the construction of the DLF problem was examined for the IEEE 123-bus system shown in Figure 4.7(a). The DLF zooming algorithm was first run with the same source bus while the zoom-in bus

Table 4.4: IEEE 123-bus system switches for the system reconfiguration

Switch	Normal condition	Reconfiguration condition
A	Closed	Open
B	Closed	Closed
C	Open	Closed
D	Closed	Open
E	Open	Closed
F	Closed	Closed

was changed from 114 to 85. The execution time for constructing the DLF problem in this case is 5.6 ms. When both the source bus and the zoom-in bus are changed from 150 and 114 to 350 and 96, respectively, the execution time is 78.5 ms. It can be observed that the total DLF solution time for the IEEE 123-bus system is still significantly small even after the DLF solution time, as listed in Table 4.3, is added to the time required for the construction of the DLF problem.

4.6 Summary

This chapter presents a novel zooming algorithm for DLF analysis in smart grids. This algorithm can solve the DLF problem for a specific zone of interest in the distribution system without the necessity of including all of the system buses in the DLF problem. This feature is utilized in the DG connection online assessment, presented in Chapter 5, to manage the curtailment of DG sources located in a specific area of interest without considering all the DG sources in the system. The algorithm can effectively reduce the size and solution time associated with the DLF problem. The simulation results show that the solution time significantly decreases as the size of the distribution system increases. The significant reduction in DLF solution offered by the zooming algorithm enables the online implementation of the DG connection assessment. The construction of the DLF problem in the algorithm involves a novel automated recursive process that is performed online without the use of any manual numeration techniques. The algorithm therefore enables fast accommodation of the continual changes in network topology of a smart grid. This automated feature thus facilitates the integration of the zooming algorithm in the proposed management scheme for DG connection online assessment, as presented in Chapter 5.

Chapter 5

A Management Scheme for Online Assessment of DG Connection in Smart Grids

5.1 Introduction

This chapter presents a management scheme for DG connection online assessment in smart grids. The work presented in this chapter builds on the techno-economic planning model presented in Chapter 3. As discussed earlier, the output power of each DG unit is assumed to include two components: unconditional and conditional. The unconditional DG component is injected into the system without curtailment. The conditional DG component is subject to curtailment based on the online condition of the distribution system.

The unconditional and conditional components are calculated using the techno-economic planning model, presented in Chapter 3. This model ensures that the IRR of a DG project is higher than the $MARR$ even with the application of DG curtailment. The goal of the proposed management scheme presented in this chapter is to control the curtailment of the conditional DG components in the distribution system. The curtailment is controlled based on an online assessment of the impact of injecting the conditional DG components on the system performance.

The management scheme is implemented based on a novel scalable optimization model. The scalable model minimizes the curtailment of the DG power by solving the optimization problem in a specific zone of interest in the distribution system without the necessity of

including the entire distribution system in the problem. The proposed management scheme utilizes the DLF zooming algorithm, presented in Chapter 4, for obtaining the DLF solution in the zone of interest. The zone of interest is determined in the management scheme based on the locations of buses and/or lines which suffer from violations to the system constraints, such as overvoltage, voltage unbalance, and reverse power flow.

This chapter is organized as follows: In Section 5.2, the proposed management scheme is presented. The determination of the zone of interest is given in Section 5.2.1, and the formulation of the proposed scalable optimization problem and the application of the DLF zooming algorithm are presented in Section 5.2.2. The simulation results validate the online operation of the proposed management scheme, as presented in Section 5.3. A summary is presented in Section 5.4.

5.2 Proposed Management Scheme

The flowchart of the proposed management scheme is shown in Figure 5.1. It is assumed that the DG sources and system loads are equipped with smart automatic meter reading (AMR) devices. The first step is to read the smart metering data and solve the DLF problem with the inclusion of all system buses and with no DG power curtailment. Constraints on overvoltage, voltage unbalance and reverse power flow are then evaluated. If none is violated, then all of the DG units will be allowed to operate without curtailment. Otherwise, if at least one of the constraints is violated, the management scheme specifies a zone of interest that includes the DG units that have the most influence on the constraints that have been violated. The process for determining the zone of interest is discussed in section 5.2.1. The proposed scalable optimization model then minimizes the power curtailment for the DG units included in the zone of interest based on the online condition of the distribution system. The final step is to use the calculated values of the curtailed DG power to obtain the permitted output DG power.

The proposed management scheme consists of two parts: the determination of the zone of interest and the formulation of the scalable optimization model problem. The details of each part are explained in the next two subsections.

5.2.1 Determination of the Zone of Interest

The primary goal of determining the zone of interest is to reduce the number of variables in the scalable optimization problem. The detection of the zone of interest is based on an

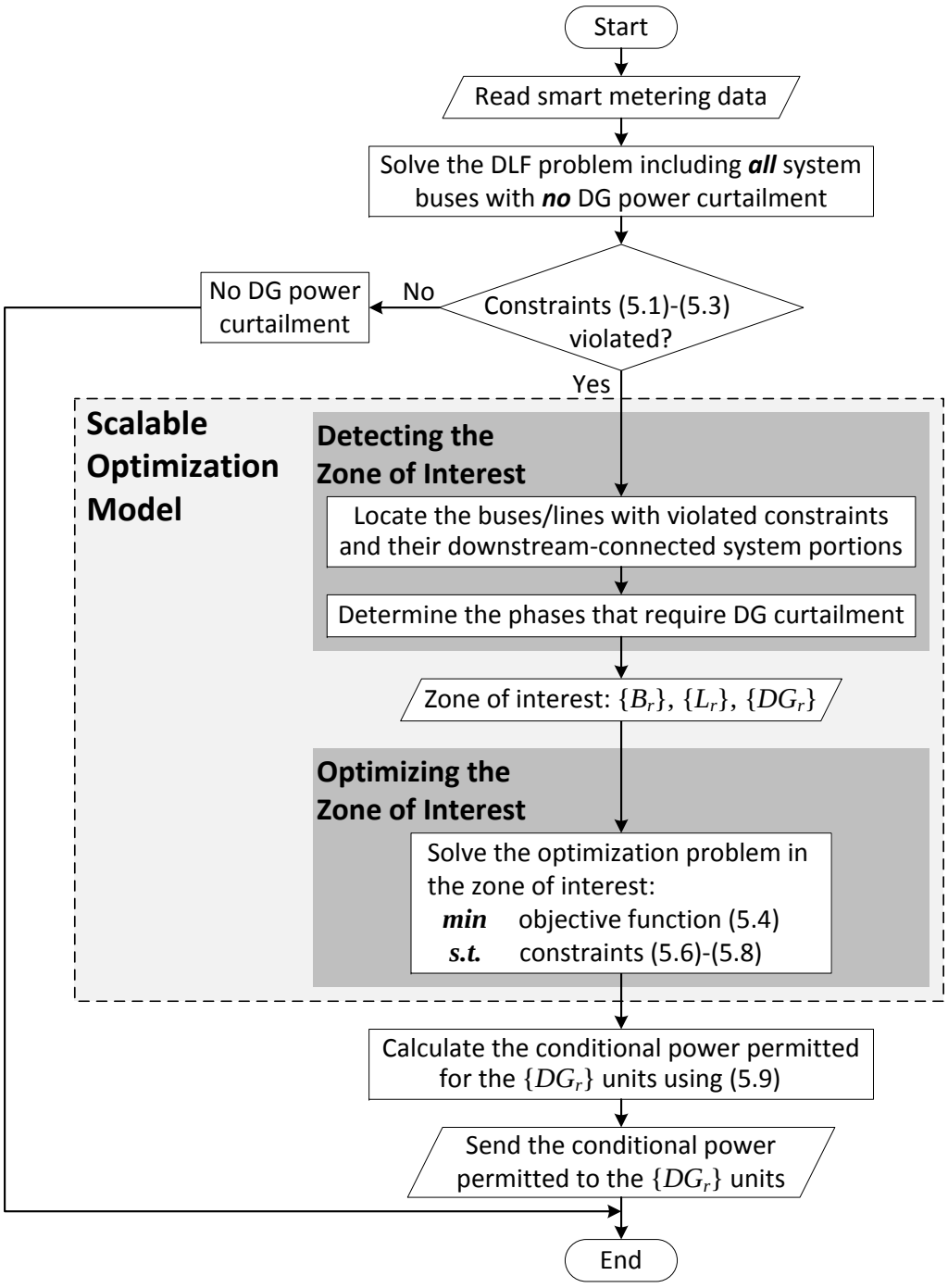

Figure 5.1: Flowchart of the proposed management scheme

evaluation of the constraints (5.1)-(5.3). The zone of interest includes only DG units that have the most influence on any violation in these constraints.

1- Voltage Constraints:

$$V_{min} \leq |V_{i_x}| \leq V_{max}, \quad \forall i \in B \tag{5.1}$$

where V_{i_x} is the voltage of phase x at bus i, $x \in \{a, b, c\}$; V_{min} and V_{max} are the minimum and maximum allowable system voltages, respectively; and B is the set of buses in the distribution system.

2- Reverse Power Flow Constraints

$$|P_{rev-l_x}| < P_{rev-l_{x_{max}}}, \quad \forall l \in L \tag{5.2}$$

where P_{rev-l_x} is the active reverse power flow of phase x of line l, $P_{rev-l_{x_{max}}}$ is the maximum allowable active reverse power flow of phase x of line l, and L is the set of lines in the distribution system.

3- Voltage Unbalance Constraints

$$UB_i < UB_{max}, \quad \forall i \in B_{3ph} \mid B_{3ph} \subset B \tag{5.3}$$

where UB_i is the voltage unbalance index of bus i, UB_{max} is the maximum allowable voltage unbalance index, and B_{3ph} is the set of 3-phase buses in the distribution system. The voltage unbalance index at any bus i is given by (3.16) and (3.17).

In radial systems, constraints (5.1)-(5.3) can be violated by increases in the output power of the DG units, especially under minimum load conditions. These violations can therefore be corrected by curtailing the DG output power feeding the locations where the constraints have been violated. If a constraint is violated at a specific bus or line in a radial system, the zone of interest includes all of the system portions that are connected downstream at that bus or line. The downstream-connected portions of the system were chosen as the zone of interest because they include all of the DG units that can feed any possible reverse power to the location where the constraint was violated. Determining the downstream-connected portions of the system at any bus is performed using the PC matrix of the system as described in Section 4.3.1.

The process for determining the zone of interest consists of two steps. The first step is to locate the buses and/or lines with violated constraints. For each of these buses and/or lines, the downstream-connected portions of the system are identified. For example, Figure 5.2 shows a simple radial system. Assuming the voltage constraint in (5.1) is violated at bus 4

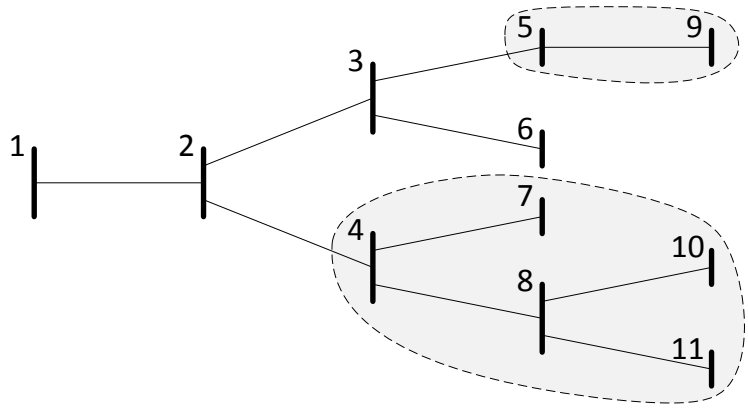

Figure 5.2: Simple radial distribution system, the shaded portions denote the zone of interest

and the unbalance constraint in (5.3) is violated at bus 5, the zone of interest in this case includes buses 4 and 5 in addition to the system portions fed by buses 4 and 5. This zone of interest is shaded in grey in Figure 5.2.

The second step is to ascertain the phases that can be excluded from the zone of interest. Constraints (5.1)-(5.3) are utilized as a means of determining the excluded phases. In a distribution system with high DG penetration, constraint (5.1) can be violated in the case of overvoltage due to reverse power flow, which is typically caused by high DG output under minimum load conditions. A violation of constraint (5.1) can be remedied by curtailing the output power of the DG units connected to the phase where the overvoltage is occurring. Only the phase that has a phase voltage higher than V_{max} is therefore included in the zone of interest; other phases are excluded.

High reverse power can result in violation of constraint (5.2). As with constraint (5.1), this type of violation requires power curtailment of the DG units connected to the phase that has an active reverse power flow higher than the maximum allowable active reverse power flow $P_{rev-l_{x_{max}}}$. Therefore, only phases with active reverse power flow higher than $P_{rev-l_{x_{max}}}$ are included in the zone of interest.

A violation of constraint (5.3) can be corrected by reducing the difference between the phase voltages and their average, which is calculated according to (3.17). This reduction can be achieved by curtailing the output power of the DG units connected to the phases whose phase voltages are higher than $V_{i_{avg}}$. Only phases with a phase voltage higher than $V_{i_{avg}}$ are thus included in the zone of interest.

5.2.2 Formulation of the Scalable Optimization Model Problem

The proposed problem formulation is scalable because the problem can be changed so that the size and number of variables reflect the set of system DG units, buses, and lines contained in the detected zone of interest. The problem is solved using GA. The goal of the objective function is to minimize the curtailment of the DG power; the problem formulation is as follows:

Objective function:

$$\min \sum_{dg} P_{cur_{dg}}, \quad \forall dg \in DG_r \mid DG_r \subset DG \tag{5.4}$$

where $P_{cur_{dg}}$ is the curtailed active power of the DG unit dg, DG is the set of DG units in the distribution system, and DG_r is the set of DG units with conditional components in the interest-zone.

Subject to:

1- Economic Constraints

The decision variables of the optimization problem are the curtailed power of the DG units in the zone of interest. The maximum curtailed power of each DG unit is limited to its conditional DG component. This approach guarantees the DG project is economically feasible when power curtailment is in place.

For example, as shown in the economic model results in Table 3.6 in Chapter 3, a 10 kW rooftop PV DG has an unconditional component of 85 %. For this case, substituting in (5.5), the maximum curtailed power is limited to 15 % of the DG output power. On the other hand, the unconditional component is 100 % for rooftop PV DG sources less than 7 kW. For this case, substituting in (5.5), the maximum curtailed power is zero. In other words, rooftop PV DG sources less than 7 kW are not subject to curtailment.

Limiting the maximum curtailed power using this approach ensures no power is curtailed from the unconditional DG component, which guarantees that the IRR is higher than the $MARR$ as discussed in Chapter 3. This constraint is formulated according to the following equation:

$$0 \leq P_{cur_{dg}} \leq (1 - \beta_{dg})\, P_{dg}, \quad \forall dg \in DG_r \mid DG_r \subset DG \tag{5.5}$$

where β_{dg} is the unconditional DG components of the output power of DG unit dg, calculated as described in Chapter 3. The term $(1 - \beta_{dg})$ corresponds to the conditional DG component of the output power of the DG unit dg, and P_{dg} is the output power of the DG unit dg.

2- Load Flow and Voltage Regulator Constraints

Consideration of these constraints is achieved by solving the DLF problem for the population of each GA offspring, in a manner similar to that explained in Section 3.3 in the proposed techno-economic planning model presented. However, rather than solving the DLF problem for the entire distribution system as in Section 3.3, the zooming DLF algorithm presented in Chapter 4 is employed. This algorithm enables the DLF problem to be solved for the zone of interest alone, a feature that can increase the speed of the optimization process, especially given that DLF solutions are required for the entire population of each GA offspring.

3- Voltage Constraints

$$V_{min} \leq |V_{i_x}| \leq V_{max}, \quad \forall i \in B_r \mid B_r \subset B \tag{5.6}$$

where V_{i_x} is the voltage of phase x at bus i, $x \in \{a, b, c\}$; V_{min} and V_{max} are the minimum and maximum allowable system voltages, respectively; B is the set of buses in the distribution system; and B_r is the set of buses in the zone of interest.

4- Reverse Power Flow Constraints

$$|P_{rev-l_x}| < P_{rev-l_{x_{max}}}, \quad \forall l \in L_r \mid L_r \subset L \tag{5.7}$$

where P_{rev-l_x} is the active reverse power flow of phase x of line l, $P_{rev-l_{x_{max}}}$ is the maximum allowable active reverse power flow of phase x of line l, L is the set of lines in the distribution system, and L_r is the set of lines in the zone of interest.

The value of $P_{rev-l_{x_{max}}}$ should be set by the DNO. In the presented analysis, this value was set to 30 % of the capacity of the line l.

5- Voltage Unbalance Constraints

$$UB_i < UB_{max}, \quad \forall i \in B_{r_{3ph}} \mid B_{r_{3ph}} \subset B_r \text{ and } B_r \subset B \tag{5.8}$$

where UB_i is the voltage unbalance index of bus i, UB_{max} is the maximum allowable voltage unbalance index, B_{3ph} is the set of 3-phase buses in the distribution system, and $B_{r_{3ph}}$ is the set of 3-phase buses in the zone of interest. The voltage unbalance index at any bus i is given by (3.16) and (3.17).

It should be emphasized that constraints (5.6)-(5.8) are different from constraints (5.1)-(5.3). This is because constraints (5.6)-(5.8) are applied only in the determined zone of interest. On the other hand, constraints (5.1)-(5.3) are applied in the entire system as means of ascertaining during the DG planning phase the maximum number of DG units that can be installed.

As shown in Figure 5.1, the management scheme sends the DG the amount of conditional power permitted after the optimization problem has been solved for the zone of interest. The permitted output DG power is calculated as follows:

$$P_{permitted_{dg}} = P_{dg} - P_{cur_{dg}}, \quad \forall dg \in DG_r \mid DG_r \subset DG \tag{5.9}$$

The proposed scalable optimization model utilizes GA to find the minimize DG curtailment in the system. In addition to the advantages of using GA discussed in Section 3.3, GA allows for determining satisfactory feasible solutions in a timely manner. This can be achieved by setting a time limit for the solving optimization problem. This time limit should be less than the sampling period of the smart meters in the system (typically 15 min).

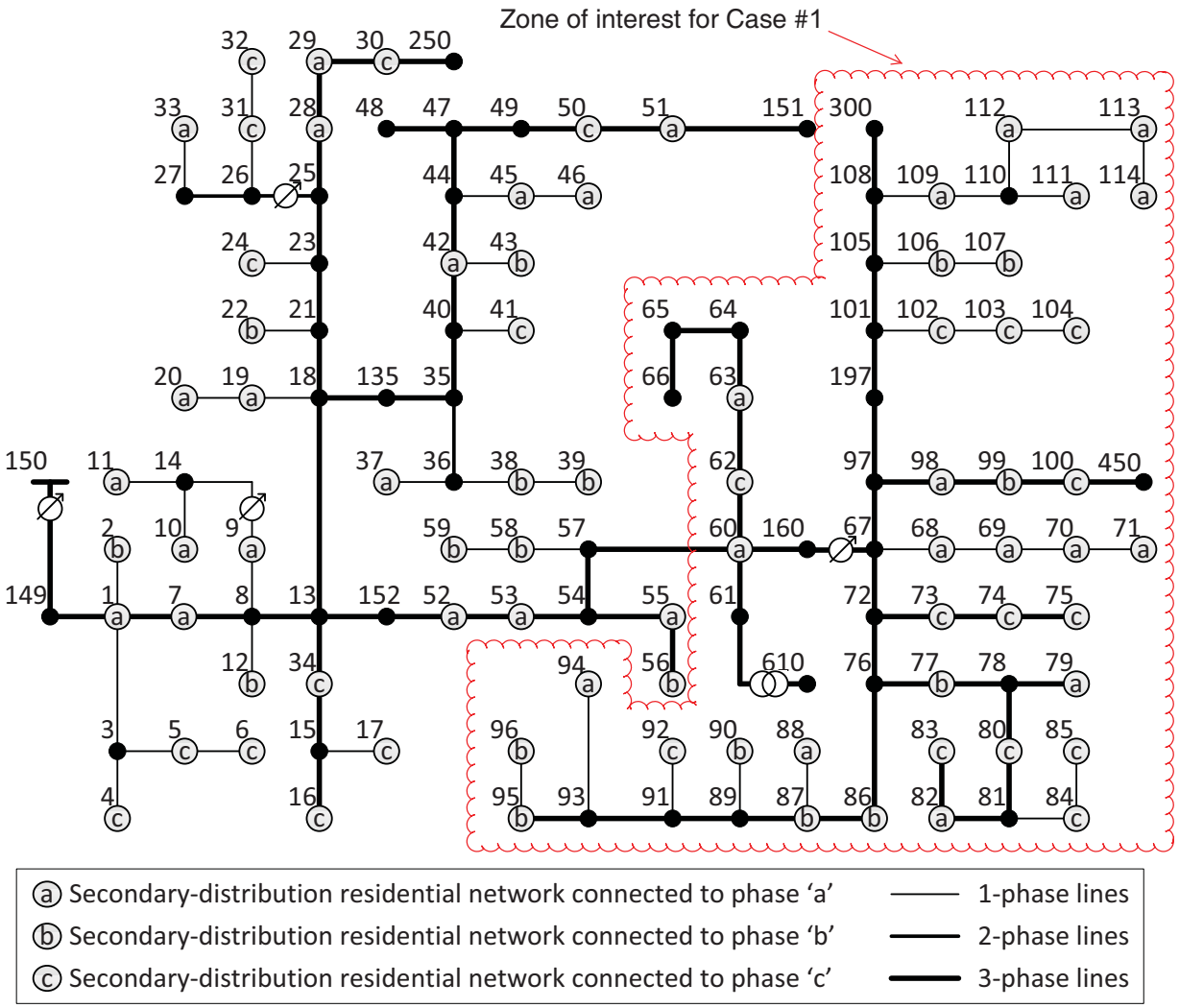

Figure 5.3: Single-line diagram of the modified IEEE 123-bus system, indicating the locations and phases of the 77 secondary-distribution residential networks. The zone of interest for Case #1 is indicated.

5.3 Simulation Results

The simulation results evaluates the performance of the proposed management scheme for DG connection online assessment. The management scheme was applied on a system with high PV DG penetration level. The simulation results include two test cases. In Case #1, the system is simulated during a Winter day. The system suffers from voltage unbalance in this test case. In Case #2, the system is simulated during a Summer day. The system in this test case suffers from reverse power flow.

The system under study is described in the next subsection. The simulation results for Case #1 and Case #2 are then presented in the two following subsections.

5.3.1 System Description

The modified IEEE 123-bus system, shown in Figure 5.3, was used for the evaluation of the proposed online assessment scheme. This system is the same system used in Chapter 3 for evaluating the proposed techno-economic planning model. The system is descried in Section 3.4. It has 77 240-120 V single-phase secondary-distribution residential networks. The layout of a 240-120 V single-phase secondary-distribution residential network is shown in Figure 5.4. Each network is supplied by a 50 kVA single-phase pole-mounted distribution transformer with a 1.9 % impedance. The locations of the 77 single-phase secondary-distribution residential networks in the IEEE 123-bus are indicated in Figure 5.3. Each network feeds 12 houses using 1/0 AWG ACSR overhead distribution feeders.

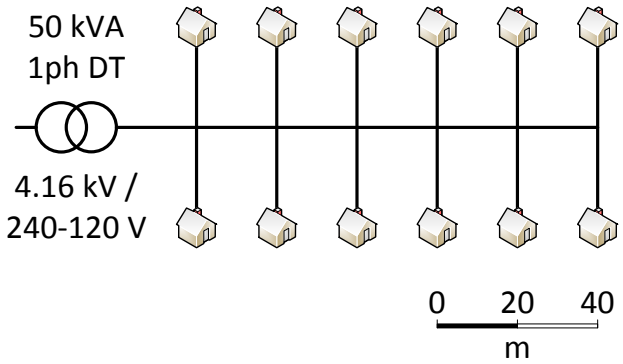

Figure 5.4: Configuration of a 240-120 V secondary-distribution residential network

All of the DG units in the system under study are assumed to be single-phase rooftop 10 kW PV DG units. The DG units are installed in the secondary-distribution residential

networks, shown in Figure 5.4. As presented in Table 3.6, the unconditional component for a 10 kW DG unit equals 85 %, and the conditional DG component equals 15 %.

The IEEE 123-bus test system was assumed to include the maximum number of installed single-phase rooftop PV DG as calculated in Scenario #3 in Section 3.4.2. In this scenario, the techno-economic planning model, proposed in Chapter 3, was applied in order to maximize the number of rooftop PV DG 10 kW units. The maximum number of PV DG units that can be installed in Scenario #3 is 286 units. The locations of the 286 PV DG units as calculated in Scenario #3 are given in Table 3.8. The DG units are assumed to be randomly located in the 240-120 V secondary-distribution residential network.

The PV DG units are modeled as PQ buses, as discussed in Section 2.5.3. The PV DG active output power is calculated based on the solar irradiance and the PV cell temperature. The PV DG reactive output power is set to zero. The parameters of the PV panel were obtained from the data sheet of the 250 W polycrystalline solar panel described in [88]. The DG output power is calculated as follows:

$$P_{dg} = N_s N_p \; V_{mp} I_{mp} \; \eta \tag{5.10}$$

where N_s and N_p are the numbers of series and parallel PV modules, respectively; V_{mp} and I_{mp} are the PV panel voltage and current at maximum power, respectively; and η is the overall efficiency of the DG PV inverter.

The value of $N_s N_p$ in (5.10) was set to 40 in order to obtain a 10 kW PV DG capacity using the 250 W polycrystalline solar panels. The efficiency η in (5.10) was set to 95 %.

The PV panel voltage and current at maximum power are obtained from

$$V_{mp}(T, G) = \; V^0_{mp} \; LIC_{V_{mp}} \; [1 - TC_{V_{mp}}(25^\circ - T)] \tag{5.11}$$

$$I_{mp}(T, G) = \; I^0_{mp} \; LIC_{I_{mp}} \; [1 - TC_{I_{mp}}(25^\circ - T)] \tag{5.12}$$

where T is the PV cell temperature in °C; G is the solar irradiance in W/m^2; $LIC_{V_{mp}}$ and $LIC_{I_{mp}}$ are the light intensity coefficients of V_{mp} and I_{mp}, respectively; $TC_{V_{mp}}$ and $TC_{I_{mp}}$ are the temperature coefficients of V_{mp} and I_{mp}, respectively; V^0_{mp} and I^0_{mp} are the values of V_{mp} and I_{mp} , respectively, at standard test conditions (G = 1000 W/m^2 and T = 25°C).

The system under study is assumed to be located in Mississauga, Ontario, Canada. The weather data were obtained from [89]. Figure 5.5 shows the hourly variations in the temperature, solar irradiance, and PV DG output power for a Summer day and a Winter day.

The residential loads in the system under study are assumed to follow the four-season daily load profiles given in [77] for a house in Canada and to have a lagging power factor of 0.9. The Summer and Winter daily load profiles are displayed in Figure 5.6.

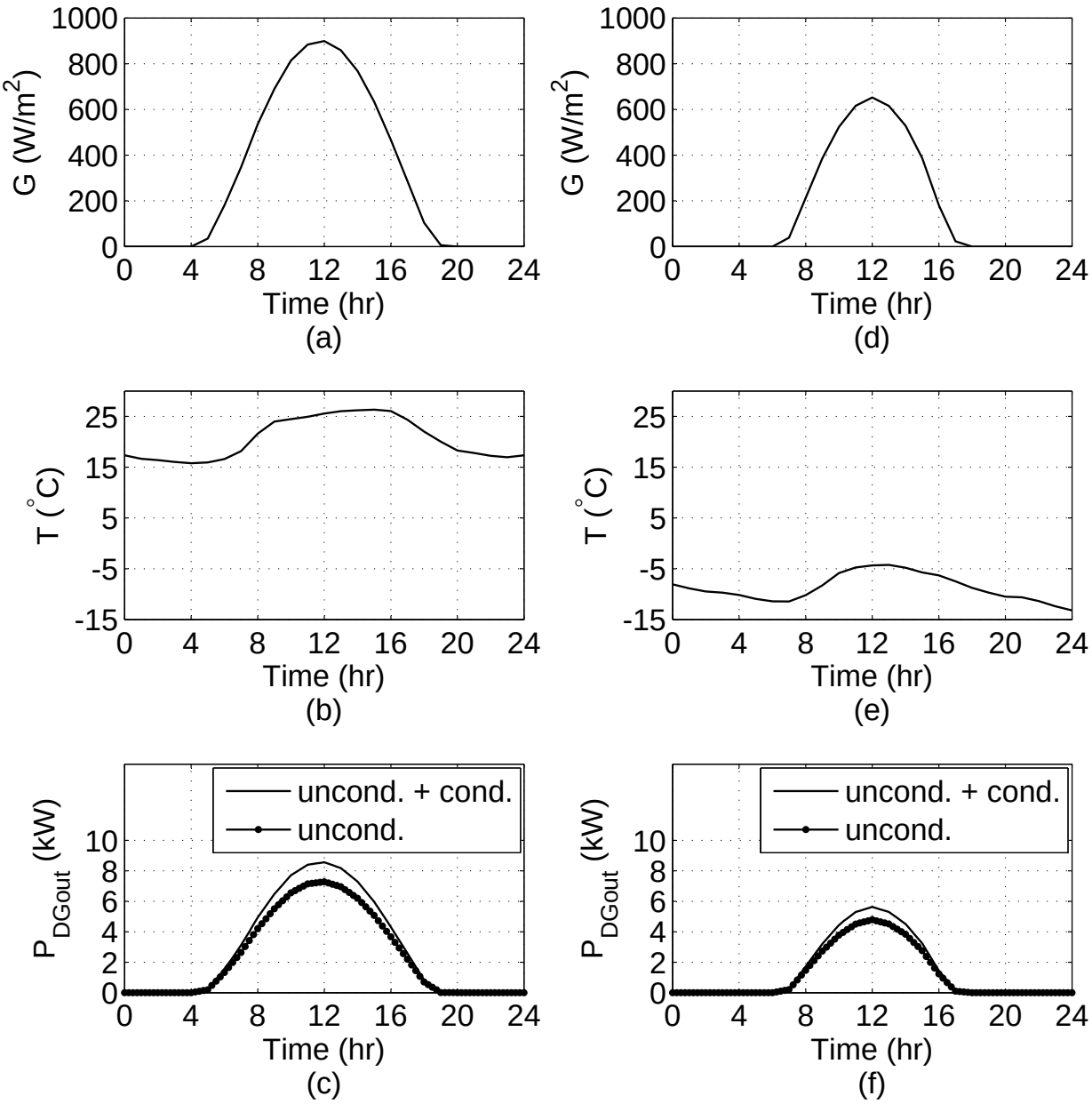

Figure 5.5: Hourly variations in (a) the temperature, (b) solar irradiance, and (c) PV DG output power for a Summer day; and (d) the temperature, (e) solar irradiance, and (f) PV DG output power for a Winter day. The unconditional power in (c) and (f) equals 85 % of the total output PV DG power.

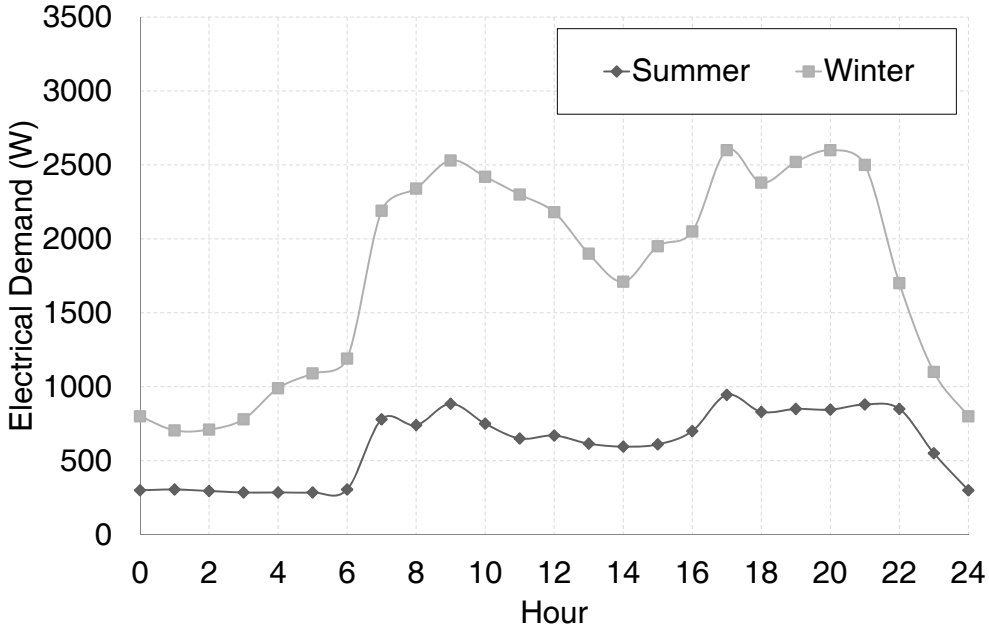

Figure 5.6: Summer and Winter daily residential load profiles given in [77] for a house in Canada

All loads and DG units in the system under study are assumed to be equipped with smart meters that have a sampling period of 15 min. The system was simulated in a MATLAB environment on a PC with an Intel® Core™ i7 2.8 GHz processor and 8 GB of RAM.

5.3.2 Case #1: Simulation Results for a Winter Day

In this case, the system was tested during a Winter day. The hourly variations in the temperature, solar irradiance, and PV DG output power are shown in Figure 5.5(d)-(f), respectively. The daily residential load profile for the Winter season is displayed in Figure 5.6.

The annual peak load in the system under study occurs in the Winter, as shown in the four-season load profile shown in Figure 3.3. The load in the system under study is highly unbalanced. Installing the 286 single-phase PV DG units adds more unbalance to the system. As a result, this test case represents a worst-case scenario regarding voltage unbalance.

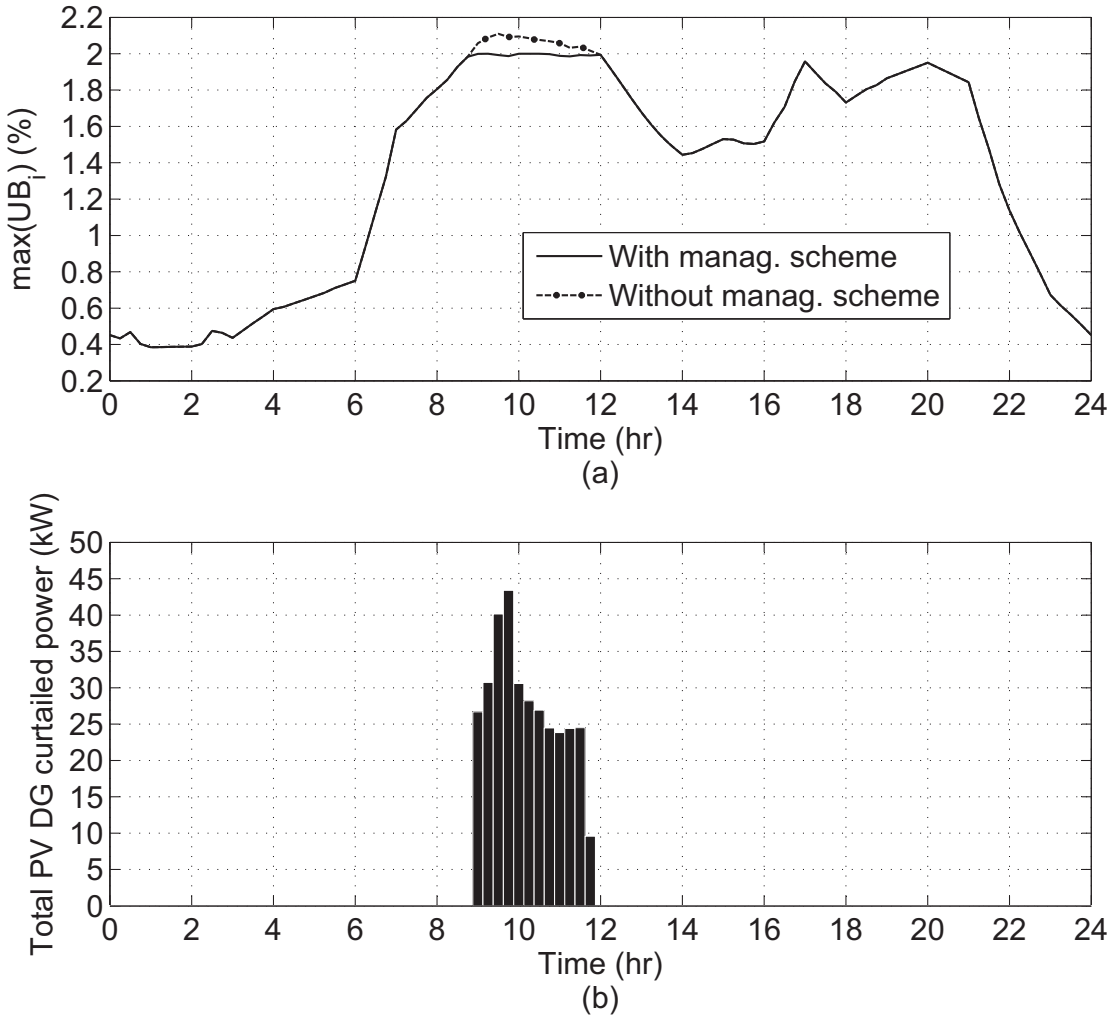

Figure 5.7: Hourly variations in (a) the maximum voltage unbalance with and without the proposed management scheme and (b) the total curtailed PV DG power in the system using the proposed management scheme during a Winter day

The proposed management scheme was executed every 15 min: an interval selected to be equal to the sampling period of the smart meters in the system. The first step in the management scheme is to determine the zone of interest and the phases that require DG curtailment. The results of the DLF algorithm calculated for all of the system buses are employed in order to identify any violated constraints. As shown in Figure 5.7(a), the voltage unbalance in the system exceeds 2 % from 9:00 AM to 11:45 PM. Next, the management scheme

locates the buses with a violated voltage unbalance, which are {60,61,62,63,65,66,160,610}, and then identifies which phases should be included in the zone of interest. For the voltage unbalance in the system under study, the phase voltages of phases b and c are higher than the average voltage calculated according to (3.17). The voltage unbalance can therefore be corrected by curtailing the output power of the DG units connected only to phases b and c in the zone of interest. The scalable optimization problem is then solved for the zone of interest. The zone of interest in this case includes all the DG units connected to phases b and c in the system portion fed from bus 60. The number of the DG units in the zone of interest is 105 units. The zone of interest for Case #1 is indicated in Figure 5.3. The final step is the calculation of the conditional power permitted, and the sending of this information to the DG units in the zone of interest.

The voltage unbalance with the proposed management scheme is indicated by the solid line in Figure 5.7(a). The voltage unbalance was successfully restored to 2 %. The total PV DG curtailed power is shown in Figure 5.7(b). The hourly variations in the maximum and minimum values for the voltage in all system buses were plotted as shown in Figure 5.8. The hourly variations in the maximum percentage reverse power in the system are shown in Figure 5.9. It can be observed from Figures 5.8 and 5.9 that the system voltage and reverse power flow are maintained within operational limits during the DG curtailment.

The smart meter sampling period can be considered as the temporal resolution of the management scheme. Reducing the smart meter sampling period can reduce any possible constraint violations in the system within the smart meter sampling period, and hence

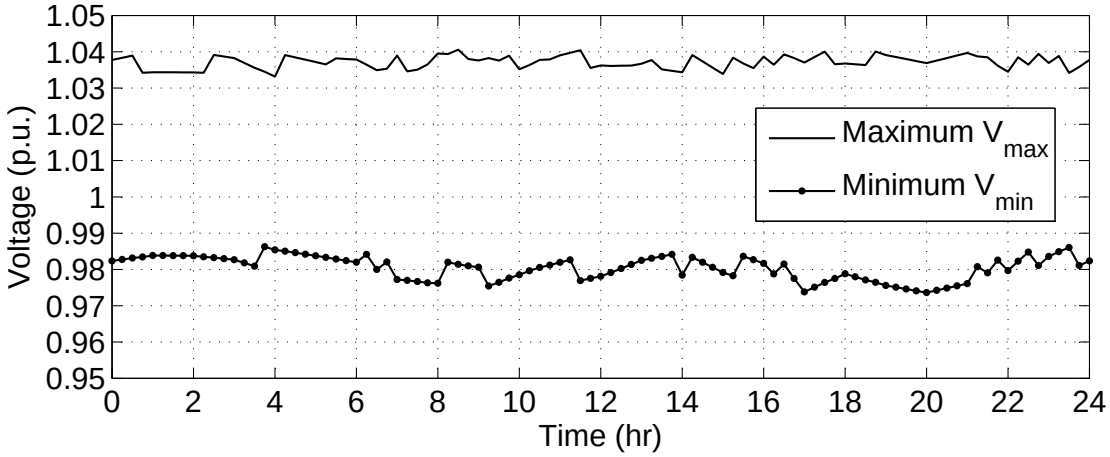

Figure 5.8: Hourly variations in the maximum V_{max} and the minimum V_{min} of the system using the proposed management scheme during a Winter day

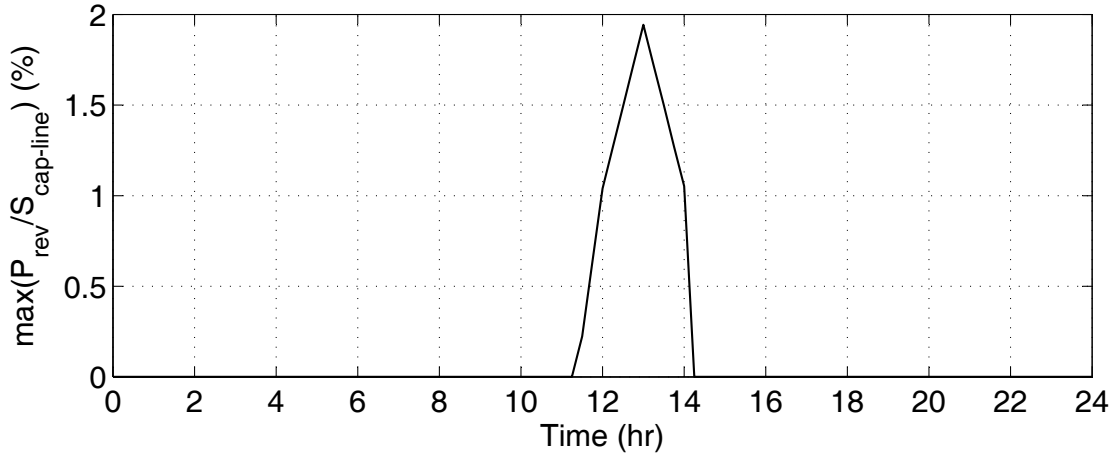

Figure 5.9: Hourly variations in the maximum percentage reverse power in the system using the proposed management scheme during a Winter day

improve the operation of the management scheme. The proposed management scheme can be executed at least for once each smart meter sampling period (15 min). The times required for the execution of the management scheme are shown in Figure 5.10. The average execution time is about 4 min, which is shorter than the smart meter sampling period. These results represent a worst-case scenario with respect to the execution time because

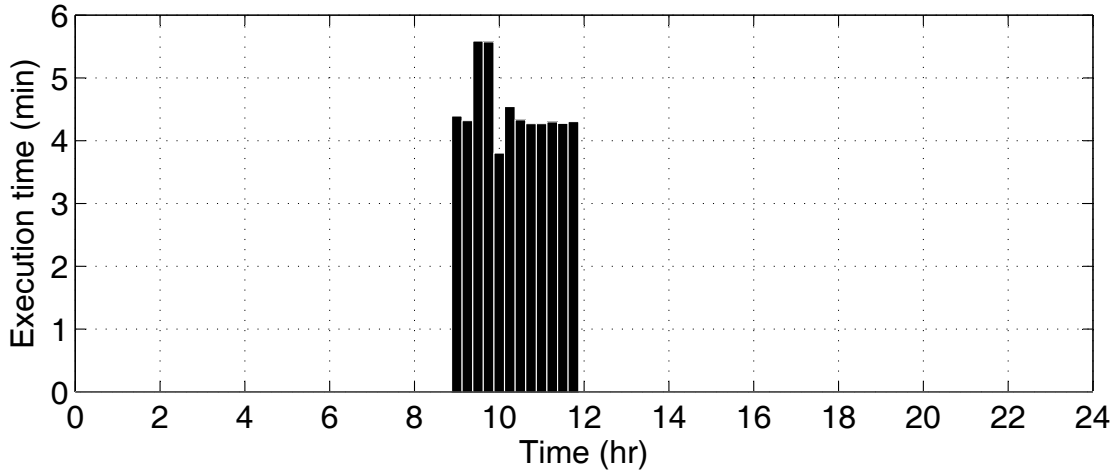

Figure 5.10: Times required for the execution of the management scheme, which runs every 15 min, during a Winter day

they were obtained for the system under study with the maximum DG capacity installed. Reducing the number of DG units installed will decrease the size of the optimization problem and thus shorten the required execution time. The results produced by the proposed management scheme therefore indicate its suitability for online operation.

Figure 5.11 shows the total generation of the 286 PV DG units in the system during the Winter day. The dotted line shows the total generated PV DG power from the conditional DG components. The broken line indicates the total generated PV DG power without implementing the management scheme, i.e. without curtailment. The solid line indicates the total generated PV DG power with implementing the management scheme, i.e. with curtailment.

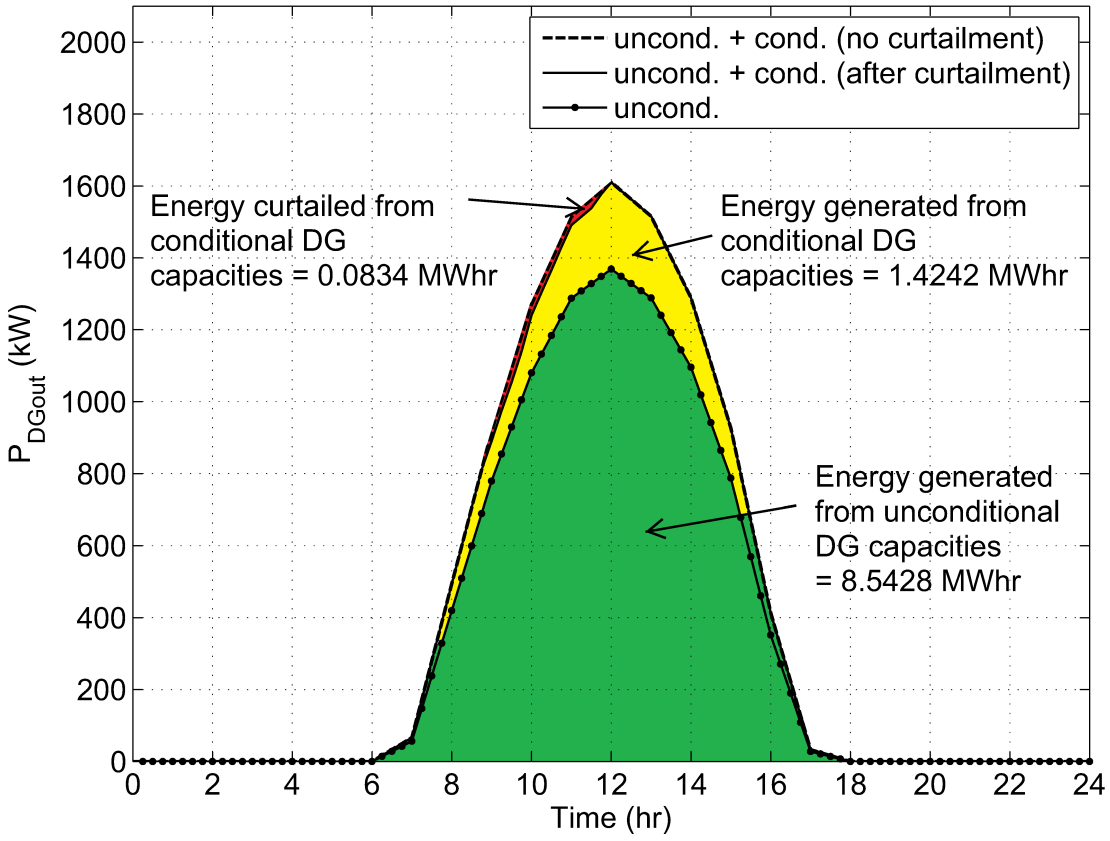

Figure 5.11: Total generated power from the 286 PV DG units during a Winter day

The total energy that can be generated from the unconditional and unconditional components of the 286 PV DG units is 10.05 MWhr during the Winter day. This total energy equals the total area in Figure 5.11. The total energy can be divided into the following three parts:

1. The energy generated from the unconditional DG components (the green area in Figure 5.11). This energy equals 8.5428 MWhr, which is equivalent to 85 % of the total energy.

2. The energy generated from the conditional DG components (the yellow area in Figure 5.11). This energy equals 1.4242 MWhr, which is equivalent to 14.171 % of the total energy. Since the conditional capacity is subject to curtailment, this energy is less than 15 % of the total energy.

3. The energy curtailed from the conditional DG components (the red area in Figure 5.11). This energy equals to 0.0834 MWhr, which is equivalent to 0.830 % of the total energy. This curtailed energy is equivalent to 5.532 % of the total energy that can be curtailed from the conditional DG components in the system.

5.3.3 Case #2: Simulation Results for a Summer Day

In this case, the system was tested during a Summer day. The hourly variations in the temperature, solar irradiance, and PV DG output power are shown in Figure 5.5(a)-(c), respectively. The daily residential load profile for the Summer season is displayed in Figure 5.6.

This test case represents a worst-case scenario for systems equipped with PV DG generation. Typically, the system loading is minimum and the PV DG generation is maximum during Summer. As a result, there is a high possibility of reverse power flow in the system. Reverse power flow can increase system losses and cause system overvoltage.

Figure 5.12(a) shows the hourly variations in the maximum reverse power flow with and without the proposed management scheme. The reverse power flow is expressed as a percentage from the line capacity. According to the reverse power flow constraint in (5.7), the maximum allowable percentage is 30 %.

As shown in Figure 5.12(a), the reverse power flow in the system exceeds 30 % from 10:45 AM to 1:15 PM. The management scheme locates the lines that violate the reverse power flow constraint. These lines are {150-149, 149-1, 1-7, 7-8, 8-13}. As shown in

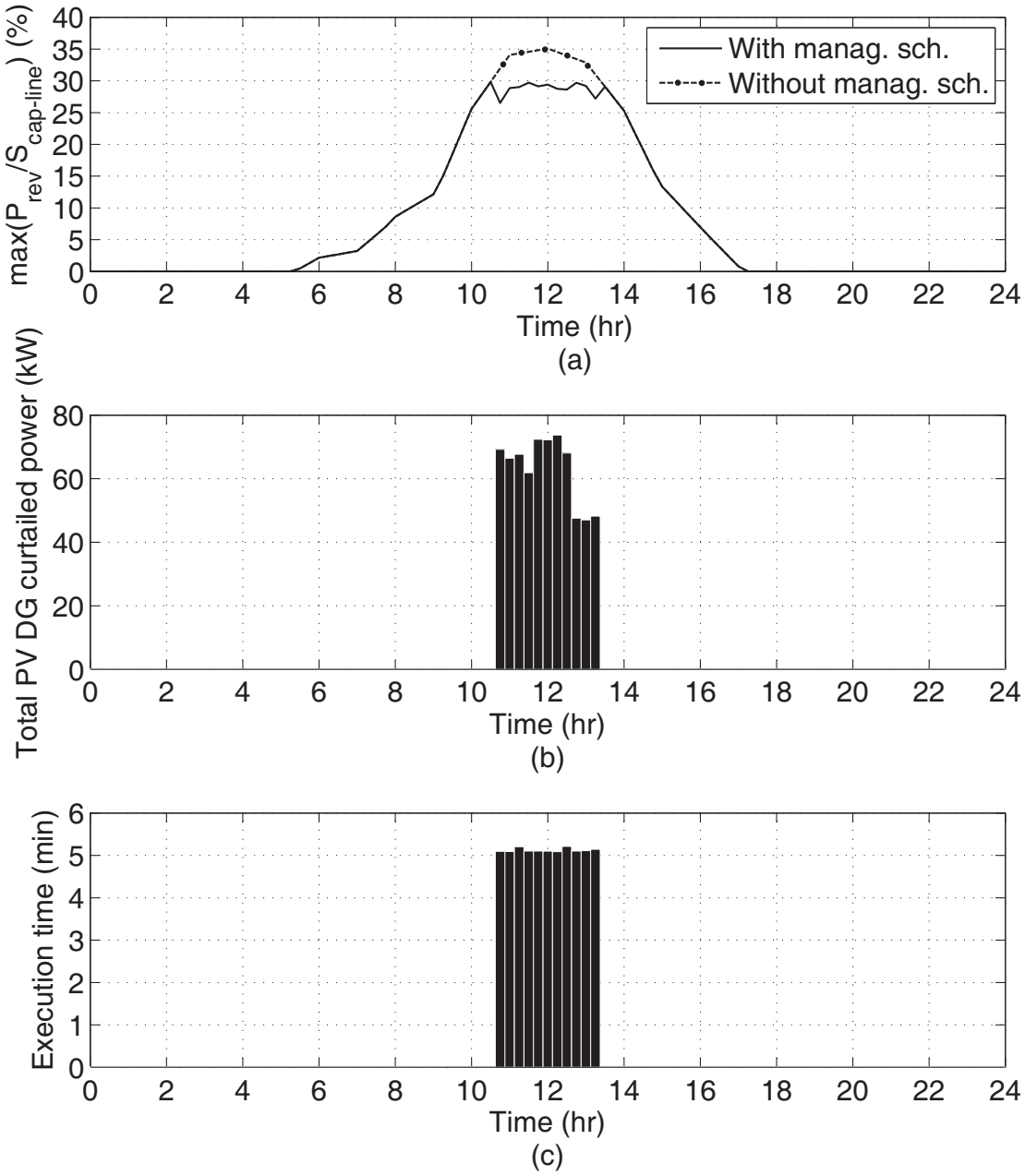

Figure 5.12: Hourly variations in (a) the maximum reverse power flow with and without the proposed management scheme, (b) the total curtailed PV DG power in the system using the proposed management scheme, and (c) times required for the execution of the management scheme, which runs every 15 min, during a Summer day

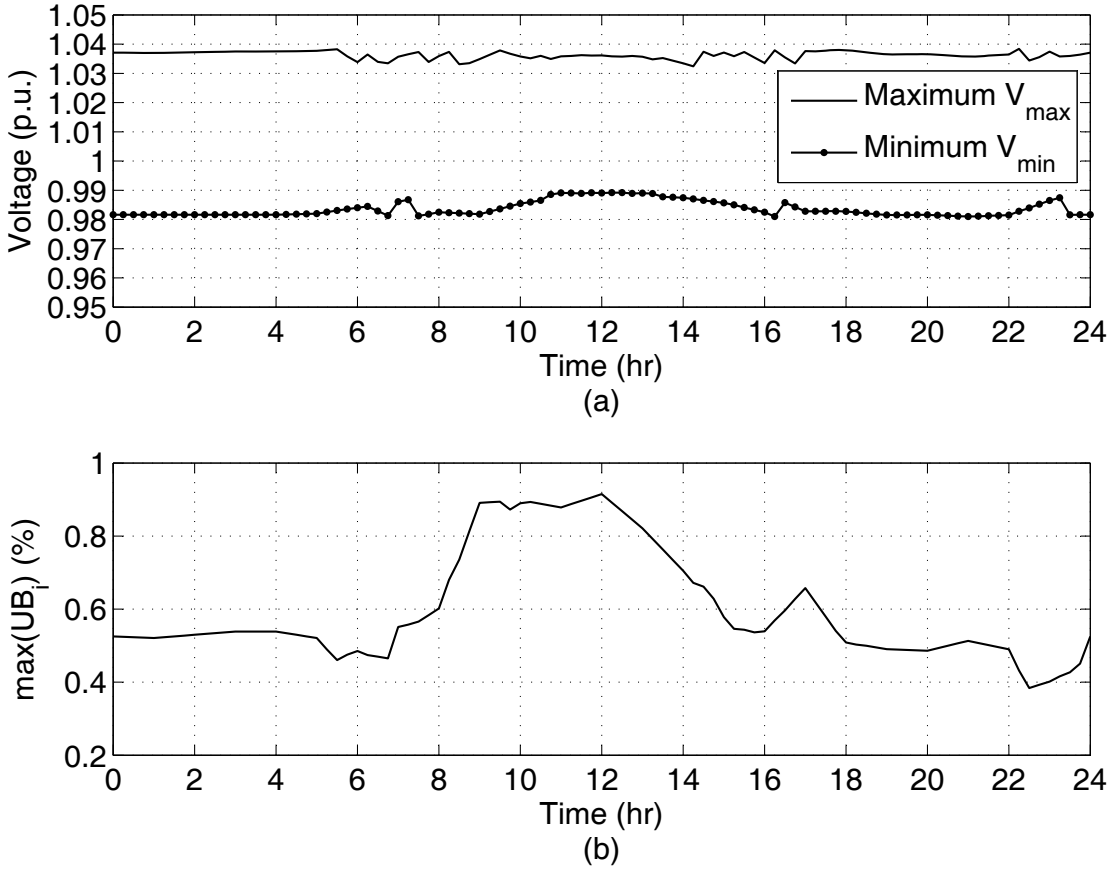

Figure 5.13: Hourly variations in (a) the maximum V_{max} and the minimum V_{min} and (b) the maximum voltage unbalance of the system using the proposed management scheme during a Summer day

Figure 5.3, these lines form the path connecting the source bus (150) to bus (13). The reverse power flow violation occurs in phase c. The reverse power flow can therefore corrected by curtailing the output power of the DG units connected to phase c in the system. The zone of interest in this case includes all the DG units connected to phase c in the system. This zone of interest includes 115 DG units.

The reverse power flow with the proposed management scheme is indicated by the solid line in Figure 5.12(a). The reverse power flow was successfully restored to less than 30 %. The total PV DG curtailed power is displayed in Figure 5.12(b). The times required for the execution of the management scheme are shown in Figure 5.12(c). The average execution time is about 5 min, which is shorter than the smart meter sampling period.

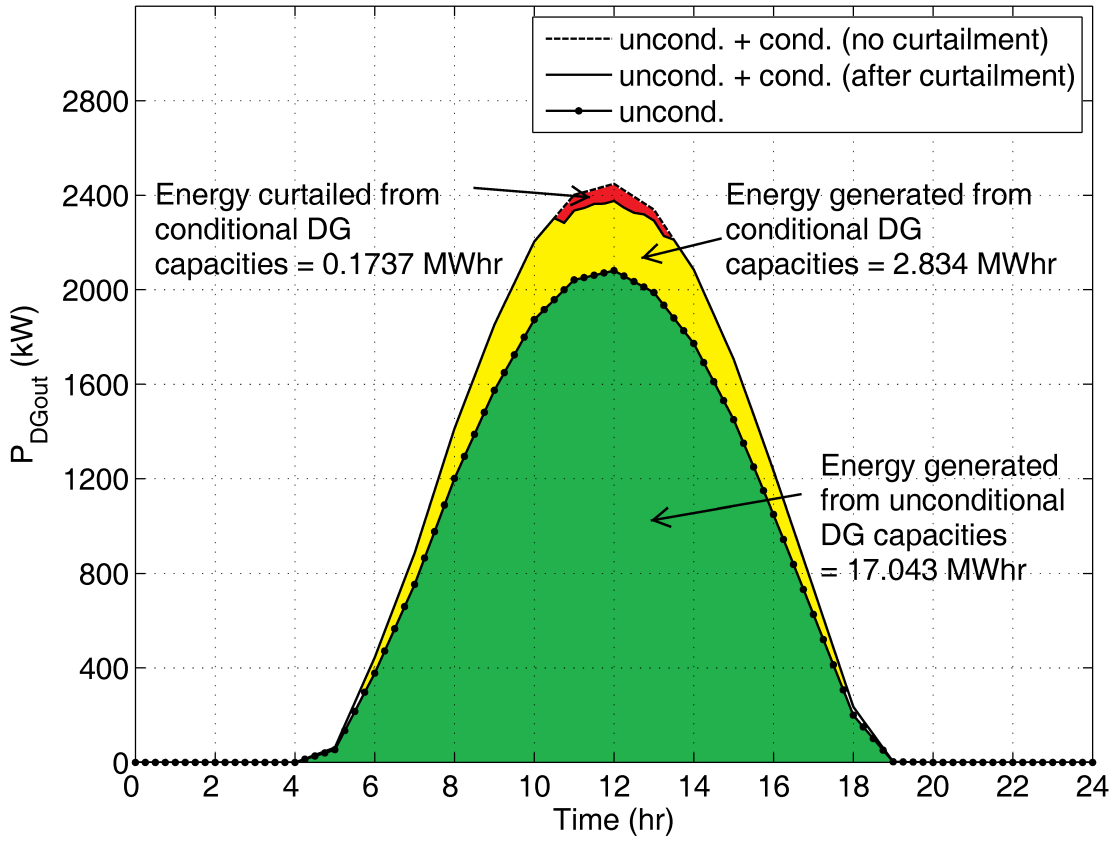

Figure 5.14: Total generated power from the 286 PV DG units during a Summer day

The hourly variations in the maximum and minimum values for the voltage in all system buses were plotted as shown in Figure 5.13(a). The hourly variations in the maximum voltage unbalance in the system are shown in Figure 5.13(b). It can be observed from Figure 5.13 that the system voltage and voltage unbalance are maintained within operational limits during the DG curtailment.

Figure 5.14 shows the total generation of the 286 PV DG units in the system during the Summer day. The dotted line shows the total generated PV DG power due to the conditional DG components. The broken line indicates the total generated PV DG power without implementing the management scheme, i.e. without curtailment. The solid line indicates the total generated PV DG power with implementing the management scheme, i.e. with curtailment.

The total energy that can be generated from the unconditional and unconditional com-

ponents of the 286 PV DG units is 20.051 MWhr during the Summer day, which is double the total energy in Case #1. This total energy equals the total area in Figure 5.14. Similar to Case #1, the total energy in Case #2 can be divided into the following three parts:

1. The energy generated from the unconditional DG components (the green area in Figure 5.14). This energy equals 17.043 MWhr, which is equivalent to 85 % of the total energy.

2. The energy generated from the conditional DG components (the yellow area in Figure 5.14). This energy equals 2.834 MWhr, which is equivalent to 14.134 % of the total energy. Since the conditional component is subject to curtailment, this energy is less than 15 % of the total energy.

3. The energy curtailed from the conditional DG components (the red area in Figure 5.14). This energy equals to 0.1737 MWhr, which is equivalent to 0.866 % of the total energy. This curtailed energy is equivalent to 5.775 % of the total energy that can be curtailed from the conditional DG components in the system.

5.4 Summary

The work presented in this Chapter builds on the techno-economic planning model introduced in Chapter 3. In this chapter, a proposed management scheme is employed to control the conditional DG component in the distribution system calculated by the proposed techno-economic planning model. The management scheme utilizes a novel scalable optimization model to minimize the curtailment of conditional DG component considering the online condition of the distribution system. The scalable optimization model enables DG curtailment to be managed in a specific zone of interest without the necessity of including the entire distribution system in the optimization model. The scalable optimization model can therefore effectively reduce the required execution time for the online management scheme. The simulation results show that the proposed management scheme can successfully mitigate the problems associated with high renewable DG penetration levels, such as reverse power flow, overvoltage, and voltage unbalance, with minimum curtailed energy. The proposed DG connection online assessment therefore allows renewable generation to access capacities not currently available under the microFIT regulations.

Chapter 6

Conclusions

6.1 Summary and Conclusions

The objective of the research presented in this thesis is to increase the connectivity of renewable DG sources in smart grids. To achieve this objective, this thesis presents new approaches for DG planning and operation to enable increasing the penetration of renewable energy generation in distribution systems.

The first phase of this work introduces a techno-economic planning model for increasing renewable DG sources in distribution systems under FIT programs. As discussed in Chapter 3, the techno-economic planning model divides the output power of each DG unit into two components, namely the unconditional and conditional components. The unconditional component is the portion of DG output power that is not susceptible to curtailment, and the conditional component is the amount of DG output power that is subject to curtailment. This model represents the main framework on which the proposed DG connection online assessment, presented in Chapter 5, is based.

The unconditional DG component, which is not subject to curtailment, is determined using the economic part of the proposed planning model. This component is calculated such that the IRR of the DG project is equal to the $MARR$. This approach guarantees that the DG project is economically feasible for DG investors when a DG power curtailment method is in place. The technical part of the proposed planning model includes an optimization model for maximizing the number of DG units to be installed in the system based on technical and economic constraints. The simulation results include a comparative study between the proposed planning model and the current microFIT regulations.

The study shows that limiting the aggregated DG capacity, as in the current microFIT regulations, results in a significant reduction in renewable energy capacity when compared to implementing the proposed planning model. The results also show that the application of DG power curtailment can significantly increase the renewable DG capacity installed in the system.

The second phase of this work introduces a novel "zooming" DLF algorithm for smart grids. As presented in Chapter 4, this algorithm is called zooming due to its ability to solve the DLF problem in a specific area of interest without necessitating the inclusion of all of the system buses, hence decreasing the solution time. The zooming DLF algorithm is employed in the management scheme for DG connection online assessment, presented in Chapter 5. The zooming feature enables minimizing the curtailed DG power in a specific area in the system. This area is determined based on the location of the overvoltage, voltage unbalance, or reverse power flow in the system.

The zooming DLF algorithm features an automated process for constructing and solving the DLF problem. The zooming algorithm can therefore interact with fast continual changes of smart grid loads and network topology. The significant reduction in DLF solution time along with the ability of interacting with network topology changes are essential for implementing the proposed management scheme for DG connection online assessment, presented in Chapter 5.

The third phase of this work introduces a management scheme for DG connection online assessment. As presented in Chapter 5, this scheme employs the smart grid communication and metering infrastructure to manage the curtailment of the conditional DG components in the system.

The management scheme for DG connection online assessment is implemented using a novel scalable optimization model that utilizes the zooming feature of the DLF presented in Chapter 4. The scalable optimization model minimizes the DG curtailment based on the system online conditions. The simulation results demonstrate the ability of the proposed management scheme to accommodate high penetration of renewable DG sources in smart grids.

6.2 Contributions

The main contributions of this thesis can be highlighted as follows:

1. The development of a novel "zooming" algorithm for DLF analysis in systems with flexible network topologies. The zooming algorithm enables the online processing of

the continual changes that take place in the network topology and loads of a smart grid. A key contribution in the proposed algorithm is the ability to significantly decrease the DLF solution time by solving the DLF problem for a specific zone of interest in the distribution system without the necessity of including all of the system buses in the DLF problem.

2. The development of an economic model for calculating the unconditional DG component, which is insusceptible to curtailment, that yields an adequate profit for DG investors. This proposed approach ensures that the DG project remains economically feasible when DG power curtailment is in place.

3. The development of a techno-economic planning model for maximizing the number of renewable DG sources with unconditional/conditional components. The developed model allows renewable generation to access capacities not currently available under the microFIT regulations. This is achieved while preserving all the system operational constraints and ensuring the economic feasibility of the DG projects.

4. The development of a management scheme for DG connection online assessment. The proposed scheme utilizes a novel scalable optimization problem for managing the curtailment of conditional DG components. The scalability feature of this model enables solving the optimization problem in a specific zone of interest without including the entire distribution system, hence reducing the problem size and the execution time for the online assessment scheme. The proposed scheme can effectively solve the overvoltage, voltage unbalance, and reverse power flow problems while minimizing the DG curtailed power.

6.3 Directions for Future Work

Based on the research presented in this thesis, the following subjects are suggested for future studies:

1. The development of the DLF zooming algorithm to solve the DLF problem in weekly-meshed distribution systems.

2. The application of the DLF zooming algorithm to perform short circuit analysis in a specific area of interest in the distribution system without including all of the system buses.

3. The application of the proposed techno-economic planning model for energy storage projects.

4. The development of a probabilistic model to determine the curtailed energy from a DG source under the proposed online assessment scheme. This curtailed energy can be used to estimate the overall IRR of the DG project while the curtailment is in place.

5. The development of the proposed online assessment scheme by using a multi objective optimization model to achieve multiple objectives simultaneously, such as minimizing system losses and DG curtailment simultaneously.

Appendix A

Cash Flows of the Candidate DG Capacities Studied in Chapter 3

Tables A.1-A.6 show the after-tax cash flows of the candidate DG capacities used in Chapter 3. These candidate capacities are 2 kW, 3 kW, 4 kW, 5 kW, 7 kW, and 10 kW. The after-tax cash flows are calculated using the analysis described in Section 3.2.3. The parameters of the economic model used in the calculations are listed in Table 3.4.

Table A.1: After-tax cash flow for a 2 kW rooftop PV DG unit using the analysis described in Section 3.2.3

End of year	Before-tax cash flow	Depreciation charges	Taxable income	Taxes	After-tax cash flow	Inflation index	After-tax cash flow with inflation
			B + C	*-0.3 × D*	*B + E*		*F / G*
A	*B*	*C*	*D*	*E*	*F*	*G*	*H*
0	-12460				-12460	1	-12460
1	903.47	-4984.00	-4080.53	1224.16	2127.63	1.02	2085.91
2	903.47	-5980.80	-5077.33	1523.20	2426.67	1.04	2332.44
3	903.47	-1196.16	-292.69	87.81	991.28	1.06	934.10
4	903.47	-239.23	664.24	-199.27	704.20	1.08	650.57
5	903.47	-47.85	855.63	-256.69	646.78	1.10	585.81
6	903.47	-9.57	893.90	-268.17	635.30	1.13	564.13
7	903.47	-1.91	901.56	-270.47	633.00	1.15	551.07
8	903.47	-0.38	903.09	-270.93	632.55	1.17	539.87
9	903.47	-0.08	903.40	-271.02	632.45	1.20	529.21
10	903.47	-0.02	903.46	-271.04	632.43	1.22	518.82
11	903.47	0.00	903.47	-271.04	632.43	1.24	508.64
12	903.47	0.00	903.47	-271.04	632.43	1.27	498.67
13	903.47	0.00	903.47	-271.04	632.43	1.29	488.89
14	903.47	0.00	903.47	-271.04	632.43	1.32	479.30
15	903.47	0.00	903.47	-271.04	632.43	1.35	469.91
16	903.47	0.00	903.47	-271.04	632.43	1.37	460.69
17	903.47	0.00	903.47	-271.04	632.43	1.40	451.66
18	903.47	0.00	903.47	-271.04	632.43	1.43	442.80
19	903.47	0.00	903.47	-271.04	632.43	1.46	434.12
20	903.47	0.00	903.47	-271.04	632.43	1.49	425.61

Table A.2: After-tax cash flow for a 3 kW rooftop PV DG unit using the analysis described in Section 3.2.3

End of year	Before-tax cash flow	Depreciation charges	Taxable income	Taxes	After-tax cash flow	Inflation index	After-tax cash flow with inflation
			B + C	*-0.3 × D*	*B + E*		*F / G*
A	*B*	*C*	*D*	*E*	*F*	*G*	*H*
0	-14610				-14610	1	-14610
1	1355.21	-5844.00	-4488.79	1346.64	2701.85	1.02	2648.87
2	1355.21	-7012.80	-5657.59	1697.28	3052.49	1.04	2933.95
3	1355.21	-1402.56	-47.35	14.21	1369.41	1.06	1290.43
4	1355.21	-280.51	1074.70	-322.41	1032.80	1.08	954.15
5	1355.21	-56.10	1299.11	-389.73	965.48	1.10	874.46
6	1355.21	-11.22	1343.99	-403.20	952.01	1.13	845.36
7	1355.21	-2.24	1352.96	-405.89	949.32	1.15	826.44
8	1355.21	-0.45	1354.76	-406.43	948.78	1.17	809.77
9	1355.21	-0.09	1355.12	-406.54	948.67	1.20	793.81
10	1355.21	-0.02	1355.19	-406.56	948.65	1.22	778.22
11	1355.21	0.00	1355.20	-406.56	948.65	1.24	762.96
12	1355.21	0.00	1355.21	-406.56	948.65	1.27	748.00
13	1355.21	0.00	1355.21	-406.56	948.65	1.29	733.33
14	1355.21	0.00	1355.21	-406.56	948.65	1.32	718.95
15	1355.21	0.00	1355.21	-406.56	948.65	1.35	704.86
16	1355.21	0.00	1355.21	-406.56	948.65	1.37	691.04
17	1355.21	0.00	1355.21	-406.56	948.65	1.40	677.49
18	1355.21	0.00	1355.21	-406.56	948.65	1.43	664.20
19	1355.21	0.00	1355.21	-406.56	948.65	1.46	651.18
20	1355.21	0.00	1355.21	-406.56	948.65	1.49	638.41

Table A.3: After-tax cash flow for a 4 kW rooftop PV DG unit using the analysis described in Section 3.2.3

End of year	Before-tax cash flow	Depreciation charges	Taxable income	Taxes	After-tax cash flow	Inflation index	After-tax cash flow with inflation
			B + C	*-0.3 × D*	*B + E*		*F / G*
A	*B*	*C*	*D*	*E*	*F*	*G*	*H*
0	-16960				-16960	1	-16960
1	1806.94	-6784.00	-4977.06	1493.12	3300.06	1.02	3235.35
2	1806.94	-8140.80	-6333.86	1900.16	3707.10	1.04	3563.15
3	1806.94	-1628.16	178.78	-53.64	1753.31	1.06	1652.18
4	1806.94	-325.63	1481.31	-444.39	1362.55	1.08	1258.79
5	1806.94	-65.13	1741.82	-522.55	1284.40	1.10	1163.32
6	1806.94	-13.03	1793.92	-538.18	1268.77	1.13	1126.63
7	1806.94	-2.61	1804.34	-541.30	1265.64	1.15	1101.82
8	1806.94	-0.52	1806.42	-541.93	1265.02	1.17	1079.68
9	1806.94	-0.10	1806.84	-542.05	1264.89	1.20	1058.41
10	1806.94	-0.02	1806.92	-542.08	1264.87	1.22	1037.63
11	1806.94	0.00	1806.94	-542.08	1264.86	1.24	1017.28
12	1806.94	0.00	1806.94	-542.08	1264.86	1.27	997.33
13	1806.94	0.00	1806.94	-542.08	1264.86	1.29	977.78
14	1806.94	0.00	1806.94	-542.08	1264.86	1.32	958.61
15	1806.94	0.00	1806.94	-542.08	1264.86	1.35	939.81
16	1806.94	0.00	1806.94	-542.08	1264.86	1.37	921.38
17	1806.94	0.00	1806.94	-542.08	1264.86	1.40	903.32
18	1806.94	0.00	1806.94	-542.08	1264.86	1.43	885.60
19	1806.94	0.00	1806.94	-542.08	1264.86	1.46	868.24
20	1806.94	0.00	1806.94	-542.08	1264.86	1.49	851.22

Table A.4: After-tax cash flow for a 5 kW rooftop PV DG unit using the analysis described in Section 3.2.3

End of year	Before-tax cash flow	Depreciation charges	Taxable income	Taxes	After-tax cash flow	Inflation index	After-tax cash flow with inflation
			B + C	*-0.3 × D*	*B + E*		*F / G*
A	*B*	*C*	*D*	*E*	*F*	*G*	*H*
0	-19250				-19250	1	-19250
1	2258.68	-7700.00	-5441.32	1632.40	3891.08	1.02	3814.78
2	2258.68	-9240.00	-6981.32	2094.40	4353.08	1.04	4184.04
3	2258.68	-1848.00	410.68	-123.20	2135.48	1.06	2012.31
4	2258.68	-369.60	1889.08	-566.72	1691.96	1.08	1563.11
5	2258.68	-73.92	2184.76	-655.43	1603.25	1.10	1452.11
6	2258.68	-14.78	2243.90	-673.17	1585.51	1.13	1407.89
7	2258.68	-2.96	2255.72	-676.72	1581.96	1.15	1377.19
8	2258.68	-0.59	2258.09	-677.43	1581.25	1.17	1349.58
9	2258.68	-0.12	2258.56	-677.57	1581.11	1.20	1323.00
10	2258.68	-0.02	2258.66	-677.60	1581.08	1.22	1297.04
11	2258.68	0.00	2258.68	-677.60	1581.08	1.24	1271.60
12	2258.68	0.00	2258.68	-677.60	1581.08	1.27	1246.67
13	2258.68	0.00	2258.68	-677.60	1581.08	1.29	1222.22
14	2258.68	0.00	2258.68	-677.60	1581.08	1.32	1198.26
15	2258.68	0.00	2258.68	-677.60	1581.08	1.35	1174.76
16	2258.68	0.00	2258.68	-677.60	1581.08	1.37	1151.73
17	2258.68	0.00	2258.68	-677.60	1581.08	1.40	1129.15
18	2258.68	0.00	2258.68	-677.60	1581.08	1.43	1107.01
19	2258.68	0.00	2258.68	-677.60	1581.08	1.46	1085.30
20	2258.68	0.00	2258.68	-677.60	1581.08	1.49	1064.02

Table A.5: After-tax cash flow for a 7 kW rooftop PV DG unit using the analysis described in Section 3.2.3

End of year	Before-tax cash flow	Depreciation charges	Taxable income	Taxes	After-tax cash flow	Inflation index	After-tax cash flow with inflation
			B + C	*-0.3 × D*	*B + E*		*F / G*
A	*B*	*C*	*D*	*E*	*F*	*G*	*H*
0	-24500				-24500	1	-24500
1	3162.15	-9800.00	-6637.85	1991.35	5153.51	1.02	5052.46
2	3162.15	-11760.00	-8597.85	2579.35	5741.51	1.04	5518.56
3	3162.15	-2352.00	810.15	-243.05	2919.11	1.06	2750.74
4	3162.15	-470.40	2691.75	-807.53	2354.63	1.08	2175.31
5	3162.15	-94.08	3068.07	-920.42	2241.73	1.10	2030.40
6	3162.15	-18.82	3143.34	-943.00	2219.15	1.13	1970.54
7	3162.15	-3.76	3158.39	-947.52	2214.64	1.15	1927.97
8	3162.15	-0.75	3161.40	-948.42	2213.73	1.17	1889.40
9	3162.15	-0.15	3162.00	-948.60	2213.55	1.20	1852.20
10	3162.15	-0.03	3162.12	-948.64	2213.52	1.22	1815.85
11	3162.15	-0.01	3162.15	-948.64	2213.51	1.24	1780.24
12	3162.15	0.00	3162.15	-948.65	2213.51	1.27	1745.33
13	3162.15	0.00	3162.15	-948.65	2213.51	1.29	1711.11
14	3162.15	0.00	3162.15	-948.65	2213.51	1.32	1677.56
15	3162.15	0.00	3162.15	-948.65	2213.51	1.35	1644.67
16	3162.15	0.00	3162.15	-948.65	2213.51	1.37	1612.42
17	3162.15	0.00	3162.15	-948.65	2213.51	1.40	1580.80
18	3162.15	0.00	3162.15	-948.65	2213.51	1.43	1549.81
19	3162.15	0.00	3162.15	-948.65	2213.51	1.46	1519.42
20	3162.15	0.00	3162.15	-948.65	2213.51	1.49	1489.63

Table A.6: After-tax cash flow for a 10 kW rooftop PV DG unit using the analysis described in Section 3.2.3

End of year	Before-tax cash flow	Depreciation charges	Taxable income	Taxes	After-tax cash flow	Inflation index	After-tax cash flow with inflation
			B + C	*-0.3 × D*	*B + E*		*F / G*
A	*B*	*C*	*D*	*E*	*F*	*G*	*H*
0	-31400				-31400	1	-31400
1	4517.36	-12560.00	-8042.64	2412.79	6930.15	1.02	6794.27
2	4517.36	-15072.00	-10554.64	3166.39	7683.75	1.04	7385.38
3	4517.36	-3014.40	1502.96	-450.89	4066.47	1.06	3831.93
4	4517.36	-602.88	3914.48	-1174.34	3343.02	1.08	3088.43
5	4517.36	-120.58	4396.78	-1319.04	3198.32	1.10	2896.82
6	4517.36	-24.12	4493.24	-1347.97	3169.39	1.13	2814.32
7	4517.36	-4.82	4512.54	-1353.76	3163.60	1.15	2754.10
8	4517.36	-0.96	4516.40	-1354.92	3162.44	1.17	2699.11
9	4517.36	-0.19	4517.17	-1355.15	3162.21	1.20	2646.00
10	4517.36	-0.04	4517.32	-1355.20	3162.16	1.22	2594.08
11	4517.36	-0.01	4517.35	-1355.21	3162.15	1.24	2543.20
12	4517.36	0.00	4517.36	-1355.21	3162.15	1.27	2493.34
13	4517.36	0.00	4517.36	-1355.21	3162.15	1.29	2444.45
14	4517.36	0.00	4517.36	-1355.21	3162.15	1.32	2396.52
15	4517.36	0.00	4517.36	-1355.21	3162.15	1.35	2349.53
16	4517.36	0.00	4517.36	-1355.21	3162.15	1.37	2303.46
17	4517.36	0.00	4517.36	-1355.21	3162.15	1.40	2258.29
18	4517.36	0.00	4517.36	-1355.21	3162.15	1.43	2214.01
19	4517.36	0.00	4517.36	-1355.21	3162.15	1.46	2170.60
20	4517.36	0.00	4517.36	-1355.21	3162.15	1.49	2128.04

Appendix B

Distribution Load Flow Results for the Forward/Backward Method and the Proposed Zooming Algorithm Presented in Chapter 4

Tables B.1 and B.2 show the DLF results for the zones of interest of the IEEE 37-bus and 123-bus systems, respectively, as discussed in Chapter 4. The results are obtained using the Forward/Backward (F/B) method and the proposed DLF zooming algorithm presented in Chapter 4. For the F/B method, the DLF problem is solved for all the system buses. On the other hand, in the case of the proposed zooming algorithm the DLF problem is solved only in the zone of interest. The DLF results of the buses included in the zone of interest only are displayed in Tables B.1 and B.2. The zone of interest in the IEEE 123-bus system contains single-phase feeders. The DLF results of the missing phases of the single-phase feeders are written as not applicable (N/A) data in Table B.2.

Table B.1: DLF results of the IEEE 37-bus system for the zone of interest using the F/B method for the entire system and the proposed zooming method

Bus	Phase 'a'				Phase 'b'				Phase 'c'			
	V (pu)		δ (degrees)		V (pu)		δ (degrees)		V (pu)		δ (degrees)	
	F/B	Zooming	F/B	Zooming	F/B	Zooming	F/B	Zooming	F/B	Zooming	F/B	Zooming
799	1.00000	1.00000	0.000	0.000	1.00000	1.00000	-120.000	-120.000	1.00000	1.00000	120.000	120.000
701	0.98711	0.98705	-0.204	-0.205	0.99270	0.99244	-120.226	-120.229	0.98099	0.98096	119.677	119.673
702	0.97932	0.97922	-0.354	-0.354	0.98861	0.98813	-120.333	-120.338	0.97168	0.97165	119.494	119.485
703	0.96947	0.96936	-0.516	-0.516	0.98769	0.98715	-120.453	-120.459	0.96431	0.96428	119.389	119.379
730	0.96264	0.96255	-0.640	-0.638	0.98796	0.98732	-120.448	-120.455	0.95719	0.95718	119.446	119.435
709	0.96028	0.96019	-0.670	-0.668	0.98792	0.98726	-120.458	-120.465	0.95547	0.95546	119.467	119.455
708	0.95630	0.95621	-0.738	-0.735	0.98892	0.98824	-120.473	-120.480	0.95252	0.95252	119.521	119.509
733	0.95225	0.95217	-0.796	-0.793	0.98981	0.98911	-120.499	-120.505	0.95015	0.95015	119.575	119.563
734	0.94705	0.94697	-0.894	-0.891	0.99103	0.99032	-120.508	-120.514	0.94562	0.94562	119.642	119.629
737	0.94046	0.94038	-0.964	-0.961	0.99283	0.99212	-120.580	-120.586	0.94370	0.94370	119.745	119.733
738	0.93858	0.93851	-1.006	-1.003	0.99359	0.99288	-120.582	-120.589	0.94203	0.94203	119.775	119.762
711	0.93886	0.93879	-1.045	-1.042	0.99400	0.99328	-120.545	-120.551	0.93992	0.93992	119.771	119.758
741	0.93895	0.93887	-1.058	-1.055	0.99413	0.99342	-120.533	-120.539	0.93924	0.93924	119.771	119.758

Table B.2: DLF results of the IEEE 123-bus system for the zone of interest using the F/B method for the entire system and the proposed zooming method

Bus	Phase 'a'				Phase 'b'				Phase 'c'			
	V (pu)		δ (degrees)		V (pu)		δ (degrees)		V (pu)		δ (degrees)	
	F/B	Zooming	F/B	Zooming	F/B	Zooming	F/B	Zooming	F/B	Zooming	F/B	Zooming
149	1.00000	1.00000	0.000	0.000	1.00000	1.00000	-120.000	-120.000	1.00000	1.00000	120.000	120.000
1	0.98643	0.98614	-0.679	-0.713	0.99837	0.99849	-120.336	-120.332	0.99047	0.99010	119.636	119.624
7	0.97635	0.97584	-1.178	-1.239	0.99726	0.99747	-120.604	-120.598	0.98426	0.98364	119.397	119.376
8	0.96980	0.96915	-1.511	-1.589	0.99645	0.99672	-120.781	-120.774	0.98015	0.97935	119.232	119.206
13	0.96104	0.96023	-1.973	-2.078	0.99489	0.99523	-121.031	-121.021	0.97398	0.97293	118.959	118.922
152	0.96104	0.96023	-1.973	-2.078	0.99489	0.99523	-121.031	-121.021	0.97398	0.97293	118.959	118.922
52	0.95445	0.95383	-2.367	-2.490	0.99395	0.99427	-121.292	-121.274	0.97022	0.96898	118.720	118.664
53	0.95145	0.95092	-2.551	-2.683	0.99333	0.99364	-121.420	-121.399	0.96837	0.96704	118.593	118.527
54	0.94974	0.94928	-2.658	-2.796	0.99284	0.99315	-121.499	-121.475	0.96722	0.96584	118.509	118.437
57	0.94615	0.94589	-2.973	-3.125	0.99028	0.99052	-121.711	-121.681	0.96420	0.96265	118.302	118.213
60	0.93865	0.93885	-3.682	-3.866	0.98581	0.98591	-122.120	-122.076	0.95719	0.95529	117.864	117.737
160	0.93865	0.93885	-3.682	-3.866	0.98581	0.98591	-122.120	-122.076	0.95719	0.95529	117.864	117.737
67	0.93583	0.93625	-3.969	-4.164	0.98519	0.98528	-122.319	-122.272	0.95480	0.95286	117.742	117.601
97	0.93477	0.93521	-4.029	-4.224	0.98466	0.98475	-122.344	-122.296	0.95406	0.95208	117.722	117.579
197	0.93477	0.93521	-4.029	-4.224	0.98466	0.98475	-122.344	-122.296	0.95406	0.95208	117.722	117.579
101	0.93394	0.93438	-4.077	-4.272	0.98437	0.98445	-122.360	-122.312	0.95347	0.95149	117.709	117.566
105	0.93257	0.93301	-4.123	-4.318	0.98420	0.98428	-122.408	-122.360	0.95377	0.95179	117.741	117.599
108	0.93105	0.93149	-4.201	-4.396	0.98486	0.98494	-122.422	-122.375	0.95362	0.95165	117.787	117.644
109	0.92680	0.92724	-4.290	-4.485	N/A	N/A	N/A	N/A	N/A	N/A	N/A	N/A
110	0.92482	0.92526	-4.331	-4.526	N/A	N/A	N/A	N/A	N/A	N/A	N/A	N/A
112	0.92418	0.92462	-4.345	-4.540	N/A	N/A	N/A	N/A	N/A	N/A	N/A	N/A
113	0.92216	0.92259	-4.388	-4.583	N/A	N/A	N/A	N/A	N/A	N/A	N/A	N/A
114	0.92169	0.92213	-4.397	-4.592	N/A	N/A	N/A	N/A	N/A	N/A	N/A	N/A

References

[1] T. Couture, C. Cory, K. nad Kreycik, and W. E., "A policymakers guide to feed-in tariff policy design," National Renewable Energy Laboratory (NREL), U.S. Dept. of Energy, Tech. Rep., 2010.

[2] S. Moore, V. Durant, and W. E. Mabee, "Determining appropriate feed-in tariff rates to promote biomass-to-electricity generation in eastern ontario, canada," *Energy Policy*, vol. 63, no. 0, pp. 607 – 613, 2013.

[3] V. Uran and S. Krajcar, "A methodology for analysis of the renewable electricity feed-in tariff markets," *International Journal of Electrical Power & Energy Systems*, vol. 53, no. 0, pp. 1 – 9, 2013.

[4] C. Dong, "Feed-in tariff vs. renewable portfolio standard: An empirical test of their relative effectiveness in promoting wind capacity development," *Energy Policy*, vol. 42, no. 0, pp. 476 – 485, 2012.

[5] S. Jenner, F. Groba, and J. Indvik, "Assessing the strength and effectiveness of renewable electricity feed-in tariffs in european union countries," *Energy Policy*, vol. 52, no. 0, pp. 385 – 401, 2013, special Section: Transition Pathways to a Low Carbon Economy.

[6] R. Tonkoski, D. Turcotte, and T. H. M. EL-Fouly, "Impact of high pv penetration on voltage profiles in residential neighborhoods," *IEEE Transactions on Sustainable Energy*, vol. 3, no. 3, pp. 518–527, 2012.

[7] R. Shayani and M. de Oliveira, "Photovoltaic generation penetration limits in radial distribution systems," *IEEE Transactions on Power Systems*, vol. 26, no. 3, pp. 1625–1631, 2011.

[8] H. Mostafa, R. El-Shatshat, and M. Salama, "Multi-objective optimization for the operation of an electric distribution system with a large number of single phase solar generators," *IEEE Transactions on Smart Grid*, vol. 4, no. 2, pp. 1038–1047, June 2013.

[9] "IEEE Guide for Conducting Distribution Impact Studies for Distributed Resource Interconnection," *IEEE Std 1547.7-2013*, pp. 1–137, Feb 2014.

[10] FIT Program. Ontario Power Authority. [Online]. Available: http://fit.powerauthority.on.ca/fit-program

[11] microFIT Program. Ontario Power Authority. [Online]. Available: http://microfit.powerauthority.on.ca/

[12] (2013) Distributed Generation Technical Interconnection Requirements, Interconnections at Voltages 50 kV and Below. Hydro One. [Online]. Available: http://www.hydroone.com/Generators/Documents/Distribution/Distributed%20Generation%20Technical%20Interconnection%20Requirements.pdf

[13] (2010) Technical Interconnection Requirements for Distributed Generation, Micro Generation & Small Generation, 3-Phase, less than 30 kW. Hydro One. [Online]. Available: http://www.hydroone.com/Generators/Documents/Feed-In%20Tariff/microFIT_TIR_for_Distributed_Generation.pdf

[14] MicroFIT program, Bi-weekly reports. Ontario Power Authority. [Online]. Available: http://microfit.powerauthority.on.ca/microfit-program-resources/version-2-program-updates/bi-weekly-reports

[15] (2014, January) MicroFIT program, Bi-weekly reports, Data as of January 6, 2014. Ontario Power Authority. [Online]. Available: http://microfit.powerauthority.on.ca/sites/default/files/bi-weekly_reports/mFIT%20Report%20Bi-Weekly%20Jan_6_2014.pdf

[16] R. Tonkoski, L. A. C. Lopes, and T. H. M. EL-Fouly, "Coordinated active power curtailment of grid connected pv inverters for overvoltage prevention," *IEEE Transactions on Sustainable Energy*, vol. 2, no. 2, pp. 139–147, 2011.

[17] D. Lew *et al.*, "Wind and solar curtailment: Preprint," National Renewable Energy Laboratory, Golden, CO, Tech. Rep. NREL/CP-5500-60245, Sep. 2013, to be presented at the International Workshop on Large-Scale Integration of Wind Power Into Power Systems as Well as on Transmission Networks for Offshore

Wind Power Plants London, England October 22 24, 2013. [Online]. Available: http://www.nrel.gov/docs/fy13osti/60245.pdf

[18] S. Alyami, Y. Wang, C. Wang, J. Zhao, and B. Zhao, "Adaptive real power capping method for fair overvoltage regulation of distribution networks with high penetration of pv systems," pp. 1–1, 2014.

[19] G. Mokhtari, A. Ghosh, G. Nourbakhsh, and G. Ledwich, "Smart robust resources control in lv network to deal with voltage rise issue," *IEEE Transactions on Sustainable Energy*, vol. 4, no. 4, pp. 1043–1050, Oct 2013.

[20] G. Mokhtari, G. Nourbakhsh, F. Zare, and A. Ghosh, "Overvoltage prevention in {LV} smart grid using customer resources coordination," *Energy and Buildings*, vol. 61, no. 0, pp. 387 – 395, 2013. [Online]. Available: http://www.sciencedirect.com/science/article/pii/S0378778813000911

[21] Y. Wang, P. Zhang, W. Li, W. Xiao, and A. Abdollahi, "Online overvoltage prevention control of photovoltaic generators in microgrids," *Smart Grid, IEEE Transactions on*, vol. 3, no. 4, pp. 2071–2078, Dec 2012.

[22] S. Weckx, C. Gonzalez, and J. Driesen, "Combined central and local active and reactive power control of pv inverters," *IEEE Transactions on Sustainable Energy*, vol. 5, no. 3, pp. 776–784, July 2014.

[23] X. Su, M. Masoum, and P. Wolfs, "Optimal pv inverter reactive power control and real power curtailment to improve performance of unbalanced four-wire lv distribution networks," *IEEE Transactions on Sustainable Energy*, vol. 5, no. 3, pp. 967–977, July 2014.

[24] *CAN3-C235-83 (R2010) - Preferred Voltage Levels for AC Systems, 0 to 50 000 V*, CSA Std., 2010.

[25] C. L. Masters, "Voltage rise: the big issue when connecting embedded generation to long 11 kv overhead lines," *Power Engineering Journal*, vol. 16, no. 1, pp. 5–12, Feb 2002.

[26] M. Hashemi and V. Agelidis, "Evaluation of voltage regulation mitigation methods due to high penetration of pv generation in residential areas," in *2013 International Conference on Renewable Energy Research and Applications (ICRERA)*, Oct 2013, pp. 1180–1189.

[27] M. Alam, K. Muttaqi, and D. Sutanto, "Mitigation of rooftop solar pv impacts and evening peak support by managing available capacity of distributed energy storage systems," *IEEE Transactions on Power Systems*, vol. 28, no. 4, pp. 3874–3884, Nov 2013.

[28] X. Liu, A. Aichhorn, L. Liu, and H. Li, "Coordinated control of distributed energy storage system with tap changer transformers for voltage rise mitigation under high photovoltaic penetration," *Smart Grid, IEEE Transactions on*, vol. 3, no. 2, pp. 897–906, June 2012.

[29] J. Barton and D. Infield, "Energy storage and its use with intermittent renewable energy," *Energy Conversion, IEEE Transactions on*, vol. 19, no. 2, pp. 441–448, June 2004.

[30] J. von Appen, T. Stetz, M. Braun, and A. Schmiegel, "Local voltage control strategies for pv storage systems in distribution grids," *IEEE Transactions on Smart Grid*, vol. 5, no. 2, pp. 1002–1009, March 2014.

[31] "Ieee standard for interconnecting distributed resources with electric power systems," *IEEE Std 1547-2003*, pp. 1–28, July 2003.

[32] L. Ochoa, C. Dent, and G. Harrison, "Distribution network capacity assessment: Variable dg and active networks," *IEEE Transactions on Power Systems*, vol. 25, no. 1, pp. 87–95, 2010.

[33] W. H. Kersting, *Distribution System Modeling And Analysis*, ser. The Electric Power Engineering Series. Taylor & Francis, 2007.

[34] A. Botea, J. Rintanen, and D. Banerjee, "Optimal reconfiguration for supply restoration with informed a search," *IEEE Transactions on Smart Grid*, vol. 3, no. 2, pp. 583–593, 2012.

[35] M. Abdel-Akher, K. Nor, and A. Rashid, "Improved three-phase power-flow methods using sequence components," *IEEE Transactions on Power Systems*, vol. 20, no. 3, pp. 1389–1397, 2005.

[36] J. Martinez and J. Mahseredjian, "Load flow calculations in distribution systems with distributed resources. a review," in *2011 IEEE Power and Energy Society General Meeting*, 2011, pp. 1–8.

[37] J. Grainger and W. Stevenson, *Power system analysis*, ser. McGraw-Hill series in electrical and computer engineering: Power and energy. McGraw-Hill, 1994.

[38] R. Zimmerman and H.-D. Chiang, "Fast decoupled power flow for unbalanced radial distribution systems," *IEEE Transactions on Power Systems*, vol. 10, no. 4, pp. 2045–2052, Nov 1995.

[39] D. R. R. Penido, L. R. de Araujo, S. Carneiro, J. L. R. Pereira, and P. Garcia, "Three-phase power flow based on four-conductor current injection method for unbalanced distribution networks," *IEEE Transactions on Power Systems*, vol. 23, no. 2, pp. 494–503, May 2008.

[40] L. R. de Araujo, D. R. R. Penido, S. C. Jnior, J. L. R. Pereira, and P. A. N. Garcia, "Comparisons between the three-phase current injection method and the forward/backward sweep method," *International Journal of Electrical Power & Energy Systems*, vol. 32, no. 7, pp. 825 – 833, 2010.

[41] M. F. AlHajri and M. El-Hawary, "Exploiting the radial distribution structure in developing a fast and flexible radial power flow for unbalanced three-phase networks," *IEEE Transactions on Power Delivery*, vol. 25, no. 1, pp. 378–389, 2010.

[42] K. Lo and C. Zhang, "Decomposed three-phase power flow solution using the sequence component frame," *IEE Proceedings C, Generation, Transmission and Distribution*, vol. 140, no. 3, pp. 181–188, May 1993.

[43] X.-P. Zhang, "Fast three phase load flow methods," *IEEE Transactions on Power Systems*, vol. 11, no. 3, pp. 1547–1554, Aug 1996.

[44] M. Kamh and R. Iravani, "Unbalanced model and power-flow analysis of microgrids and active distribution systems," *IEEE Transactions on Power Delivery*, vol. 25, no. 4, pp. 2851–2858, 2010.

[45] W. H. Kersting and D. L. Mendive, "An application of ladder network theory to the solution of three phase radial load flow problem," in *the IEEE PES Winter Meeting, New York*, 1976.

[46] W. Kersting, "A method to teach the design and operation of a distribution system," *IEEE Transactions on Power Apparatus and Systems*, vol. PAS-103, no. 7, pp. 1945–1952, July 1984.

[47] U. Eminoglu and M. Hocaoglu, "Distribution systems forward/backward sweep-based power flow algorithms: a review and comparison study," *Electric Power Components and Systems*, vol. 37, no. 1, pp. 91–110, 2008.

[48] M. Mishra and D. Das, "Evolution of Distribution System Load Flow Methods - a Bibliographic Review," *Journal of the Institution of Engineers (India). Electrical Engineering Division*, vol. 91, pp. 42–48, September 2010.

[49] J.-H. Teng, "A direct approach for distribution system load flow solutions," *IEEE Transactions on Power Delivery*, vol. 18, no. 3, pp. 882 – 887, July 2003.

[50] F. Zhang and C. Cheng, "A modified newton method for radial distribution system power flow analysis," *IEEE Transactions on Power Systems*, vol. 12, no. 1, pp. 389–397, Feb 1997.

[51] K. Mahmoud and M. Abdel-Akher, "Efficient three-phase power-flow method for unbalanced radial distribution systems," in *2010 15th IEEE Mediterranean Electrotechnical Conference - MELECON 2010*, April 2010, pp. 125–130.

[52] L. Zhang, W. Tang, and H. Guan, "The back/forward sweep-based power flow method for distribution networks with dgs," in *2009 2nd International Conference on Power Electronics and Intelligent Transportation System (PEITS)*, vol. 1, Dec 2009, pp. 145–149.

[53] S. Mishra, "A simple algorithm for unbalanced radial distribution system load flow," in *TENCON 2008 - 2008 IEEE Region 10 Conference*, Nov 2008, pp. 1–6.

[54] S. Khushalani, J. Solanki, and N. Schulz, "Development of three-phase unbalanced power flow using pv and pq models for distributed generation and study of the impact of dg models," *IEEE Transactions on Power Systems*, vol. 22, no. 3, pp. 1019–1025, Aug 2007.

[55] D. Das, H. S. Nagi, and D. Kothari, "Novel method for solving radial distribution networks," *IEE Proceedings-Generation, Transmission and Distribution*, vol. 141, no. 4, pp. 291–298, Jul 1994.

[56] D. Rajicic, R. Ackovski, and R. Taleski, "Voltage correction power flow," *IEEE Transactions on Power Delivery*, vol. 9, no. 2, pp. 1056–1062, Apr 1994.

[57] A. Augugliaro, L. Dusonchet, S. Favuzza, M. Ippolito, and E. R. Sanseverino, "Backward solution of pv nodes in radial distribution networks," *Electric Power Systems Research*, vol. 79, no. 4, pp. 669 – 679, 2009.

[58] W. Wu and B. Zhang, "A three-phase power flow algorithm for distribution system power flow based on loop-analysis method," *International Journal of Electrical Power & Energy Systems*, vol. 30, no. 1, pp. 8 – 15, 2008.

[59] S. Khushalani and N. Schulz, "Unbalanced distribution power flow with distributed generation," in *2005/2006 IEEE PES Transmission and Distribution Conference and Exhibition*, May 2006, pp. 301–306.

[60] W. Kersting and W. Phillips, "Distribution feeder line models," *IEEE Transactions on Industry Applications*, vol. 31, no. 4, pp. 715–720, Jul 1995.

[61] IEEE Task Force on Load representation for Dynamic Performance, "Load representation for dynamic performance analysis [of power systems]," *IEEE Transactions on Power Systems*, vol. 8, no. 2, pp. 472–482, 1993.

[62] "IEEE Recommended Practice for Interconnecting Distributed Resources with Electric Power Systems Distribution Secondary Networks," *IEEE Std 1547.6-2011*, pp. 1–38, Sept 2011.

[63] G. J. Thuesen and W. J. Fabrycky, *Engineering Economy*, 8th ed., ser. Prentice-Hall International Series in Industrial and Systems Engineering. Prentice Hall, 1993.

[64] D. Young, *Modern Engineering Economy*. J. Wiley, 1993.

[65] C. Park and G. Sharp-Bette, *Advanced Engineering Economics*. Wiley, 1990.

[66] G. Smith, *Engineering-Economy: Analysis of Capital Expenditures*, 4th ed. Iowa State University Press, 1987.

[67] Multiple Projects on the Same Deemed Single Property. Ontario Power Authority. [Online]. Available: http://fit.powerauthority.on.ca/fit-program/eligibility-requirements/eligibility-requirements-all-projects/multiple-on-same-deemed-single-property

[68] (2010, August) FIT Guidelines: Multiple Projects on One Property. Ontario Power Authority. [Online]. Available: https://fit.powerauthority.on.ca/Storage/11109_FIT_Guidelines_-_Multiple_FIT_Projects_on_One_Property_VERSION_2_Final.pdf

[69] Renewable Energy Project Finance in the U.S.: 2010-2013 Overview and Future Outlook. Mintz Levin Cohn Ferris Glovsky and Popeo PC. [Online]. Available: http://www.mintz.com/DesktopModules/Bring2mind/DMX/Download.aspx?EntryId=231&PortalId=0&DownloadMethod=attachment

[70] Y. Atwa, E. El-Saadany, M. Salama, R. Seethapathy, M. Assam, and S. Conti, "Adequacy evaluation of distribution system including wind/solar dg during different modes of operation," *Power Systems, IEEE Transactions on*, vol. 26, no. 4, pp. 1945–1952, Nov 2011.

[71] Photovoltaic potential and solar resource maps of Canada. Natural Resources Canada. [Online]. Available: http://pv.nrcan.gc.ca

[72] Canadian Wind Energy Atlas. Environment Canada. [Online]. Available: http://www.windatlas.ca/

[73] Wind Maps. National Renewable Energy Laboratory (NREL). [Online]. Available: http://www.nrel.gov/gis/wind.html

[74] Solar Maps. National Renewable Energy Laboratory (NREL). [Online]. Available: http://www.nrel.gov/gis/solar.html

[75] A. Von Jouanne and B. Banerjee, "Assessment of voltage unbalance," *IEEE Transactions on Power Delivery*, vol. 16, no. 4, pp. 782–790, Oct 2001.

[76] Distribution Test Feeders. IEEE Power & Energy Society. [Online]. Available: http://ewh.ieee.org/soc/pes/dsacom/testfeeders/

[77] C. D. Aussant, A. S. Fung, V. I. Ugursal, and H. Taherian, "Residential application of internal combustion engine based cogeneration in cold climatecanada," *Energy and Buildings*, vol. 41, no. 12, pp. 1288 – 1298, 2009.

[78] Prices For Solar PV Supplies. Solacity Inc. [Online]. Available: http://www.solacity.com

[79] The GST/HST Implications of the Acquisition of Solar Panels Under the micro Feed-in Tariff Program in Ontario. Canada Revenue Agency. [Online]. Available: http://www.cra-arc.gc.ca/E/pub/gi/gi-122/gi-122-e.pdf

[80] (2014, January) FIT/microFIT Price Schedule (January 1, 2014). Ontario Power Authority. [Online]. Available: http://microfit.powerauthority.on.ca/sites/default/files/page/2014%20FIT%20Price%20Schedule_Final_20131107.pdf

[81] Photovoltaic potential and solar resource maps of Canada, Mississauga, Ontario. Natural Resources Canada. [Online]. Available: http://pv.nrcan.gc.ca/index.php?n=1753&m=u&lang=e

[82] Ontario's FIT/microFIT Programs. Canada Revenue Agency. [Online]. Available: http://www.cra-arc.gc.ca/tx/bsnss/thrtpcs/nt-ft/q1-eng.html

[83] The Green Source Funding Database - Accelerated Capital Cost Allowance. Environment Canada. [Online]. Available: https://www.ec.gc.ca/financement-funding/sv-gs/search_results_e.cfm?action=details&id=319&start_row=1&all_records_details=

[84] M. M. A. Salama, E. A. A. Mansour, A. Y. Chikhani, and R. Hackam, "Control of reactive power in distribution systems with an end-load and varying load condition," *IEEE Transactions on Power Apparatus and Systems*, vol. PAS-104, no. 4, pp. 941 –947, July 1985.

[85] W. H. Kersting, "Radial distribution test feeders," in *IEEE Power Engineering Society Winter Meeting*, vol. 2, 2001, pp. 908–912.

[86] N. Deo, *Graph Theory With Applications To Engineering And Computer Science*, ser. Prentice-Hall series in automatic computation. Prentice-Hall Of India Pvt. Limited, 2004.

[87] T. Cormen, C. Leiserson, R. Rivest, and C. Stein, *Introduction To Algorithms*. MIT Press, 2001.

[88] SLK60P6L SLV/WHT 220W-255W Poly-Crystalline Solar Modules. Siliken Canada. [Online]. Available: http://www.highlandsolar.ca/media/SLK60P6L_with_Linear_Warranty.pdf

[89] Weather Data, Department of Geography. University of Toronto, Mississauga. [Online]. Available: http://www.utm.utoronto.ca/geography/resources/meteorological-station/weather-data